

UNIVERSITY OF OKLAHOMA

GRADUATE COLLEGE

POTENTIAL FIELD STUDIES OF THE CENTRAL SAN LUIS BASIN AND SAN
JUAN MOUNTAINS, COLORADO AND NEW MEXICO, AND SOUTHERN
AND WESTERN AFGHANISTAN

A DISSERTATION

SUBMITTED TO THE GRADUATE FACULTY

in partial fulfillment of the requirements for the

Degree of

DOCTOR OF PHILOSOPHY

By

BENJAMIN JOHN DRENTH

Norman, Oklahoma

2009

POTENTIAL FIELD STUDIES OF THE CENTRAL SAN LUIS BASIN AND SAN
JUAN MOUNTAINS, COLORADO AND NEW MEXICO, AND SOUTHERN
AND WESTERN AFGHANISTAN

A DISSERTATION APPROVED FOR THE
CONOCOPHILLIPS SCHOOL OF GEOLOGY AND GEOPHYSICS

BY

Dr. G. Randy Keller, Chair

Dr. V.J.S. Grauch

Dr. Carol Finn

Dr. R. Douglas Elmore

Dr. Ze'ev Reches

Dr. Carl Sondergeld

TABLE OF CONTENTS

Introduction.....	1
Chapter A: Geophysical Constraints on Rio Grande Rift Structure in the Central San Luis Basin, Colorado and New Mexico.....	2
Chapter B: A Geophysical Study of the San Juan Mountains Batholith, southwestern Colorado.....	61
Chapter C: Geophysical Expression of Intrusions and Tectonic Blocks of Southern and Western Afghanistan.....	110
Conclusions.....	154

LIST OF TABLES

Chapter A: Geophysical Constraints on Rio Grande Rift Structure in the Central San Luis Basin, Colorado and New Mexico

Table A1: Geophysical characteristics of units in model A-A'41

Chapter B: A Geophysical Study of the San Juan Mountains Batholith, southwestern Colorado

Table B1: Surficial densities used to calculate gravity map88

Table B2: Batholith complex properties89

LIST OF FIGURES

Chapter A: Geophysical Constraints on Rio Grande Rift Structure in the Central San Luis Basin, Colorado and New Mexico	
Figure A1: Physiography and geography of the San Luis basin.....	42
Figure A2: Simplified geology and physiography of the study area.....	43
Figure A3: Isostatic residual gravity anomaly map of the study area.....	44
Figure A4: Density-depth function for Santa Fe Group rift sediments.....	45
Figure A5: Gravitational effect of pre-rift (pre-Santa Fe Group) rocks.....	46
Figure A6: Elevation of the base of Santa Fe Group sediments.....	46
Figure A7: Reduced-to-pole aeromagnetic anomalies.....	47
Figure A8: Aeromagnetic anomalies and elevation of southern San Luis Hills.....	47
Figure A9: Filtered reduced-to-pole aeromagnetic anomalies.....	48
Figure A10: Estimates of depth to magnetic sources.....	48
Figure A11: Geophysical profiles and model along A-A'.....	49
Figure A12: Summary of selected new geologic conclusions.....	50
 Chapter B: A Geophysical Study of the San Juan Mountains Batholith, southwestern Colorado	
Figure B1: Physiography and geography of the San Juan Mountains region.....	90
Figure B2: Geology of the San Juan Mountains region.....	91
Figure B3: Conventional complete Bouguer gravity map.....	92
Figure B4: Elevation map of the San Juan Mountains region.....	93
Figure B5: Regional gravity anomalies.....	94
Figure B6: Density model used for surficial rocks.....	95

Figure B7: New gravity anomaly map.....	96
Figure B8: Difference between new and conventional gravity maps.....	97
Figure B9: Gravity map results using alternate reduction density.....	98
Figure B10: Horizontal gradient magnitude of new gravity map.....	99
Figure B11: Seismic refraction picks and model.....	100
Figure B12: Gravity profile models.....	101
Chapter C: Geophysical Expression of Intrusions and Tectonic Blocks of Southern and Western Afghanistan	
Figure C1: Regional physiography and tectonic elements.....	133
Figure C2: Geology of southern and western Afghanistan.....	134
Figure C3: Elevation map of southern and western Afghanistan.....	135
Figure C4: Reduced-to-pole aeromagnetic anomalies.....	136
Figure C5: Magnetic potential anomalies.....	137
Figure C6: Complete Bouguer gravity anomalies.....	138
Figure C7: Isostatic residual gravity anomalies.....	139
Figure C8: Synthetic data example showing mapping techniques used.....	140
Figure C9: Terraced reduced-to-pole aeromagnetic anomalies.....	141
Figure C10: Terraced isostatic residual gravity anomalies.....	142
Figure C11: Magnetic source depth estimates.....	143
Figure C12: Geophysical profile models along A-A'.....	144
Figure C13: Interpreted distribution of strongly magnetized intrusions.....	145
Figure C14: Interpreted pattern of crustal extrusion.....	146
Figure C15: Aeromagnetic gradients and Quaternary faults.....	147

ABSTRACT

This dissertation includes three separate chapters, each demonstrating the interpretive utility of potential field (gravity and magnetic) geophysical datasets at various scales and in various geologic environments. The locations of these studies are the central San Luis Basin of Colorado and New Mexico, the San Juan Mountains of southwestern Colorado, and southern and western Afghanistan.

The San Luis Basin is the northernmost of the major basins that make up the Rio Grande rift, and interpretation of gravity and aeromagnetic data reveals patterns of rifting, rift-sediment thicknesses, distribution of pre-rift volcanic and sedimentary rocks, and distribution of syn-rift volcanic rocks. Syn-rift Santa Fe Group sediments have a maximum thickness of ~2 km in the Sanchez graben near the eastern margin of the basin along the central Sangre de Cristo fault zone. Under the Costilla Plains, thickness of these sediments is estimated to reach ~1.3 km. The Santa Fe Group sediments also reach a thickness of nearly 1 km within the Monte Vista graben near the western basin margin along the San Juan Mountains. A narrow, north-south-trending structural high beneath San Pedro Mesa separates the graben from the structural depression beneath the Costilla Plains. Aeromagnetic anomalies are interpreted to mainly reflect variations of remanent magnetic polarity and burial depth of the 5.3-3.7 Ma Servilleta basalt of the Taos Plateau volcanic field. Magnetic-source depth estimates indicate patterns of subsidence following eruption of the basalt and show that the Sanchez graben has been the site of maximum subsidence.

One of the largest and most pronounced gravity lows in North America lies over the rugged San Juan Mountains in southwestern Colorado. A buried, low-density silicic

batholith related to an Oligocene volcanic field coincident with the San Juan Mountains has been the accepted interpretation of the source of the gravity low since the 1970s. However, this interpretation was based on gravity data processed with standard techniques that break down in the SJVF region. We applied an unconventional processing procedure that uses geologically appropriate densities for the uppermost crust and digital topography to mostly remove the effect of the low density units that underlie the topography associated with the SJVF. We also reinterpreted vintage seismic refraction data that indicate the presence of two low-velocity zones under the SJVF. Assuming that the source of the gravity low on the improved gravity anomaly map is the same as the source of the low seismic velocities, integrated modeling defined the dimensions and overall density contrast of the batholith complex. Models show that the thickness of the batholith complex varies significantly laterally, with the greatest thickness (~20 km) under the western SJVF, and lesser thicknesses (< 10 km) under the eastern SJVF.

The Afghan block, a series of Gondwanan terranes that lie between the Eurasian and Indian plates, is coincident with most of southern and western Afghanistan. Recently acquired regional aeromagnetic and aerogravity datasets were used to examine the geophysical expressions of plutons related to magmatic arcs, major tectonic blocks within the broader Afghan block, Himalayan deformation, and the Helmand basin. Numerous plutons are reflected as aeromagnetic highs, allowing these to be mapped in areas where they do not crop out. The Farah and Helmand blocks have distinctive geophysical expressions that separate them from the adjacent Eurasian and Indian plates. West-

southwestward crustal extrusion, an effect of the Himalayan orogeny, is indicated to have occurred with greater displacement along the Farah block than along the Helmand block.

INTRODUCTION

This dissertation includes three different chapters, each involving the geologic interpretation of gravity and magnetic geophysical datasets. The scales of the studies presented here are variable, from mapping of individual structures in the San Luis Basin to mapping at the scale of most of the country of Afghanistan. Goals of the three chapters include delineating the geometry of the central San Luis Basin of the Rio Grande rift, the geometry of the batholith under the San Juan Mountains, and describing the geophysical expression of the tectonic blocks and plutons in southern and western Afghanistan.

Each chapter is intended to be a scientific paper on its own, and these chapters are currently in various stages of preparation for journal publication. Chapter A on the central San Luis Basin has received approval for publication by the U.S. Geological Survey, and will shortly receive final approval from the Geological Society of America for publication in a Special Paper on the Rio Grande rift. Chapter B, on the San Juan Mountains batholith, is close to being ready for review. A publication based on Chapter C, on the tectonics of western and southern Afghanistan, is still in preparation.

Chapter A: Geophysical Constraints on Rio Grande Rift Structure in the Central San Luis Basin, Colorado and New Mexico

ABSTRACT

Interpretation of gravity and aeromagnetic data reveals patterns of rifting, rift-sediment thicknesses, distribution of pre-rift volcanic and sedimentary rocks, and distribution of syn-rift volcanic rocks in the central San Luis Basin, the northernmost of the major basins that make up the Rio Grande rift. Rift-sediment thicknesses for the central San Luis Basin calculated using a three-dimensional gravity inversion indicate that syn-rift Santa Fe Group sediments have a maximum thickness of ~2 km in the Sanchez graben near the eastern margin of the basin along the central Sangre de Cristo fault zone. Under the Costilla Plains, thickness is estimated to reach ~1.3 km, although no independent thickness constraints exist, and a range of thicknesses of 600 m to 2 km are geophysically reasonable. Considerable ambiguity exists regarding what rocks may lie between the bottom of the Santa Fe Group sediments and Precambrian basement beneath the Costilla Plains, and the presence of Mesozoic and Paleozoic sedimentary rocks cannot be ruled out. The Santa Fe Group sediments also reach a thickness of nearly 1 km within the Monte Vista graben near the western basin margin along the San Juan Mountains. A narrow, north-south-trending structural high beneath San Pedro Mesa with about 2 km of positive relief with respect to the base of the Sanchez graben separates the graben from the structural depression beneath the Costilla Plains. Geophysical data provide new evidence that this high is rooted in the Precambrian basement. A structural high composed of pre-rift rocks, long inferred to extend from under the San Luis Hills to

the Taos Plateau, is confirmed and found to be denser than previously believed, with little or no overlying Santa Fe Group sediments. Major faults in the study area are delineated by geophysical data and models; these faults include significant vertical offsets (≥ 1 km) of Precambrian rocks along the central and southern zones of the Sangre de Cristo fault system. Other faults with similarly large offsets of the Santa Fe Group include a fault bounding the western margin of San Pedro Mesa, and other faults that bound the Monte Vista graben in an area previously assumed to be a simple hinge zone at the western edge of the San Luis Basin. A major north-south-trending structure interpreted to be a down-to-the-east normal fault or fault zone occurs at the boundary between the Costilla Plains and the San Luis Hills structural high and is shown in our gravity modeling. This fault does not have much expression as a major rift fault; it is likely related to pre-rift tectonic events. Aeromagnetic anomalies are interpreted to mainly reflect variations of remanent magnetic polarity and burial depth of the 5.3-3.7 Ma Servilleta basalt of the Taos Plateau volcanic field. Magnetic-source depth estimates indicate patterns of subsidence following eruption of the basalt and show that the Sanchez graben has been the site of maximum subsidence.

INTRODUCTION

The San Luis Basin is the northernmost of the major basins that comprise the Rio Grande rift, extending for roughly 250 km north-south through south-central Colorado and northern New Mexico. The present-day geomorphic basin is bounded on the west by the San Juan Mountains and volcanic field in Colorado and the Tusas Mountains in New Mexico, and on the east by the Sangre de Cristo Mountains (Fig. A1). The central

portion of the San Luis Basin is loosely defined as the region that includes an eastward-offset embayment in the Sangre de Cristo range, the Culebra reentrant (Upson, 1939; Wallace, 2004), the San Luis Hills, Costilla Plains, San Pedro Mesa, the narrow valley coincident with the Sanchez graben between San Pedro Mesa and the Culebra Range, and the region lying between the San Luis Hills and San Juan Mountains to the west (Figs. A1& A2). The general subsurface geometry of the central portion of the basin is poorly understood, although the surface geology is well constrained by recent mapping (e.g., Thompson and Machette, 1989; Kirkham, 2004; Thompson et al., 2007a; Machette et al., 2008).

This study uses recently acquired gravity and aeromagnetic geophysical datasets, along with geologic map data and subsurface constraints derived from interpreted drill hole logs, to interpret the configuration of tectonic elements present along an east-west transect through a portion of the central San Luis Basin. The main goal of this study is to determine how the Rio Grande rift is manifested within the central San Luis Basin, including the following specific goals: to estimate the thickness of rift-fill sediments that are critical hosts of groundwater supplies (Topper et al., 2003); to determine what the rift-sediment thickness distribution indicates about basin structure and temporal pattern of rifting; to evaluate the distribution of syn-rift volcanic rocks and implications for the history of rifting; to interpret the extent and structural configuration of pre-rift rocks and their relationship to the rift; and to better delineate rift-bounding structures than surface geologic mapping is able to do.

GEOLOGIC BACKGROUND

The region occupied by the San Luis Basin has been structurally and topographically high for much of its history from the Paleozoic to the Late Eocene, spanning the Ancestral Rocky Mountain and Laramide orogenies. Subsequent extension associated with continental rifting occurred along much of the uplifted orogen (Sales, 1983; Kellogg, 1999; Kluth, 2007). Like most of the southern Rocky Mountain region, the area currently underlain by the San Luis Basin was occupied by middle-Tertiary volcanic rocks of the southern Rocky Mountain volcanic field (Steven, 1975; Lipman, 2007). Extension of the central San Luis Basin began ~28-25 Ma, following eruption of the uppermost ash-flow tuffs of the San Juan volcanic field (Lipman, 1975a, b; Lipman and Mehnert, 1975; Thompson and Dungan, 1985; Thompson and Machette, 1989; Thompson et al., 1991; Lipman, 2007) In some areas of the basin, the Santa Fe Group lies directly on Precambrian basement, whereas much of the central and western portion of the basin includes a thick section of Oligocene volcanic rocks between the Santa Fe Group and Precambrian basement rocks.

Faults generally trend along directions similar to preexisting north-northwest-trending Precambrian faults, a pattern reflected in basin-margin and intra-basin faults and structures (Tweto, 1979a, b). The general structure of the basin is commonly considered to be an east-tilted half graben, with a hinge zone along its margin with the San Juan Mountains, a major north-south-trending normal fault system bounding its eastern margin with the Sangre de Cristo Mountains, and a north-south-trending structural high through the basin center (e.g., Tweto, 1979b). This simplistic picture is more complicated in the central San Luis Basin, where deformation along the margin of the Sangre de Cristo

Mountains has formed the Culebra reentrant (Fig. A1), and San Pedro Mesa represents a secondary intra-rift structural high.

The Sangre de Cristo fault system forms the eastern tectonic boundary of the entire San Luis Basin and is divided into northern, central, and southern zones (Personius and Machette, 1984; Ruleman and Machette, 2007). The southern portion of the central zone occurs in the study area along the margin between the Culebra Range and Sanchez graben (Fig. A2), and has a relatively gentle geomorphologic expression that suggests a lower slip rate compared to the northern and southern zones and/or the fact that the footwall of the fault is underlain by basin-fill sediments (Ruleman and Machette, 2007). The northern portion of the southern Sangre de Cristo fault zone forms the western boundary of San Pedro Mesa. Offset along the fault increases to the south into New Mexico, where a sharp range front fault is evident south of the village of Costilla. The down-to-west Mesita fault (Thompson et al., 2007b), synthetic to the southern Sangre de Cristo fault zone, trends north-south through the central Costilla Plains (Fig. A2), although offset is only about 13 m at the surface.

Precambrian igneous and metamorphic rocks, mainly granitic/gneissic in composition, form the western portion of the Culebra Range and are bounded on the west by the central Sangre de Cristo fault zone. A recently mapped outcrop of Precambrian rock lies near the western margin of San Pedro Mesa (Fig. A2) (Kirkham, 2006; Thompson et al., 2007a), where the basin floor was previously assumed to have little or no relief (e.g., Keller et al., 1984). Magnetotelluric soundings provided the first indication that this outcrop was rooted at depth (B. Rodriguez, personal comm., 2006), showing that significant relief of Precambrian rock is present below the mesa. A

borehole in the southern Sanchez graben, the Williamson well (Fig. A2) (Kirkham et al., 2005; Thompson et al., 2007a), reached Precambrian rocks at a depth of 1.9 km, where they are directly overlain by Santa Fe Group sediments. No additional Precambrian rock crops out or has been encountered in boreholes in the study area west of San Pedro Mesa.

Because the study area has been structurally and topographically high during much of its geologic history, little or no Paleozoic or Mesozoic rocks have been thought to remain in the study area (e.g. Brister and Gries, 1994). While this is likely the case in the Sanchez graben, as demonstrated by drilling, the presence of Mesozoic and possibly Paleozoic rocks (Shirley, 1995; Watkins et al., 1995; Morel and Watkins, 1997; Hoy and Ridgway, 2002) in the northern San Luis Basin (outside the study area) suggests that these rocks may exist at depth within the study area under the Costilla Plains. Younger pre-rift sedimentary rocks, such as Eocene sediments, may also exist in significant thicknesses under the Costilla Plains but do not exceed 10 m in thickness where they crop out on the margin of San Pedro Mesa (Thompson et al., 2007a).

As much as 600 m of Oligocene volcanic rocks crop out in the San Luis Hills (Thompson and Machette, 1989; Thompson et al., 1991) and likely form much of the lower portion of the basin. These rocks are correlative with the 35-30 Ma Conejos Formation that makes up a portion of the San Juan volcanic field to the west; in the San Luis Hills these rocks include intermediate-composition lava flows and volcaniclastic sedimentary deposits as young as 29 Ma (R.A. Thompson, personal comm., 2008). The Conejos Formation is assumed to extend into the subsurface to the west, where it is a major basin-filling unit within the Monte Vista graben, a north-south-trending depocenter that extends far north of the study area and was mainly active prior to what is typically

considered Rio Grande rift extension (Brister and Gries, 1994). These rocks again reach the surface immediately west of the Monte Vista graben in the San Juan Mountains (included in rocks mapped as Tv, Fig. A2). The extent of the Conejos Formation in the subsurface under the Costilla Plains is unknown, although poor-quality seismic reflection data suggest that it may be present as an eastward-thinning package below Santa Fe Group sediments under at least a portion of the Costilla Plains (Uitti, 1980). However, it does not crop out on San Pedro Mesa (Thompson et al., 2007a) and was not encountered by the Williamson well in the Sanchez graben. Ash-flow tuffs, erupted from the San Juan and Latir (south of study area) volcanic fields (Lipman et al., 1986), are likely to overlie the Conejos Formation in much of the study area, although their thicknesses are unknown. Erosional topography that formed on the Conejos Formation between ~29 and ~26 Ma in the San Luis Hills area was partially filled by basalts of the Hinsdale Formation that now remain as mesa-capping outcrops (Dungan et al., 1989; Thompson and Machette, 1989). The Hinsdale basalts also crop out on southern San Pedro Mesa above another package of Tertiary volcanic rocks (Thompson et al., 2007a). These basalts are regionally dated 27 to 6 Ma, but are dated between 27 and 25 Ma in the San Luis Hills (Lipman and Mehnert, 1975; Thompson and Machette, 1989).

Intermediate composition intrusions crop out in the San Luis Hills (stars on Fig. A2, unit Tiq of Thompson and Machette, 1989) and correlate in age with the Conejos Formation, although their extent at depth is unknown. Other Oligocene intrusions crop out in the southern Rocky Mountain region (Lipman, 2007) and are typically associated with gravity lows (Plouff and Pakiser, 1972; Lipman, 1983; Cordell et al., 1985).

The San Luis Hills are a horst that is structurally high, composed of pre-rift rocks, and flanked by structural lows filled by rift sediments around its margin. The hills are part of a 150-200 km, north-south-trending, mostly buried horst that is thought to exist underneath the San Luis Valley (e.g., Keller et al., 1984; Grauch and Keller, 2004). Locally, the northwestern tectonic margin of the hills is inferred to be a concealed down-to-the-northwest fault (Tweto, 1979a, b), informally known as the Manassa fault (Fig. A2). Other faults have been inferred along the eastern margin of the San Luis Hills, in both a north-south zone along the Rio Grande and a northeast-southwest zone along the southern margin of the northeastern San Luis Hills (Burroughs, 1972; Tweto, 1979a, b; Thompson et al., 1991), although detailed geologic mapping (Thompson and Machette, 1989) did not include these structures since they have little or no surface expression.

Santa Fe Group sediments comprise the basin fill in the central San Luis Basin. Locally, in the transect area, these deposits post-date the youngest ash-flow tuffs from the southeastern San Juan volcanic field ($< \sim 28$ Ma) and are as young as mid-Pleistocene age (Ingersoll et al., 1990; Brister and Gries, 1994). Lithologies encountered in wells are primarily weakly to strongly consolidated claystone, sandstone, and conglomerate.

Interbedded with the uppermost Santa Fe Group sediments are numerous flows of the regionally extensive 5.3-3.7 Ma Servilleta basalt of the ~ 6 -2 Ma Taos Plateau volcanic field (Lipman and Mehnert, 1975; Lipman, 1979; Dungan et al., 1984; Dungan et al., 1989; Appelt, 1998). These flows are less than 200 m thick in the study area and generally less than 70 m thick (indicated by shallow borehole data, available from the Colorado Division of Water Resources).

Within the study area, basalt flows crop out along the northern Taos Plateau and on San Pedro Mesa. Multiple wells indicate that the basalt is shallowly buried (generally < 350 m, data available from Colorado Division of Water Resources) beneath the Costilla Plains. Total thicknesses range from approximately 200 m on the Taos Plateau, to ~140 m in the Sanchez graben (encountered in the Williamson well), to 30-65 m on San Pedro Mesa and beneath the Costilla Plains. Basalts of similar age crop out on the northeastern flank of Los Mogotes volcano (Fig. A2) (Lipman and Mehnert, 1975; Appelt, 1998). Other rocks associated with the Taos Plateau volcanic field include dacites that form large volcanic domes, such as Ute Mountain in the southern part of the study area (unit Td, Fig. A2).

GEOPHYSICAL DATA AND METHODS

GRAVITY METHODS

Gravity anomalies reflect lateral variations of density, with gravity highs occurring over regions of relatively high densities, such as mountains composed of crystalline basement, and gravity lows occurring over large volumes of low-density materials, such as unconsolidated sediments. Large density contrasts between low-density rift-filling sediments, such as the Santa Fe Group, and older rocks make gravity data useful for defining the configuration of basins within the Rio Grande rift (Cordell, 1978; Daggett et al., 1986; Grauch et al., 2006).

Regional quality (1-5 km station spacing) gravity data were extracted from the PACES gravity database that is maintained by the University of Texas at El Paso (<http://gis.utep.edu>) and supplemented with the acquisition of about 130 new stations in

the San Pedro Mesa-Culebra reentrant region during 2006 and 2007. The PACES database consists of data collected over decades by many previous workers and was compiled as the result of a major cooperative effort between federal agencies and universities (Keller et al., 2006). Standard techniques (e.g., Blakely, 1995) were used to process the gravity data and calculate complete Bouguer anomalies, including corrections for predicted gravitational attraction at the elevation and latitude of the observation point (theoretical and free air corrections), effects of homogeneous masses underneath (Bouguer correction), and effects of topographic masses (terrain corrections). The standard reduction density of 2670 kg/m^3 (Hinze, 2003) was used for the Bouguer and terrain corrections. An additional step of computing isostatic residual anomalies was performed, in order to remove the effect of long-wavelength anomalies that correlate with regional topography. This method is only one possible way of removing a regional field and results in a gravity anomaly map (Fig. A3) that is a better representation of upper-crustal density variations than a more standard complete Bouguer anomaly map (Simpson et al., 1986; Blakely, 1995). Computation of isostatic residual anomalies requires estimates of crustal thickness and Moho density contrast, but these values do not need to be accurate to yield useful results. Estimates of these parameters resulting from a lengthy investigation for gravity data for the state of New Mexico (Heywood, 1992) were used in this study, including a Moho density contrast of 300 kg/m^3 and a normal (assuming ground surface at sea level) crustal thickness of 20 km.

Previous three-dimensional gravity models of the San Luis Basin (Keller et al., 1984) facilitated mapping of major tectonic elements and thickness of the Santa Fe Group. However, this work assumed a single density contrast (350 kg/m^3) between the

Santa Fe Group and older rocks, and had limited data in several key areas where new data have since been acquired.

For this study we implemented a more sophisticated approach to determine basin geometry: an inverse method that attempts to separate the gravitational effect of the low-density Santa Fe Group sediments from that of older, denser rocks (Jachens and Moring, 1990; Blakely and Jachens, 1991; Blakely, 1995). Unlike other basin-depth estimation methods, this approach allows user-defined density-depth functions for the basin fill while also accommodating density variations of the pre-rift rocks. The method includes the following steps. First, an initial approximation for the gravity field caused by the pre-rift rocks is computed from only those gravity stations located on outcrops of those rocks and then is subtracted from the isostatic residual gravity anomaly field. The result is a crude approximation of the gravity field due to variations in the thickness of the Santa Fe Group alone. This residual field was inverted for sediment thickness using a density-depth function (Fig. A4) estimated from well logs in the Albuquerque and Española Basins to the south and assumed to be valid for the northern Rio Grande rift (Grauch et al., 2006). The inversion is based on a method that assumes the basin extends infinitely laterally and iteratively solves for basin depths (Bott, 1960; Blakely, 1995). Next, the calculated gravitational effect of the resulting Santa Fe Group thickness distribution was subtracted from the isostatic residual field at the pre-rift gravity stations, in order to produce an improved estimate of the gravity field of all pre-rift rocks. The entire process is iteratively repeated until the difference between observed and calculated thicknesses becomes minimal. Results include a gravity map due to all pre-Santa Fe Group (pre-rift) rocks (Fig. A5), thickness distribution of Santa Fe Group deposits (Fig. A5), and a

structural elevation on the base of the Santa Fe Group computed by subtracting the thickness distribution from the surface topography (Fig. A6). Constraints on the depth to the bottom of the Santa Fe Group for the inversion came from mapped locations of older rocks (places where the Santa Fe Group thickness is zero) (Tweto, 1979a; Green, 1992; Anderson and Jones, 1994; Green and Jones, 1997; Thompson et al., 2007a), interpretations of drilling records (HRS Water Consultants, 1987; Brister, 1990; Kirkham et al., 2005), and results of seismic reflection surveys (Gries and Brister, 1989).

The presence of Servilleta basalt within the basin may lead to errors in estimates of Santa Fe Group thickness, particularly in areas where the volume of the basalt is large relative to the size of the basin (locations where basalt thicknesses exceed ~100 m, Santa Fe Group thicknesses are less than 1 km, and no borehole or seismic constraints exist). However, the relatively small volume of the basalt compared to the volume of the basin in most of the study area corresponds to a small error (< 6%) in the final computed depths. The basalts have densities of about 2700 kg/m³ (M. Anderson, Colorado College, personal comm., 2008) and displace densities of 2170 kg/m³ in the upper 1.25 km of sediments. The difference in assumed mass leads to incorrect Santa Fe Group thickness estimates where no independent thickness constraints are placed on the model. This effect may have led to an underestimation of the thickness of the Santa Fe Group beneath the Taos Plateau, where basalt thicknesses reach 200 m and few independent constraints exist on the depth to the base of the Santa Fe Group.

MAGNETIC METHODS

Magnetic anomalies reflect spatial variations of total magnetization, the vector sum of induced and remanent magnetizations. Induced magnetization, an instantaneous property, is proportional to magnetic susceptibility and has the same direction as the present-day ambient field (inclination of 64 degrees, declination of 10 degrees in the study area). Remanent magnetization is a long-lived property, is related to a rock's formation and geologic history, and may be directed in a different direction than the induced magnetization. Volcanic rocks commonly carry large-magnitude components of remanent magnetization. In regions with near-surface volcanic rocks and locally high topographic relief, magnetic anomalies can be produced in several different ways, depending on rock magnetic properties, volume and depth of the rock unit, and relation to topography. In this study area, magnetic lows can be sourced by reversely polarized, highly magnetic rocks (generally represented by relatively large-magnitude magnetic lows), weakly magnetized rocks (commonly represented by subtle, broad lows), or terrain and/or anomaly shape effects such as topographically low areas surrounded by or adjacent to normally magnetized topography. Magnetic anomaly highs can alternatively be interpreted as caused by normally magnetized rocks, magnetic rocks with induced magnetization that is much greater than the remanent magnetization, or topographically low areas surrounded by or adjacent to reversely magnetized topography. Terrain and anomaly shape effects can be particularly well developed along edges of magnetic rock units, such as truncated basalt flows that compose topography. Linear changes in magnetic patterns may also be caused by source edges, such as basalt flows offset by faulting or linear paleotopography.

Data from three high-resolution (200 meter flightline spacing, 150 m above the ground) total-field aeromagnetic surveys acquired during 2003-2005 were draped to a surface 100 m above the ground and merged to create an aeromagnetic map of the study area (Bankey et al., 2004; Bankey et al., 2005; Bankey et al., 2006). A reduction-to-pole transformation, a standard geophysical technique to center anomalies over their sources, was applied to the aeromagnetic data using an inclination of 64 degrees and declination of 10 degrees (Fig. A7) (Baranov and Naudy, 1964; Blakely, 1995). Identification of strongly or weakly magnetized terrain and identification of correlations between outcropping rock units and aeromagnetic anomalies is best done by careful inspection of these relations in map view. An example is presented here, using a larger scale view of the southern San Luis Hills that combines reduced-to-pole aeromagnetic anomalies, terrain, and mapped geology (Fig. A8). There, Hinsdale basalt and Conejos Formation rocks form individual topographic features, and aeromagnetic anomalies are well correlated positively with outcrop boundaries, indicating that the terrain is moderately to strongly magnetized and that the magnetization directions are close to the ambient field direction.

The geophysical expression of relatively deep and/or broad geologic sources can be enhanced by filtering anomalies according to wavelength, since deep/broad sources produce longer wavelength anomalies than do surficial sources. Here, we applied a low-pass filter with a 5 km filter cutoff to the reduced-to-pole aeromagnetic anomalies in order to isolate anomalies broader than the short wavelengths observed over individual topographic features in the San Luis Hills (Fig. A9), and thereby removed anomalies clearly related to terrain and surface geology.

Quantitative estimates of depth to magnetic sources help facilitate geologic interpretation by differentiating shallow from deep sources, allowing delineation of different tectonic patterns. Unlike the low-pass filter approach to separating deep from shallow sources, these calculations provide direct estimates of source depth beneath the ground surface. Numerous depth estimation techniques exist, and for this study we chose to use the local wavenumber method, since this method has been shown to be effective for aeromagnetic datasets (such as this one) with low noise levels (Thurston and Smith, 1997; Smith et al., 1998; Phillips, 2000, 2007; Phillips et al., 2007). In this approach, spatial derivatives of the measured magnetic field are related to the depth of magnetic sources, resulting in a distribution of depth estimates (Fig. A10). These results indicate the estimated depth to the top of the shallowest magnetic sources, which may be strongly magnetized rocks that crop out (such as basalt on the surface of San Pedro Mesa) or are buried (such as basalts buried in the Sanchez graben).

GEOPHYSICAL EXPRESSION OF GEOLOGIC FEATURES

The San Luis Basin is expressed geophysically by a north-south trending gravity low that reflects the relatively low density of the Santa Fe Group sediments compared to the Precambrian basement (Cordell, 1978). Within this trend is a gravity high trending north-south through the area north of Alamosa coincident with a buried intra-rift horst (Gaca and Karig, 1966; Keller et al., 1984; Kluth and Schaftenaar, 1994). The gravity high also continues south of Alamosa over the San Luis Hills and into New Mexico, where a structural high has long been inferred (Lipman, 1979; Grauch and Keller, 2004). The following section discusses the geophysical characteristics of the main tectonic

features present within the central San Luis Basin and key results of geophysical data analyses.

Culebra Range and Eastern Basin Boundary

The eastern boundary of the San Luis Basin in the study area is geologically defined by the central Sangre de Cristo fault zone, and geophysically by the gradient that separates a gravity high on the east from a gravity low on the west (Fig. A3). The gravity low west of the fault zone is caused by thick, low-density Santa Fe Group sediments in the Sanchez graben. The gravity high is caused by higher-density Precambrian rocks.

The gravity high over the Culebra Range is not as large as the high caused by pre-rift rocks within the basin to the west over the San Luis Hills (Fig. A3). The high gravity values over the Culebra Range decrease to the south, with the lowest values observed in northern New Mexico (Fig. A3). Two possible explanations exist for such low gravity values over Precambrian rocks. The first is that during the Laramide orogeny, Precambrian rocks of the modern Sangre de Cristo range were thrust over Cretaceous and Tertiary sedimentary rocks of the Raton Basin east of the study area, so that the low-density sedimentary rocks now lie under Precambrian crystalline rocks that form the high mountains (Trevino et al., 2004). This is supported by recent mapping of the eastern Culebra Range that demonstrates that the scenario is spatially/geometrically reasonable (Fridrich and Kirkham, 2007). Another possibility is that a silicic intrusion or series of intrusions within the Culebra Range are less dense than the Precambrian country rocks, causing the low gravity values. Silicic intrusions in the region are mainly Precambrian or Tertiary in age and have been interpreted to be sources for gravity lows elsewhere in the

Sangre de Cristo Mountains (Cordell and Keller, 1984; Cordell et al., 1985; Grauch and Keller, 2004; Quezada et al., 2004).

San Pedro Mesa-Sanchez graben

Recent gravity data acquisition for this study revealed a ~12 mGal gravity high over the west-central portion of San Pedro Mesa (SPM, Fig. A3), with the highest anomaly amplitude located over the newly discovered outcrop of Precambrian basement rock. The southern Sangre de Cristo fault zone bounds this anomaly on the west (Ruleman and Machette, 2007; Thompson et al., 2007a). Relatively high gravity values trend south near the western edge of San Pedro Mesa into New Mexico, merging with a high over the Sangre de Cristo Mountains near Costilla where Precambrian rocks crop out (SDC on Fig. A3). North of the San Pedro Mesa basement outcrop (SPM and north of SPM on Fig. A3), gravity values decrease and merge with lower amplitude, broader gravity anomalies over the northern Sanchez graben and the town of San Luis. Gravity values smoothly decrease to a greater extent to the east of the basement outcrop on San Pedro Mesa, until a low is reached over the southern Sanchez graben (SG), where Precambrian rocks were encountered at a depth of 1.9 km in the Williamson well. These observations are consistent with the hypothesis developed from magnetotelluric soundings that the Precambrian basement outcrop on San Pedro Mesa is rooted and is not a detached fragment from a previous orogeny underlain by low-density sediments (see profile model section below).

The interpretation of rooted basement under San Pedro Mesa was built into the gravity inversion by forcing the basement to reach the surface at the outcrop location, with the result being a north-south-trending basement high along the western margin of

the mesa (Fig. A6). The deepest portion of the Sanchez graben lies just north of the Colorado-New Mexico state border. A broad, relatively shallow area of the basin occurs beneath the northern Sanchez graben and the town of San Luis (SL). The inversion results also show that vertical displacement on north-south-trending faults bounding both east and west sides of San Pedro Mesa decreases to the north.

Aeromagnetic anomalies over San Pedro Mesa display a complex pattern of short-wavelength, often high-amplitude highs and lows (Fig. A7). This is a common aeromagnetic anomaly signature over basalts. Paleomagnetic measurements of oriented core samples of basalt along the mesa show the presence of both normal and reverse polarities of remanent magnetization (M. Hudson, personal comm., 2007), which explains the alternating normal-reverse anomaly signature observed along the mesa edge. Landslide blocks immediately below the western edge of the mesa include large slabs of Servilleta basalt, producing complex north-south-trending aeromagnetic highs and lows that lie adjacent to the southern Sangre de Cristo fault zone.

Aeromagnetic anomalies tend to be more subdued over the Sanchez graben and the area around San Luis, indicating deeper sources. The Williamson well places Servilleta basalt flows at a depth of about 270 m in the southern Sanchez graben. Anomaly sources throughout the remainder of the graben are interpreted as being buried basalt.

Magnetic-source depth estimates (Fig. A10) indicate shallow (< 350 m) depths over San Pedro Mesa and the basalt-capped mesa northwest of San Luis, reflecting the effect of shallowly buried and outcropping basalts. Zones of relatively deep (>450 m) solutions include most of the southern Sanchez graben, as well as two smaller zones

south and north of San Luis. Some of these zones are bounded by recently mapped faults that cross the graben along a northwest-southeast trend (near label SG, Fig. A10) (Thompson et al., 2007a).

Costilla Plains

The Costilla Plains are expressed geophysically by a broad gravity low reflecting a large thickness of Santa Fe Group sediments, bounded on the west and east by gravity highs associated with the San Luis Hills and San Pedro Mesa, respectively (Fig. A3). Along the western margin of San Pedro Mesa, a gravity gradient tracks the location of the southern Sangre de Cristo fault zone, reflecting shallow basement to the east and deep basement to the west. A larger magnitude gradient trends north-south along the western margin of the low, near the Rio Grande, with gravity values increasing to the west where pre-rift rocks crop out in the San Luis Hills (see following paragraphs). The broad gravity low over the Costilla Plains reaches its lowest values along the state border and into Sunshine Valley (SV on Fig. A3).

The north-south-trending gravity gradient corresponding roughly to the location of the Rio Grande, with high values west of the river and low values to the east, indicates a fundamental difference in the composition and/or structure of pre-rift rocks from the southern San Luis Hills area to the Costilla Plains. The north-south trend of the gradient as expressed in the pre-rift gravity map (Fig. A5) is consistent with pre-rift tectonic patterns observed throughout the San Luis Basin region (Tweto, 1979b) and suggests that pre-rift tectonics may have influenced the formation of the western boundary of the Costilla Plains. An alternative hypothesis is that the gradient is reflective of a major syn-

rift fault, although there is little surface evidence for such a structure (e.g., Thompson and Machette, 1989).

In order to address this question, end-member models of the possible source of the gravity gradient were tested using the gravity inversion. The thickness of Santa Fe Group sediments under the Costilla Plains has been interpreted to reach a maximum of about 2 km, on the basis of poor-quality seismic reflection data (Uitti, 1980), which would support the hypothesis that the gradient reflects a major syn-rift fault. The first test used the seismic reflection estimate to represent the maximum possible thickness of the Santa Fe Group, emphasizing the hypothesized syn-rift effect of the N-S trending gravity gradient. The second test forced the pre-rift gravity field under the Costilla Plains to be similar to the gravity field over the northeastern San Luis Hills (see following section), which had the effect of producing a minimum Santa Fe Group thickness and emphasizing the pre-rift effect of the gravity gradient. The second test resulted in a maximum thickness of only 500 m for the Santa Fe Group, contrasted to the ~2 km estimated from seismic data, which we consider to be a maximum reasonable thickness. Given the large uncertainty of the seismic interpretation and the lack of surficial evidence for a major syn-rift fault along the Rio Grande, we chose to present a compromise model that was not constrained by the seismic reflection interpretation, assigned a significant portion of the Rio Grande gravity gradient to the pre-rift field, and produced a maximum Santa Fe Group thickness of 1.3 km, with the greatest thickness under the southern Costilla Plains (Fig. A5).

Structural offset along the southern Sangre de Cristo fault zone is estimated from the inversion results to be 500 m to 1 km, with offset increasing to the south. A

northwest-trending splay of this fault zone off the northern end of San Pedro Mesa (CP1 on Fig. A6) is also reflected in the inversion results, as a down-to-the-southwest normal fault with an approximate offset of 300-400 m. Another north-south-trending structural offset (CP2 on Fig. A6) about 6 km west of the western edge of San Pedro Mesa is most clearly apparent near the state border, but can be extended to a total length of ~16 km using the gravity inversion results (dashed white line, Fig. A6). This offset bounds the most depressed portion of the Costilla Plains structural low and corresponds to the location of down-to-the-west normal faults mapped near the state border (CP2). The western boundary of the structural low is bounded by the down-to-west Mesita fault (Fig. A6) that has about 13 m of displacement, an inconsistent relation that may indicate the fault has been reactivated from an earlier down-to-east normal fault.

The southwestern structural boundary of the Costilla Plains is indicated to be a broad fault zone or ramp along a north-northwest trend in the area of Ute Mountain along which the basin structure narrows to the south into Sunshine Valley, although independent constraints are lacking in this region. Ute Mountain is the site of a data artifact in the inversion results (Fig. A6), where subtraction of the thickness distribution from the surface topography failed to remove the entire effect of Ute Mountain. In other words, this should *not* be taken as an indication that a structural high exists beneath Ute Mountain.

The aeromagnetic map (Fig. A7) displays a similar pattern of short-wavelength anomalies over the Costilla Plains as the one over San Pedro Mesa. The anomaly patterns probably reflect Servilleta basalt buried at a shallow depth beneath sediments. Near the western edge of San Pedro Mesa, anomalies appear to follow the trends of

nearby anomalies caused by alternating remanent polarities of basalt exposed on the mesa, suggesting lateral continuity of basalt flows across the southern Sangre de Cristo fault zone into the Costilla Plains subsurface. The anomaly patterns over the entire Costilla Plains may also be explained by alternating remanent polarities of basalts within the basin fill, but this interpretation is tentative due to lack of exposure. Linear anomalies in the aeromagnetic map (Fig. A7) coincide with the trace of the Mesita fault as well as faults exposed in the southeastern portion of the Costilla Plains, likely indicating where faults offset basalt. A profound change in anomaly character also occurs across the Mesita fault, with high values to the east and low values to the west (Fig. A7). This may be an expression of an important geologic boundary, such as an extension of Conejos Formation rocks into the subsurface from the west. Another possibility is that the Mesita fault has in the past been a more important structure than it is today (only showing ~13 m of offset), and that emplacement of Servilleta basalt was affected by the fault. This could have resulted in different individual flows with different magnetic properties being present on either side of the fault.

Depth estimates show that basalts beneath the Costilla Plains are generally buried at depths of less than 350 m (Fig. A10). Water well logs from the area typically show multiple stacked flows of variable thickness (and possibly different magnetic properties) separated by sediments. The tops of the uppermost basalt flows are generally less than 350 m deep, and individual flows may be as much as 10-15 m thick. Conspicuous zones of deeper solutions exist along the southwestern portion of the fault that splays northwest off the north end of San Pedro Mesa (Fig. A10), as well as along the southern portion of

the Costilla Plains into Sunshine Valley. Seismic reflection data also indicate that the Servilleta basalt deepens near the latitude of Ute Mountain (Uitti, 1980).

San Luis Hills and Northern Taos Plateau

A broad, high-amplitude gravity high lies over the San Luis Hills and the northern Taos Plateau volcanic field (Fig. A3). Based on the significant exposures of pre-rift volcanic rocks in these areas, this anomaly has long been interpreted as reflecting a mid-basin structural high (Gaca and Karig, 1966; Keller et al., 1984; Grauch and Keller, 2004). The gravitational effect of pre-rift rocks (Fig. A5) suggests that the highest gravity values in the study area are over the San Luis Hills west of the Rio Grande in a broadly north-south orientation. A significant gravity low in the signature of pre-rift rocks exists over the northeastern San Luis Hills, implying a large difference in densities between the volumes of rocks that underlie the northeastern and western portions of the hills. The source of this low is unknown, but it may be due to relatively thick pre-rift sediments and/or sedimentary rocks, a low-density igneous intrusion of Oligocene age(?), or low-density rocks within the Precambrian basement. Inversion results also show that the structural high associated with the San Luis Hills extends to the south and west under the northern Taos Plateau with little or no (<200 m) Santa Fe Group present beneath Servilleta basalt (Fig. A6). Structures bounding the San Luis Hills include the fault zone or ramp bordering the Costilla Plains (discussed above), as well as a zone of deepening along the northwestern margin of the San Luis Hills that corresponds to the approximately located Manassa fault.

Aeromagnetic anomalies over the Taos Plateau have a similar short-wavelength character to those observed elsewhere over exposed and inferred Servilleta basalt. A

large-amplitude aeromagnetic low over Ute Mountain is likely caused by reversely polarized volcanic rocks that form the mountain. The circular anomaly resembles similar ones over individual volcanoes and vents in the Taos Plateau south of the study area, where paleomagnetic and radiometric dating evidence supports the presence of strong remanent magnetizations of both normal and reverse polarities (Grauch and Keller, 2004).

The San Luis Hills have a different geophysical character than surrounding regions covered by Servilleta basalt, and the aeromagnetic anomalies over the hills reflect a pattern of strongly magnetized topography. Hinsdale basalt caps high ridges and produces strong (> 1000 nT) positive aeromagnetic anomalies that mimic the pattern of the topography, suggesting that the basalts are dominantly normally polarized (Figs. A7 & A8). Much lower anomaly amplitudes (up to hundreds of nT) are observed over outcrops of the Conejos Formation, and relationships between aeromagnetic anomalies and topography indicate that these rocks are mainly normally polarized in the San Hills west of the Rio Grande, and mainly reversely polarized in the northeastern hills. The areas of different polarity generally correspond to different stratigraphic levels within the Conejos Formation, with normally polarized rocks corresponding to the lower Conejos Formation west of the river, and reversely polarized rocks to the east of the river corresponding to the upper Conejos Formation. This relation implies that ages of the rocks span at least one reversal of the Earth's field.

On the western side of the San Luis Hills, anomaly patterns corresponding to areas of outcropping volcanic rocks extend well beyond those outcrops, in a complex pattern of broadly east-west-trending anomalies (Figs. A7 & A8). Because cliff

exposures show that Hinsdale basalts were erupted onto a deeply incised surface cut into the Conejos rocks (Thompson and Machette, 1989), we hypothesize that the east-west-trending anomalies reflect buried paleotopography in the areas that are covered. The sources of east-west-trending lows could be channels cut into normally polarized units of the Conejos Formation that are now filled with weakly magnetized sediments or with younger, reversely polarized volcanic flows.

The anomaly patterns extending west of the San Luis Hills gradually become broader and more subdued, reflecting deeper sources. This effect is demonstrated quantitatively by predominantly greater source depth estimates in a ~10-km-wide, north-northeast-trending zone west of the San Luis Hills (Fig. A10) that corresponds to the Manassa fault as defined by the gravity inversion (Fig. A6).

A broad, sub-circular, composite aeromagnetic high >400 nT in amplitude occurs over the southern San Luis Hills (Fig. A7 & outlined on Fig. A9). At 15-20 km in diameter, this anomaly is much broader than the dominant wavelengths of anomalies related to terrain, apparent on the long-wavelength filtered map (Fig. A9). As discussed above, relatively broad anomalies reflect relatively deep and/or broad sources. Also, magnetic depth estimates include a number of deep (>450 m) solutions in this area, which may be related to the anomaly's source. Therefore, we interpret the source of this anomaly to be a buried, strongly magnetized body with the approximate dimensions of the anomaly itself, as shown on Fig. A9. This interpretation is discussed in detail below.

Monte Vista Graben and Western Basin Boundary

The Monte Vista graben in the study area lies about 50 km south of where it is well defined by seismic and borehole data northwest of Alamosa (Brister and Gries,

1994). A ~15 mGal, north-south-trending isostatic gravity low extends south into the study area, suggesting that the structures lie along a similar trend and are likely related. Thus, the name Monte Vista graben is used here.

Gravity inversion results indicate a graben with a significant thickness of Santa Fe Group sediments (Figs. A5 & A6). The western edge of the graben represents the western boundary of the San Luis Basin with the San Juan volcanic field. The abrupt structural relief imaged there suggests that this may be a fault zone, contrary to previous interpretations (e.g., Tweto, 1979b) that this is a hinge zone with unfaulted San Juan volcanic rocks dipping gently into the western San Luis Basin. The eastern boundary of the graben (MVGEB, Fig. A6) occurs along an abrupt northeast-trending margin of the structural high associated with the San Luis Hills and Taos Plateau that is similar in trend although not directly aligned with the inferred Manassa fault trend. To the south, a structural high along the state border bounds the deeper portion of the graben, although due south in New Mexico the extreme northern portion of another structural low is imaged (Fig. A6).

Aeromagnetic anomalies and depth estimates over the inferred graben are typical of outcropping or shallowly buried basalt flows, and correlate with Servilleta-like basalt flows that extend north and northeast from the Los Mogotes volcano (Figs. A2, A7, & A10). These flows overlie the inferred graben and extend into the subsurface beyond the northern edge of their outcrop, indicated by a pattern of short-wavelength aeromagnetic anomalies and shallow depth estimates.

PROFILE MODEL

In order to display the interpreted geologic relationships in a more quantitative manner, a 2.5D gravity and magnetic model along profile A-A' (Figs. A3 & A11) was constructed using the results of the gravity inversion as a starting point and well data, outcrop locations, magnetotelluric modeling (Drenth et al., in prep.), and magnetic source depth estimates as constraints (using GM-SYS software, www.geosoft.com). The gravity and magnetic model's location was chosen to most effectively capture the main tectonic features in the study area (Figs. A2 & A3). The following sections discuss details of the construction of the model and interpretation of the final model.

Model Construction and Geophysical Properties

Because the Precambrian rocks likely cause the largest and broadest variations in the pre-rift gravity effect (Fig. A11a) and their densities are unknown, the first step was to construct an equivalent density model for the Precambrian basement. The equivalent model serves as a proxy to compute and remove the broad basement effects and focus on other geologic units represented by the profile model. The equivalent basement model was constructed by assigning variable densities to vertically bounded zones that are 8 km thick until the gravity field was matched (Fig. A11d). The densities of other pre-rift rocks, such as the Conejos Formation, were not allowed to vary across the profile.

The second step was to develop the geometry of the base of the Santa Fe Group. The results of the gravity inversion (Fig. A6) provided a robust first approximation to the Santa Fe Group thickness (inverted from “rift basin effect” curve, Fig. A11a), and subsequent adjustments to the model resulted in only small differences (<10%) between the inversion results and the final model (Fig. A11d). The minor adjustments account for

thickness/depth constraints from magnetotelluric data (Drenth et al., in prep.), outcrop locations, and wells, and provided a good fit to the observed gravity profile.

The final step was to develop a model of geologic units above the basement that honored all independent constraints on depths, unit thicknesses, and physical properties. Physical rock properties (summarized in Table 1) assigned to the specific units in the model were based on unpublished field and lab measurements, published averages based on lithology (Telford et al., 1990), and fits to the model. The Conejos Formation is an example of the latter case; density logs in San Juan volcanic field (San Juan Mountains) indicate that an overall average density for the Conejos Formation is about 2500 kg/m³ (R. Gries, written comm., 2007), yet there, the unit is mainly composed of andesite flows. In the San Luis Basin, the Conejos Formation includes a significant proportion of volcanoclastic deposits that are likely to have lower densities than andesite. In the course of profile modeling it was found that a density of 2500 kg/m³ made a proper fit difficult while still honoring well constraints and the gravity inversion results. For these reasons, a density of 2400 kg/m³ was used because it produced a better fit to the observed data.

No independent constraints exist on the depth to the bottom of the Santa Fe Group sediments or to what lies under these sediments beneath the Costilla Plains, and therefore considerable uncertainty exists. The Conejos Formation, pre-rift Tertiary sedimentary rocks, or Mesozoic or Paleozoic sedimentary rocks have similar densities and cannot be distinguished on the basis of gravity modeling. These pre-rift units have likely densities ranging from 2400-2600 kg/m³, and a possible thickness distribution for them was found using an averaged density of 2500 kg/m³ (Fig. A11d, “unknown pre-rift volcanic/sedimentary rocks”).

The Santa Fe Group was modeled using the assumed density-depth function discussed above (Fig. A4), although only the upper two density zones were needed for the depths encountered along the profile. As discussed above, greater and lesser thicknesses of the Santa Fe Group were tested using the 3D inversion in order to determine geophysically reasonable end-members of thicknesses, specifically under the Costilla Plains. The model shown (Fig. A11d) is our preferred model, although different thicknesses were tested in 2D, as well as in part of the magnetotelluric modeling (Drenth et al., in prep.). No magnetic properties were assigned to these sediments. Despite measured magnetic susceptibilities on the order of 1 to 10×10^{-3} (SI units) for sediments in this and other Rio Grande rift basins (Grauch et al., 2001; Grauch and Hudson, 2007; Hudson et al., 2008), wavelengths of the aeromagnetic anomalies modeled are more regional at the profile model scale and are dominantly produced by volcanic/crystalline rocks.

Basalts are present in most of the study area, have high densities, and are strongly magnetized. Although massive basalts often have densities near 3000 kg/m^3 (Telford et al., 1990), samples of the Servilleta basalt have measured densities of about 2700 kg/m^3 (M. Anderson, personal comm., 2008). Densities have not been measured on the Hinsdale basalts but were also assigned a density of 2700 kg/m^3 . Oriented samples of Servilleta basalt were collected on San Pedro Mesa and yielded remanent intensities of 1-8 A/m in both normal and reverse polarities, with intensities varying considerably over short distances (M. Hudson, personal comm., 2007). Magnetic susceptibilities also vary considerably for these basalt samples, and a typical value of 0.015 SI units was used in the model. The Hinsdale basalt has high measured magnetic susceptibilities, although the

remanences of the basalt and similar rocks are not known. However, inspection of anomalies compared to geology and topography suggests the Hinsdale basalt is normally polarized nearly everywhere in the study area and almost certainly carries some remanence. Therefore, a very high susceptibility (0.1 SI units) was used in the model to simulate the combined effect of both the high susceptibility and normal polarity remanence.

Interpretation of Gravity-Magnetic Model (A-A')

Given the setup of the model along A-A', the interpretation of the preferred model follows. The part of the model representing Precambrian rocks is an equivalent model and is required to fit low gravity values over the Culebra Range and high values over the San Luis Hills. Accordingly, the lowest densities occur at the eastern portion of the profile and, as discussed above may represent the effect of overthrust, low-density sedimentary rocks at depth and/or a low-density intrusion in the Culebra Range. The model presented here includes low densities in the Culebra Range, and is not meant to endorse one case over the other. The highest densities of the Precambrian equivalent model occur underneath the structural high associated with the San Luis Hills and northern Taos Plateau volcanic field, although these density variations may also occur in pre-rift rocks younger than Precambrian age.

About 2 km of relief is interpreted for the Precambrian rocks between the base of the Sanchez graben and the outcrop on top of San Pedro Mesa, and is fairly well-constrained as discussed previously. This impressive, asymmetric basement ridge has an extremely steep western margin that lies roughly 1 km east of the trace of the southern Sangre de Cristo fault zone, suggesting that the fault zone is or has been wider at depth

than its current surface expression. The eastern margin of the basement high is only slightly less precipitous, plunging from the surface near the western rim of San Pedro Mesa to a depth of more than 1 km beneath its eastern rim. Independent constraints on depth to Precambrian basement in the study area are unavailable west of the outcrop on San Pedro Mesa. The model as drawn (Fig. A11d) indicates basement at nearly the shallowest levels possible, constrained by deep wells in the San Luis Hills area that do not reach basement.

Maximum thicknesses of the Santa Fe Group under the entire Costilla Plains and in the Sanchez graben are interpreted to be 1.3 and 2 km, respectively. The structural high of Precambrian rocks under San Pedro Mesa forms a prominent boundary separating the two grabens. Areas where sharp changes occur in Santa Fe Group thickness correlate well with mapped fault zones, including the central and southern Sangre de Cristo fault zones and the fault bounding the eastern margin of San Pedro Mesa (Thompson et al., 2007a). The western margin of the Costilla Plains has long been thought to be controlled by a fault (Tweto, 1979a), but no direct evidence for faulting has been found on the surface. However, the model indicates that a fault zone or ramp marks the boundary between the San Luis Hills and Costilla Plains, roughly coincident with the Rio Grande. We believe the most reasonable explanation is that these inferred structures form a zone of down-to-the-east normal faults. The timing of movement on these faults, however, is difficult to determine, given the uncertainties of what lies beneath the Santa Fe Group under the Costilla Plains.

As much as 800 m of Santa Fe Group sediments are interpreted to lie within the Monte Vista graben. The large structural offsets bounding the graben can be interpreted

as fault-controlled, contrary to the assumption that the San Luis Basin's western margin is a simple hinge zone with little structural relief.

The thicknesses, lateral extents, and dips of post-Precambrian pre-rift rocks shown in the model are only crude approximations at best, since they are not well constrained within the study area. These include Eocene and possibly Mesozoic and/or Paleozoic sedimentary rocks that may exist in the Monte Vista graben (Bristler and Gries, 1994) and that may be present under the Conejos Formation in the western San Luis Hills as suggested by borehole data. The presence of these rocks, as well as Conejos Formation and ash-flow tuffs of the San Juan volcanic field, cannot be ruled out beneath the Costilla Plains. Units that lie above Precambrian basement and pre-date Santa Fe Group rocks and sediments do not crop out on or east of San Pedro Mesa.

Aeromagnetic anomalies along the profile are well explained by variations in magnetic properties and burial depths of volcanic rocks, primarily the Servilleta basalt in most of the study area. The approximate burial depth and thickness of the basalt within the Sanchez graben are approximately known from the Williamson well 5 km south of the profile and are consistent with magnetic depth estimates. In the Sanchez graben a normal polarity was assigned to the basalt (N1, Fig. A11d), with the magnitude varied until the observed aeromagnetic anomaly was matched (1 A/m was required). A similar approach was used for the basalt that crops out on the surface of San Pedro Mesa, although there a reverse polarity signature was interpreted (R1, 4 A/m). The burial depth of basalt beneath the Costilla Plains is well known from water well logs, but the total thickness is not definitively known. The basalt is thought to be confined to the uppermost sedimentary section there, with a total thickness of roughly 70 m; we assumed

this geometry for the model across the Costilla Plains. Immediately west of San Pedro Mesa, an aeromagnetic low is interpreted to reflect dominantly reversely polarized basalt (R2, 8 A/m) that may be laterally correlative with basalt on the mesa having the same polarity signature. An area of higher aeromagnetic values to the west is interpreted to be a zone of mainly normally polarized basalt (N2, 3 A/m). Extending this alternating polarity approach west, however, is not attempted beyond assigning a reverse polarity (R3, 5 A/m) to basalt beneath the Costilla Plains, because the magnetic properties of the Sevilleta basalt are not constrained beyond San Pedro Mesa, resulting in the progressive failure of the model to match anomalies there. Andesites and dacites of San Pedro Mesa do not appear to be strongly magnetized nor do they appear to produce gravity anomalies, although the gravity station coverage over these rocks may not be adequate. Therefore, it is difficult to model their subsurface extent or to conclusively determine whether they are underlain by Santa Fe Group sediments or rest directly on Precambrian rocks. Based on the density assigned to these rocks in the profile model (2400 kg/m^3 , based on their lithology) and the limited available gravity data, it would appear that the andesites and dacites are underlain by Santa Fe Group sediments.

The Conejos Formation is likely to have strongly heterogeneous magnetic properties, given that it is volcanic (thus likely to be strongly magnetized) and volcanoclastic (likely to be weakly to moderately magnetized). The geometry of these variations, however, is not known, and the unit is modeled as having uniform properties. As discussed above, exposed Conejos Formation near the profile has mainly normal polarity (west of the Rio Grande). It is difficult to capture the geometry of the interpreted east-west-trending paleotopography of the San Luis Hills using an east-west profile,

although the inclusion in the model of Hinsdale basalt in the shallow subsurface provides a fit to some of the short-wavelength aeromagnetic anomalies over the hills.

Two strongly magnetized, shallowly buried bodies under the San Luis Hills (labeled “Intrusions?” on Fig. A11d) were included to provide a possible interpretation for longer-wavelength anomalies over the San Luis Hills. These inferred bodies do not produce a gravity low, unlike many Oligocene intrusions in the southern Rocky Mountain region. Precambrian rocks were assigned moderate magnetic susceptibilities as needed to account for the longest-wavelength trends along the profile.

DISCUSSION

Computed thickness variations of the Santa Fe Group sediments may indicate patterns of rifting over time, provided that simplifying assumptions are made about the geology. These assumptions include: the deepest Santa Fe Group sediments in the study area correspond to areas involved in rifting since its inception (28-25 Ma), dips within the Santa Fe Group are sub-horizontal, sediment supply has been constant throughout the history of rifting, computed Santa Fe Group thickness is an effective proxy for the amount of subsidence, and the Servilleta basalt (5.3-3.7 Ma) is consistent enough in age across the study area to make it a robust time horizon. The thickness of the Santa Fe Group representing the time interval from inception of rifting to the eruption of Servilleta basalt is greater in the Sanchez graben (1.2 km) than under the Costilla Plains (up to 900 m in the preferred model), suggesting that the greatest subsidence occurred close to the margin of the Culebra Range. The same time interval accounts for the ~1 km of sedimentation/subsidence in the Monte Vista graben. Rift-related subsidence appears to

have followed a similar pattern since or during emplacement of the Servilleta basalt, as indicated by a greater thickness of basalt and overlying Santa Fe Group sediments in the Sanchez graben compared to other portions of the study area. This is also expressed in the magnetic depth estimates as relatively deep solutions within the Sanchez graben (Fig. A10).

The gravity inversion and profile model provide a new perspective on faulting patterns within the central San Luis Basin (Figs. A6, A11d, & A12). The western boundary of the basin has long been assumed to be a simple hinge zone at the margin of the San Juan Mountains. However, large structural offsets are noted at the boundaries of the Monte Vista graben and are interpreted to be fault zones. The eastern boundary of the Monte Vista graben is shown to be at least partially controlled by the Manassa fault. Published maps show differing interpretations of the boundary between the San Luis Hills and Costilla Plains, with Tweto (1979 a,b) showing fault zones and Thompson and Machette (1989) omitting them due to a lack of surface expression. Results of modeling indicate that a significant fault zone or structural ramp does exist along the eastern margin of the San Luis Hills that has displaced the Costilla Plains downward. Geophysical observations and interpretations along this structure or set of structures include the following: (1) it is the location of a major gradient in the gravity field of pre-rift rocks (Fig. A5), (2) it forms the western and northwestern boundary of the Costilla Plains structural depression as shown by the gravity inversion results (Figs. A6 and A12), and (3) it may offset pre-rift rocks (Fig. A11d). Modeling further suggests that the offset along this structure may be greater for pre-rift rocks than for the Santa Fe Group (Fig. A11e), suggesting a long-lived structure possibly inherited from earlier tectonism that

had significant offset prior to rifting, relatively minor offset during formation of the rift, and is no longer active today. The western boundary of the structural depression beneath the Costilla Plains is gentler, with thinner Santa Fe Group sediments, than its eastern margin (Fig. A11d) along San Pedro Mesa and the active southern Sangre de Cristo fault zone. These observations are consistent with the western depression margin being less active throughout the history of rifting than the eastern margin. Other faults under the Costilla Plains may be responsible for the thickness variations of the Santa Fe Group sediments, including faults with recent offsets such as the Mesita fault and other faults near the western margin of San Pedro Mesa (Fig. A6). Both the central and southern zones of the Sangre de Cristo fault system, as well as the fault or fault zone that bounds San Pedro Mesa on the east, are shown by gravity modeling to be major structures (Figs. A6, A11d).

A broad (15-20 km diameter) aeromagnetic high over the southern San Luis Hills is interpreted to be produced by a buried source (Fig. A12). The anomaly only partially correlates spatially with the gravity high over the San Luis Hills (Figs. A5 & A7) and occurs over a much smaller area. The source may be an Oligocene intrusion or intrusive complex related to the pre-rift volcanic rocks in the overlying hills. In this scenario, a candidate for the material that composes the intrusion is unit Tiq of Thompson and Machette (1989), which forms a number of small outcropping intrusions of intermediate composition in the southern San Luis Hills (stars, Fig. A2) and displays moderately high magnetic susceptibilities (0.005-0.030 SI units, V. Grauch, unpublished data, 2006). Unlike other Oligocene intrusions in the southern Rocky Mountains, however, this body does not produce a gravity low. Another possibility is that the source is a relatively

strongly magnetized zone within heterogeneous Precambrian rocks, perhaps mafic or ultramafic rocks. In this scenario, the source rocks may be related to the source of the gravity high over the San Luis Hills (Fig. A5).

The north-south-trending Precambrian basement structural high that underlies western San Pedro Mesa is interpreted to have ~2 km of relief from the basement in the Sanchez graben, as indicated by borehole information from the Williamson well. Units that lie above Precambrian basement and pre-date Santa Fe Group sediments do not crop out on or east of San Pedro Mesa, indicating that the structural high underneath the mesa may have already been present when rifting began. Volcanic rocks older than Servilleta basalt on southeastern San Pedro Mesa, as well as those within the Sanchez graben, have not been found west of the mesa (e.g., Fig. A11d). Therefore, the structural high may have been a long-lived barrier separating the area that would become the Costilla Plains from the Sanchez graben, forming prior to rifting and remaining high throughout at least early stages of rifting.

CONCLUSIONS

Three-dimensional gravity inversion and modeling reveal new details of the spatial distribution of rift-sediment thicknesses within the central San Luis Basin, part of the northern Rio Grande rift, as summarized in Fig. A12. The structural depression beneath the Costilla Plains is interpreted to contain up to 1.3 km of Santa Fe Group sediments, although as little as 600 m and as much as 2 km are geophysically reasonable, with the greatest accumulation near the depression's eastern margin. The southern Sanchez graben contains about 2 km of Santa Fe Group sediments, and at the western

margin of the San Luis Basin, the Monte Vista graben is filled with up to ~1 km of Santa Fe Group. The greatest amount of rift-related subsidence apparently has been concentrated along the eastern margin of the basin adjacent to the Culebra Range, a pattern that appears to have intensified throughout the history of rifting. Areas of relatively thin sediments indicate areas of structural highs, including a narrow north-south-trending ridge of Precambrian basement rocks nearly completely buried beneath San Pedro Mesa that may be a long-lived structural high. A structural platform with <900 m of overlying sediments occurs under the northern Sanchez graben and the town of San Luis.

Modeling results show that the horst composed of pre-rift rocks exposed at the San Luis Hills extends under at least the northern Taos Plateau (Figs. A6 & A12). Less than 200 m of Santa Fe Group sediments are inferred to exist under the northern portion of the plateau. The gravity high over the San Luis Hills (Fig. A3) was thought to be due to the structural high there, although results presented here show not only a structural high but also high-density pre-rift rocks, consistent with speculation by Brister and Gries (1994).

Aeromagnetic anomalies over the Taos Plateau, Costilla Plains, San Pedro Mesa, and Sanchez graben largely reflect the burial depth and magnetic properties of the Servilleta basalt. Strongly magnetized terrain composed of Conejos Formation and Hinsdale basalt characterizes the San Luis Hills.

A number of features highlighted in this study deserve future investigation to improve our understanding of the geologic history of the central San Luis Basin. The distribution of pre-rift volcanic and sedimentary rocks under the Costilla Plains is highly

uncertain. Previous studies have implicitly or explicitly assumed that little or no Mesozoic/Paleozoic rocks exist there, but the presence of Mesozoic rocks in the northern San Luis Basin (e.g., Hoy and Ridgway, 2002) suggests that they may also exist under the Costilla Plains. The models and interpretations presented here do not rule out their presence. These rocks are currently being targeted for petroleum exploration in the northern San Luis Basin.

The origins of gravity anomalies caused by pre-rift rocks (Fig. A5) are largely unknown, other than the possibilities that the gravity low over the Culebra Range is produced by overthrust sediments and/or a low-density intrusion. The subsurface distribution of the Conejos Formation, as well as pre-rift sedimentary rocks, is not constrained. The gravity low over the northeastern San Luis Hills is noteworthy for its sub-circular extent and difference in character from the gravity high over the San Luis Hills west of the Rio Grande. The anomaly source may be a relatively thick accumulation of pre-rift sedimentary rocks, or may be magmatic in origin, such as an Oligocene intrusion.

Table A1: Geophysical characteristics of units in model A-A'

Unit	Density (kg/m ³)	Assigned magnetic susceptibility (range) (10 ⁻³ SI units)	Remanence intensity (relative where not measured)
Servilleta basalt and similar rocks	2700	15 (2-26)	1-8 A/m, normal and reverse polarities observed
Santa Fe Group	2170 and 2350	Assumed zero, possibly significant for local studies	Assumed none
Hinsdale basalt and similar rocks	2700	100 (assumed)	Not measured or modeled, but potentially very large (included in susceptibility value)
Andesite and dacite of San Pedro Mesa	2400	1 (0.001-6)	Likely small
Ash-flow tuffs of San Juan V.F.	2200	Volumetrically insignificant	Volumetrically insignificant
Conejos Formation	2400	30 (assumed)	Assumed small, but potentially large locally
Buried body under San Luis Hills (labeled Intrusions?, Fig. A11d)	2700	60 (assumed)	Likely small if intrusion, possibly important if Precambrian volcanic rocks
Eocene sedimentary rocks	2400	Assumed small	Assumed none
Cretaceous sedimentary rocks	2400-2600	Assumed small	Assumed none
Paleozoic sedimentary rocks	2600	Assumed small	Assumed none
Precambrian basement	Variable (arbitrary)	0-20 (assumed)	Assumed none

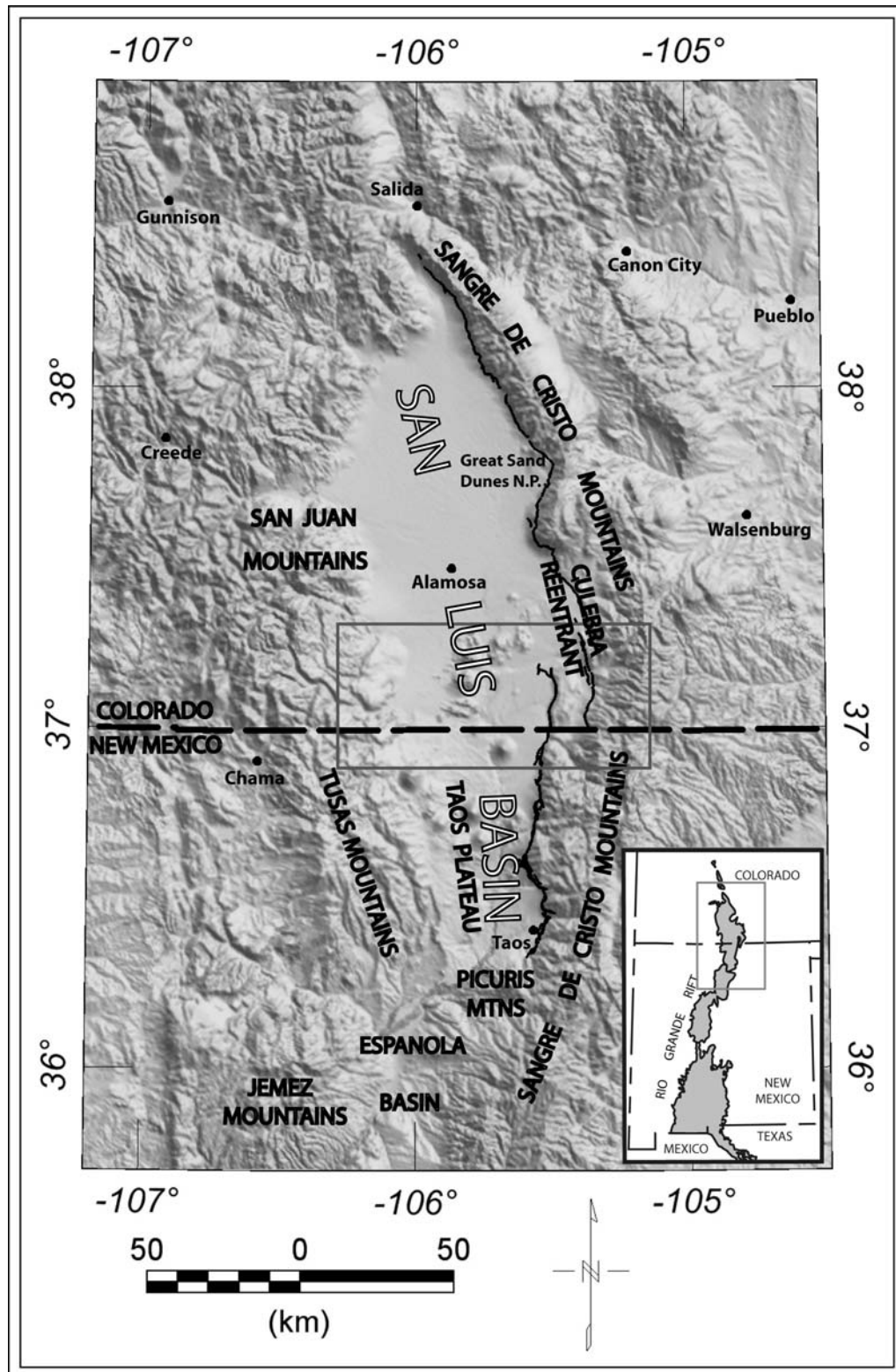
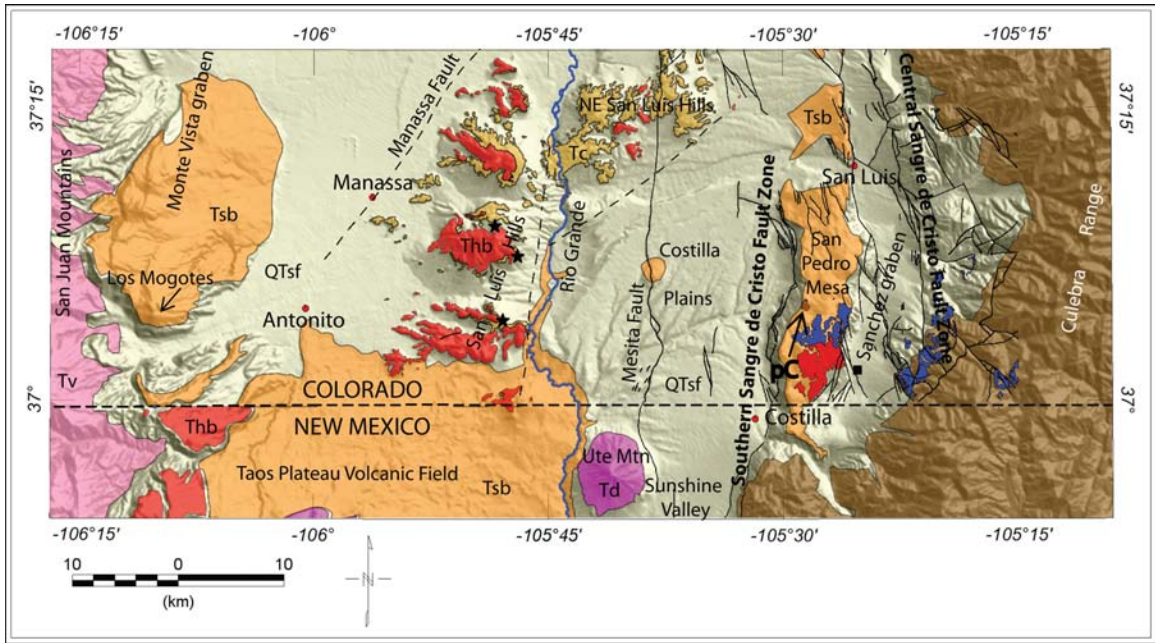


Figure A1: Physiography and geography of the San Luis basin. Gray box defines area of this study and subsequent figures. Inset map shows location of Fig. A1 in relation to the Rio Grande rift.



Explanation

SYN-RIFT UNITS		MID-TERTIARY VOLCANIC ROCKS		MISCELLANEOUS	
QTsf	Santa Fe Group and surficial deposits	■	andesite and dacite of San Pedro Mesa	■	Precambrian rocks
Tsb	Servilleta basalt and similar rocks	■	Volcanic rocks of San Juan volcanic field	- - -	fault, dashed where inferred
Td	dacite related to Taos Plateau	■	Tc Conejos Formation	—	river
Thb	Hinsdale basalt	★	Oligocene intrusions, San Luis Hills	■	Williamson well

Figure A2: Simplified geology and physiography of the study area (Burroughs, 1972; Lipman, 1975b; Tweto, 1979a; Lipman and Reed, 1989; Thompson and Machette, 1989; Green, 1992; Anderson and Jones, 1994; Thompson and Lipman, 1994; Green and Jones, 1997; Kirkham et al., 2004; Thompson et al., 2007a; Machette et al., 2008). Additional data from Machette and others, unpublished mapping; Thompson, unpublished Taos Plateau mapping.

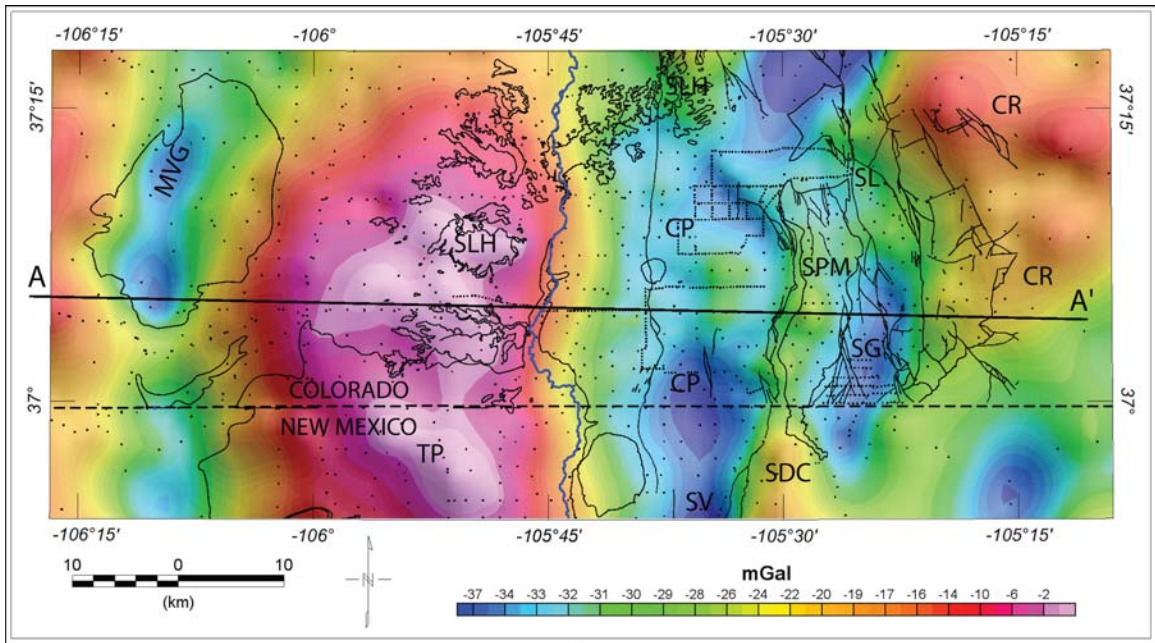


Figure A3: Isostatic residual gravity anomaly map of the study area. Selected linework from Fig. A2 included for reference. Black dots are gravity station locations. Inverted red triangles are locations of magnetotelluric (MT) soundings (Drenth et al., in prep.). Location of profile model A-A' shown. Labels: CR, Culebra Range; SDC, Sangre de Cristo Mountains; SL, San Luis; SG, Sanchez graben; SPM, San Pedro Mesa; CP, Costilla Plains; SV, Sunshine Valley; SLH, San Luis Hills; TP, Taos Plateau; MVG, Monte Vista graben.

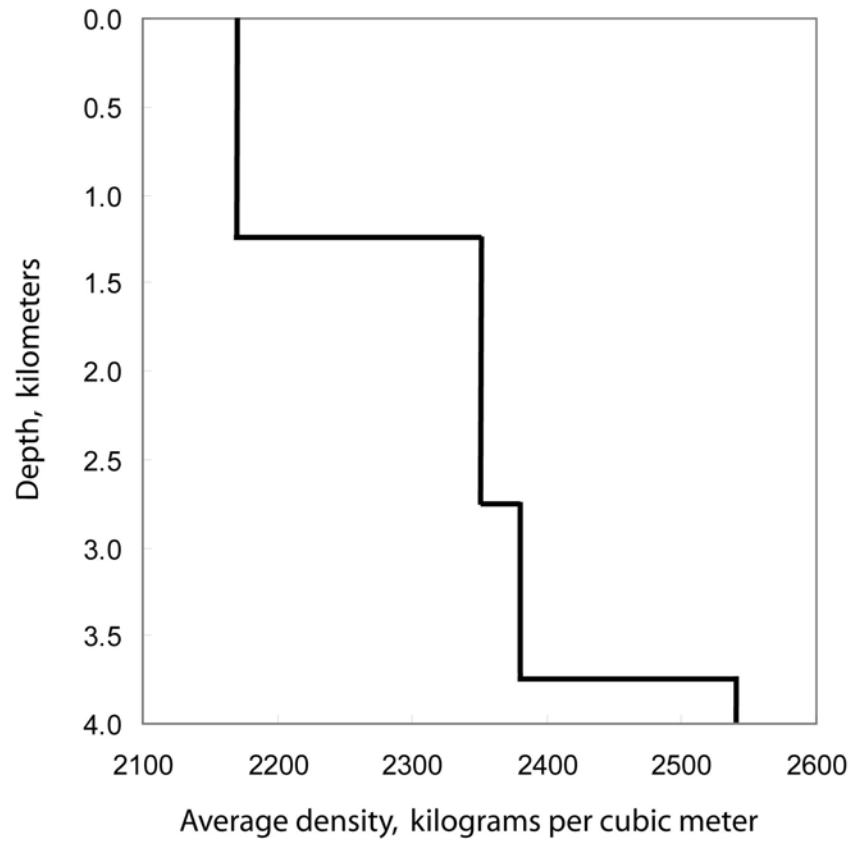


Figure A4: Density-depth function for Santa Fe Group rift sediments, from Grauch et al. (2006). Compare to Bouguer reduction density of 2670 kg/m^3 .

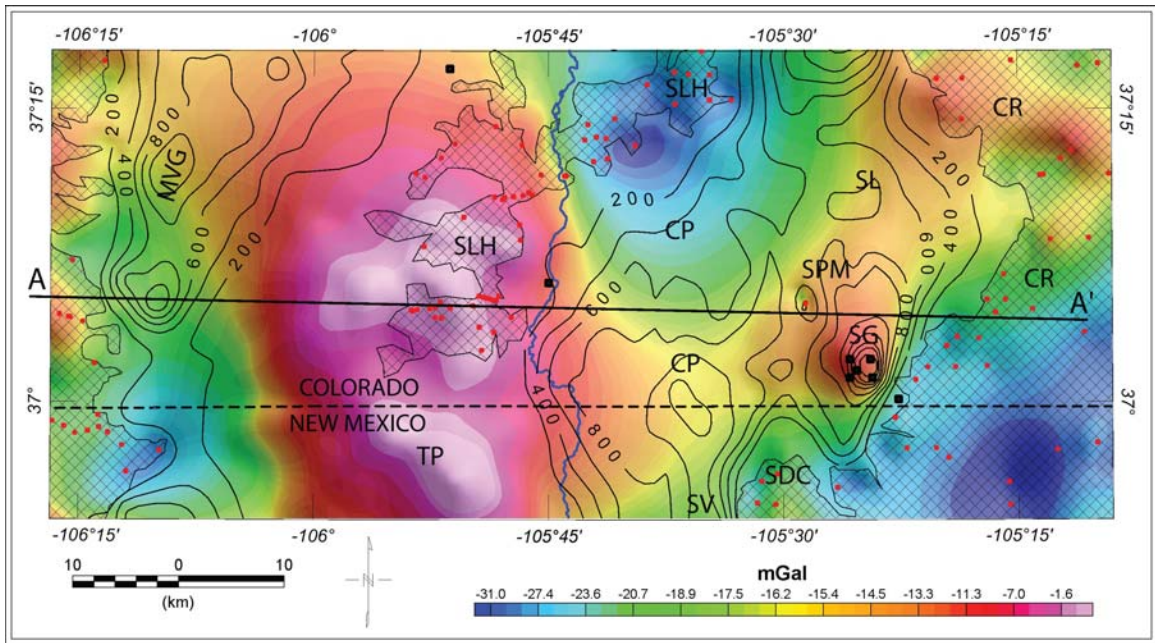


Figure A5: Gravitational effect of pre-rift (pre-Santa Fe Group) rocks, from 3-dimensional gravity inversion. Black squares are locations of well and seismic reflection constraints. Location of profile model A-A' shown. Red dots are gravity stations on pre-rift rocks; diagonal patterned areas are outcrops of pre-rift rocks. Contour lines show computed thickness of Santa Fe Group.

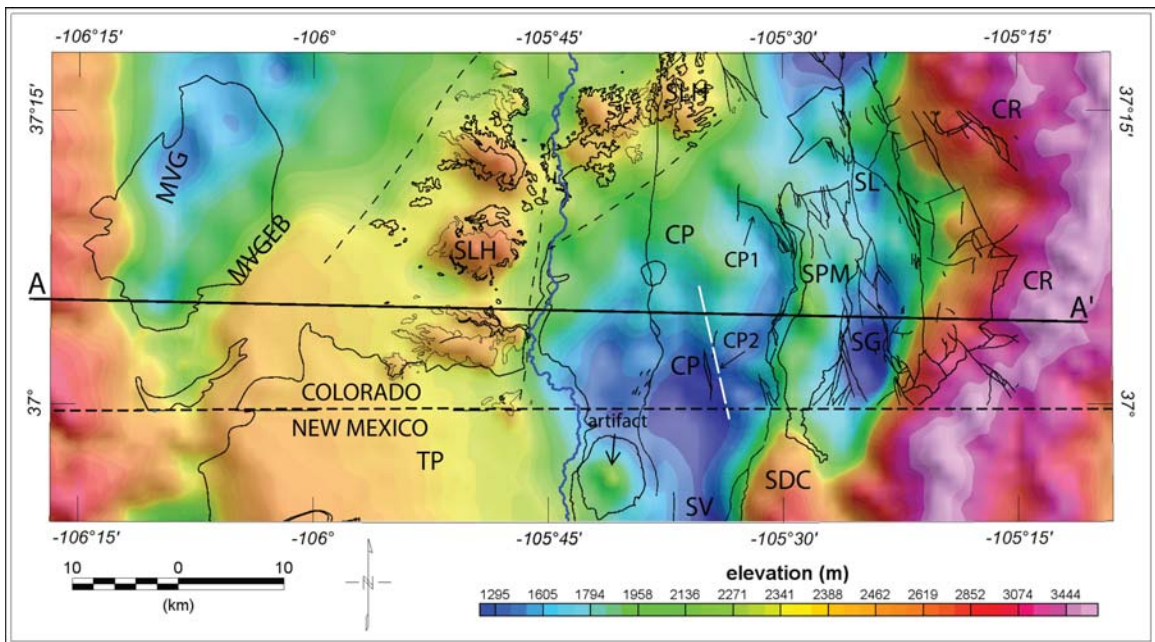


Figure A6: Elevation of the base of Santa Fe Group sediments, from 3-dimensional gravity inversion. Location of profile model A-A' shown. Additional labels: CP1, fault splay off northwest edge of San Pedro Mesa; CP2, structural boundary under Costilla Plains; MF1, possible southern extension of Mesita Fault.

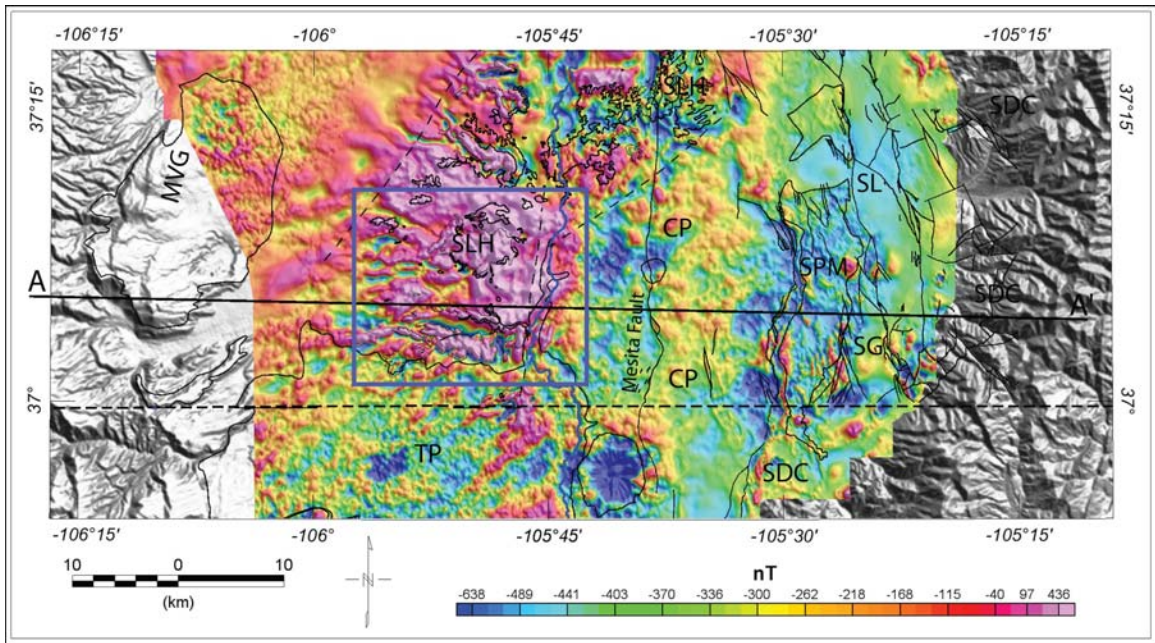


Figure A7: Reduced-to-pole aeromagnetic anomalies. Area of Fig. A8 shown by blue box. Location of profile model A-A' shown.

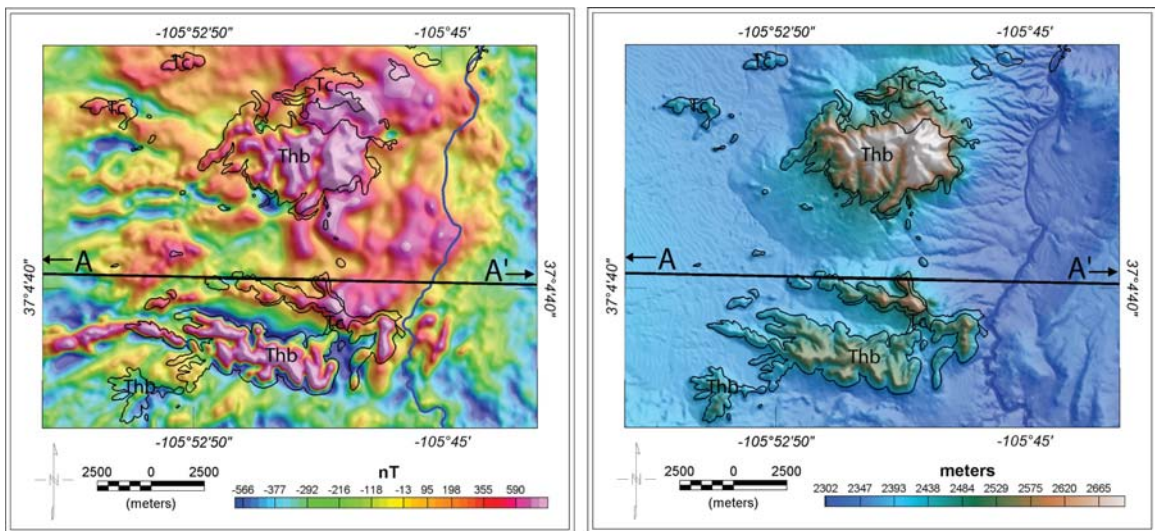


Figure A8: Reduced-to-pole aeromagnetic anomalies (left) and elevation (right) maps of the southern San Luis Hills. Outcrops of Conejos Formation (Tc) and Hinsdale basalt (Thb) shown.

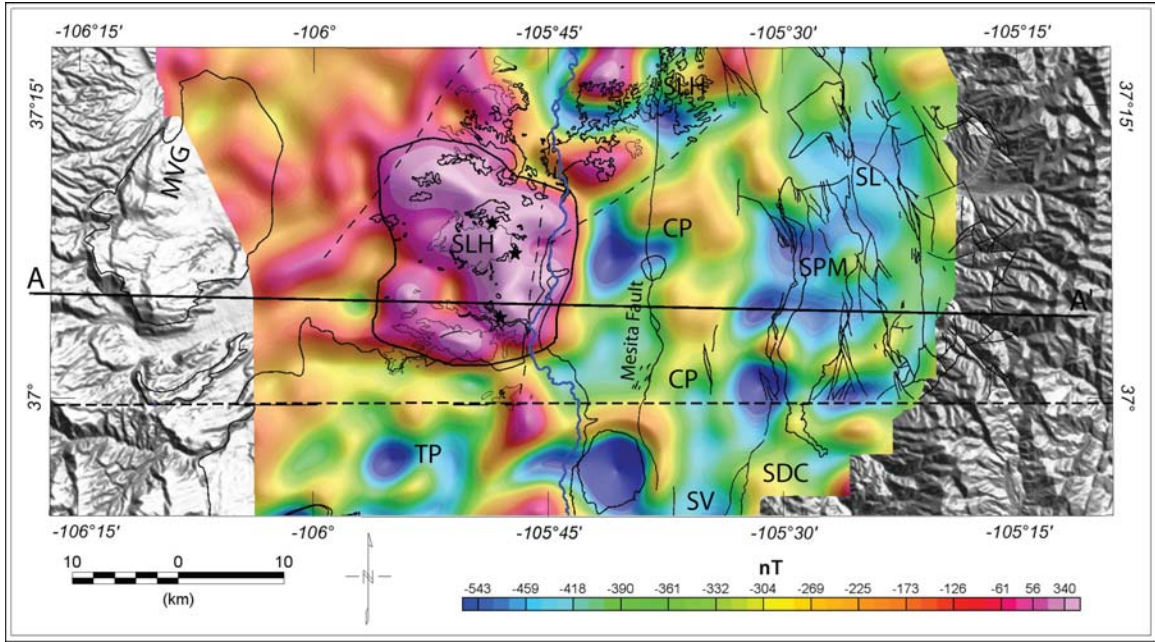


Figure A9: Filtered reduced-to-pole aeromagnetic anomalies, with wavelengths greater than 5 km retained. Stars indicate locations of Oligocene intrusions in San Luis Hills (see Fig. A2). Location of profile model A-A' shown.

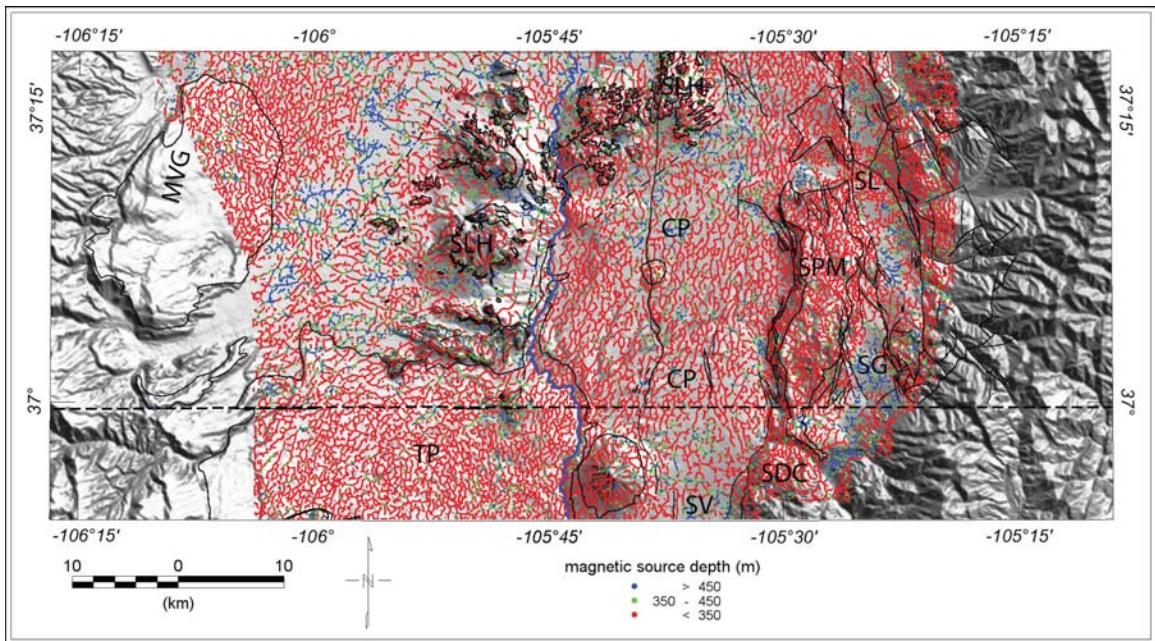


Figure A10: Estimates of depth to magnetic sources from the local wavenumber method (see text for references).

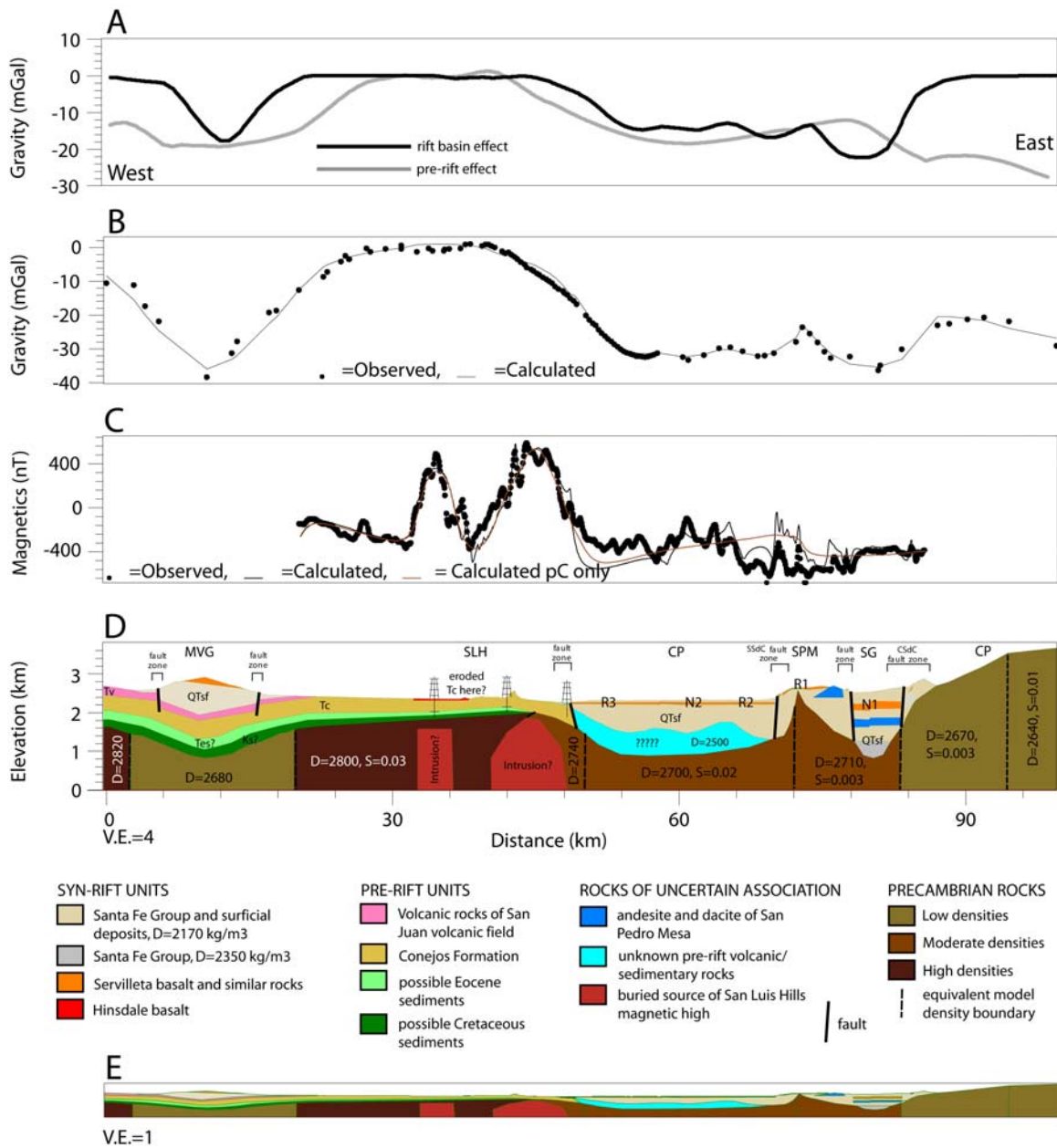


Figure A11: Geophysical profiles and model along A-A' (Fig. A3). A: Results of 3-dimensional gravity inversion, showing estimated effects of pre-rift rocks and basin geometry. B: Isostatic residual gravity anomalies (projected from within 2 km of profile location) with gravitational effect of geologic model. C: Reduced-to-pole aeromagnetic anomalies with response of geologic model. Brown line shows calculated response of Precambrian sources alone. D: Geologic model, vertically exaggerated 4 times. Densities in kg/m³ (D) and susceptibilities in SI units (S) shown for Precambrian rocks, properties of other units shown in Table 1. E: Geologic model, no vertical exaggeration.

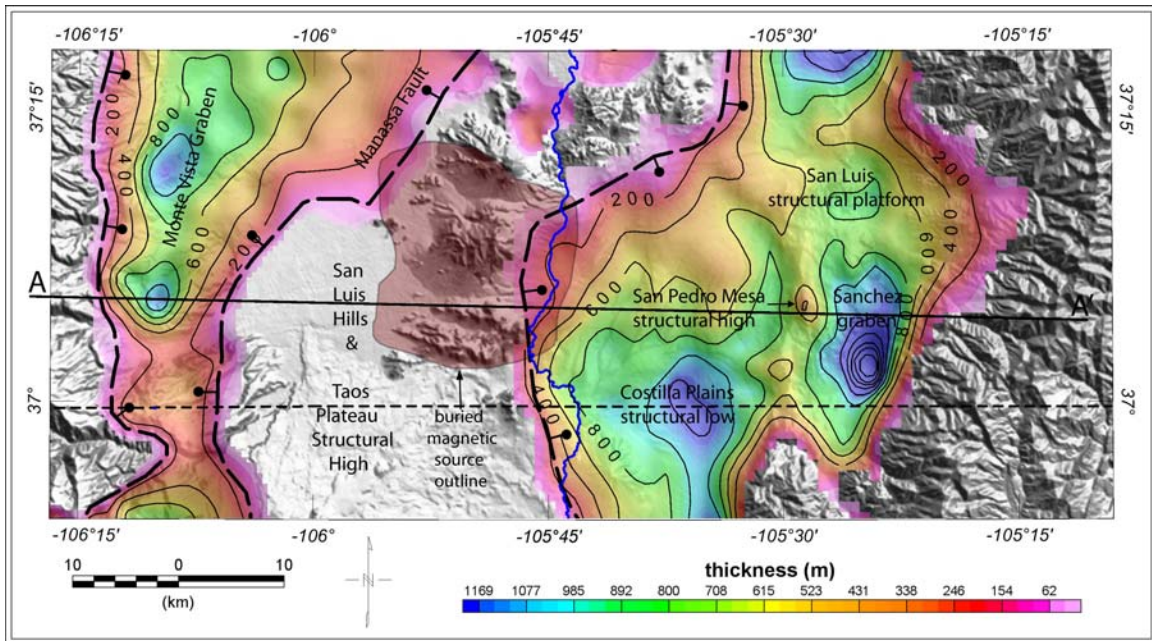


Figure A12: Summary of selected new geologic interpretations derived from geophysical data analysis. Colors and contours indicate estimated thickness of Santa Fe Group sediments from gravity inversion (CI = 200 m). Locations of inferred basin- and graben-bounding normal faults shown by dashed lines with ball on downthrown side.

REFERENCES

- Anderson, O.J., and Jones, G.E., 1994, Geologic Map of New Mexico: New Mexico Bureau of Mines and Mineral Resources, Open-file Report 408-A and B, Geologic map and 15 magnetic disks, 1:500,000 map.
- Appelt, R.M., 1998, $^{40}\text{Ar}/^{39}\text{Ar}$ geochronology and volcanic evolution of the Taos Plateau volcanic field, northern New Mexico and southern Colorado [Master's thesis]: Socorro, New Mexico Tech.
- Bankey, V., Grauch, V.J.S., and Corporation, F.A.S., 2004, Digital Aeromagnetic Data and Derivative Products from a Helicopter Survey over the Town of Blanca and Surrounding Areas, Alamosa and Costilla Counties, Colorado, U.S. Geological Survey Open-File Report 2004-1229-B.
- Bankey, V., Grauch, V.J.S., Drenth, B.J., and Geophex, L., 2006, Digital data from the Questa-San Luis and Santa Fe East helicopter magnetic surveys in Santa Fe and Taos Counties, New Mexico, and Costilla County, Colorado, U.S. Geological Survey Open-File Report 2006-1170.
- Bankey, V., Grauch, V.J.S., Webbers, A., and PRJ, I., 2005, Digital data and derivative products from a high-resolution aeromagnetic survey of the central San Luis basin, covering parts of Alamosa, Conejos, Costilla, and Rio Grande Counties, Colorado, and Taos County, New Mexico, U.S. Geological Survey Open-File Report 2005-1200.
- Baranov, V., and Naudy, H., 1964, Numerical calculation of the formula of reduction to the magnetic pole: *Geophysics*, v. 29, p. 67-79.
- Blakely, R.J., 1995, *Potential Theory in Gravity and Magnetic Applications*, Cambridge University Press, 441 p.
- Blakely, R.J., and Jachens, R.W., 1991, Regional study of mineral resources in Nevada-- Insights from three-dimensional analysis of gravity and magnetic anomalies: *Geological Society of America Bulletin*, v. 103, p. 795-803.

- Bott, M.H.P., 1960, The use of rapid digital computing methods for direct gravity interpretation of sedimentary basins: *Geophysical Journal of the Royal Astronomical Society*, v. 3, p. 63-67.
- Brister, B.S., 1990, Tertiary sedimentation and tectonics: San Juan sag-San Luis basin region, Colorado and New Mexico [Ph.D. thesis]: Socorro, New Mexico, New Mexico Institute of Mining and Technology.
- Brister, B.S., and Gries, R.R., 1994, Tertiary stratigraphy and tectonic development of the Alamosa basin (northern San Luis Basin), Rio Grande rift, south-central Colorado, *in* Keller, G.R., and Cather, S.M., eds., *Basins of the Rio Grande Rift: Structure, Stratigraphy, and Tectonic Setting*: Boulder, Geological Society of America Special Paper 291, p. 39-58.
- Burroughs, R.L., 1972, Geology of the San Luis Hills, south-central Colorado [Ph.D. thesis]: Albuquerque, University of New Mexico.
- Cordell, L., 1978, Regional geophysical setting of the Rio Grande rift: *Geological Society of America Bulletin*, v. 89, p. 1073-1090.
- Cordell, L., and Keller, G.R., 1984, Regional structural trends inferred from gravity and aeromagnetic data in the New Mexico-Colorado border region, New Mexico Geological Society Guidebook, 35th Field Conference, Rio Grande Rift: Northern New Mexico, p. 21-23.
- Cordell, L., Long, C.L., and Jones, D.W., 1985, Geophysical expression of the batholith beneath Questa caldera, New Mexico: *Journal of Geophysical Research*, v. 90, p. 11263-11269.
- Daggett, P.H., Keller, G.R., Morgan, P., and Wen, C.L., 1986, Structure of the southern Rio Grande rift from gravity interpretation: *Journal of Geophysical Research*, v. 91, p. 6157-6167.
- Drenth, B.J., Grauch, V.J.S., and Rodriguez, B.D., in prep., Geophysical Constraints on Rio Grande Rift Structure in the Central San Luis Basin, Colorado and New Mexico: Geological Society of America Special Paper.

- Dungan, M.A., Muehlberger, W.R., Leininger, L., Peterson, C., McMillan, N.J., G., G., Lindstrom, M., and Haskin, L., 1984, Volcanic and sedimentary stratigraphy of the Rio Grande Gorge and the late Cenozoic geologic evolution of the southeastern San Luis Valley, *in* Baldridge, W.S., Dickerson, P.W., Riecker, R.E., and Zidek, J., eds., New Mexico Geological Society Guidebook, 35th Field Conference, Rio Grande Rift: Northern New Mexico, p. 51-57.
- Dungan, M.A., Thompson, R.A., and Stormer, J.S., 1989, Rio Grande rift volcanism: northeastern Jemez zone, New Mexico, *in* Chapin, C.E., and Zidek, J., eds., Field excursions to volcanic terranes in the western United States, Volume 1: southern Rocky Mountain region: New Mexico Bureau of Mines and Mineral Resources Memoir 46, p. 435-486.
- Fridrich, C.J., and Kirkham, R.M., 2007, Preliminary Geologic Map of the Culebra Peak Area, Sangre de Cristo Mountains, Las Animas and Costilla Counties, Colorado: U.S. Geological Survey Open-File Report 2007-1428, 1:50,000 scale map.
- Gaca, J.R., and Karig, D.E., 1966, Gravity survey in the San Luis Valley area, Colorado, Colorado Geological Survey Open-File Report 66-46.
- Grauch, V.J.S., and Hudson, M.R., 2007, Guides to understanding the aeromagnetic expression of faults in sedimentary basins: lessons learned from the central Rio Grande rift, New Mexico: *Geosphere*, v. 3, p. 596-623.
- Grauch, V.J.S., Hudson, M.R., and Minor, S.A., 2001, Aeromagnetic expression of faults that offset basin fill, Albuquerque basin, New Mexico: *Geophysics*, v. 66, p. 707-720.
- Grauch, V.J.S., and Keller, G.R., 2004, Gravity and aeromagnetic expression of tectonic and volcanic elements of the southern San Luis Basin, New Mexico and Colorado, *in* Brister, B.S., Bauer, P.W., Read, A.S., and Lueth, V.W., eds., New Mexico Geological Society Guidebook, 55th Field Conference, Geology of the Taos Region, p. 230-243.
- Grauch, V.J.S., Sawyer, D.A., Minor, S.A., Hudson, M.R., and Thompson, R.A., 2006, Gravity and aeromagnetic studies of the Santo Domingo basin area, New Mexico, *in* Minor, S.A., ed., The Cerrillos Uplift, the La Bajada Constriction, and Hydrogeologic Framework of the Santo Domingo Basin, Rio Grande Rift, New Mexico, U.S. Geological Survey Professional Paper 1720, p. 62-86.

- Green, G.N., 1992, The Digital Geologic Map of Colorado in ARC/INFO Format, U.S. Geological Survey Open-File Report 92-0507, 9 p.
- Green, G.N., and Jones, G.E., 1997, The Digital Geologic Map of New Mexico in ARC/INFO Format: U.S. Geological Survey Open-File Report 97-0052, 9 p.
- Gries, R.R., and Brister, B.S., 1989, New interpretation of seismic lines in the San Luis Valley, south-central Colorado, *in* Harmon, E.J., ed., *Water in the Valley: Colorado Groundwater Association, 8th Annual Field Trip, Guidebook*, p. 241-254.
- Heywood, C.E., 1992, Isostatic residual gravity anomalies of New Mexico, U.S. Geological Survey Water-Resources Investigations Report 91-4065, 27 p.
- Hinze, W.J., 2003, Bouguer reduction density: why 2.67?: *Geophysics*, v. 68, p. 1559-1560.
- Hoy, R.G., and Ridgway, K.D., 2002, Syndepositional thrust-related deformation and sedimentation in an Ancestral Rocky Mountains basin, central Colorado trough, Colorado, USA: *Geological Society of America Bulletin*, v. 114, p. 804-828.
- HRS Water Consultants, I., 1987, San Luis Valley Aquifer Study, Phase One Final Report; prepared for Colorado Water Resources Power Development Authority.
- Hudson, M.R., Grauch, V.J.S., and Minor, S.A., 2008, Rock magnetic characterization of faulted sediments with associated magnetic anomalies in the Albuquerque basin, Rio Grande rift, New Mexico: *Geological Society of America Bulletin*, v. 120, p. 641-658.
- Ingersoll, R.V., Cavazza, W., Baldrige, W.S., and Shafiqullah, M., 1990, Cenozoic sedimentation and paleotectonics of north-central New Mexico: implications for initiation and evolution of the Rio Grande rift: *Geological Society of America Bulletin*, v. 102, p. 1280-1296.

- Jachens, R.W., and Moring, B.C., 1990, Maps of the thickness of Cenozoic deposits and the isostatic residual gravity over basement for Nevada, U.S. Geological Survey Open-File Report 90-404, 15 p.
- Keller, G.R., Cordell, L., Davis, G.H., Peeples, W.J., and White, G., 1984, A geophysical study of the San Luis basin, *in* Baldrige, W.S., Dickerson, P.W., Riecker, R.E., and Zidek, J., eds., New Mexico Geological Society Guidebook, 35th Field Conference, Rio Grande Rift: Northern New Mexico, p. 51-57.
- Keller, G.R., Hildenbrand, T.G., Hinze, W.J., and Li, X., 2006, The quest for the perfect gravity anomaly: Part 2 — Mass effects and anomaly inversion: Society of Exploration Geophysicists Technical Program Expanded Abstracts, v. 25, p. 864.
- Kellogg, K.S., 1999, Neogene basins of the northern Rio Grande rift: partitioning and asymmetry inherited from Laramide and older uplifts: *Tectonophysics*, v. 305, p. 141-152.
- Kirkham, R.M., 2006, Surprises in the Culebra graben, a major sub-basin within the San Luis basin of the Rio Grande rift: Geological Society of America Abstracts with Programs, v. 38, No. 6, p. 36.
- Kirkham, R.M., Brister, B.S., Grauch, V.J.S., and Budahn, J.R., 2005, Culebra graben: a major intrarift structure in the San Luis basin, Rio Grande rift: Geological Society of America Abstracts with Programs, v. 37, No. 6, p.14.
- Kirkham, R.M., Lufkin, J.L., Linday, N.R., and Dickens, K.E., 2004, Geologic map of the La Valley quadrangle, Costilla County, Colorado: Colorado Geological Survey Open-File Map 04-8, scale 1:24,000.
- Kluth, C.F., 2007, Inversion and reinversion of the northern Rio Grande rift, San Luis basin, southern Colorado: Geological Society of America Abstracts with Programs, v. 39, No. 6, p.366.
- Kluth, C.F., and Schaftenaar, C.H., 1994, Depth and geometry of the northern Rio Grande rift in the San Luis basin, south-central Colorado, *in* Keller, G.R., and Cather, S.M., eds., Basins of the Rio Grande Rift: Structure, Stratigraphy, and Tectonic Setting: Boulder, Geological Society of America Special Paper 291, p. 27-37.

- Lipman, P.W., 1975a, Evolution of the Platoro caldera complex and related volcanic rocks, southeastern San Juan Mountains, Colorado, U.S. Geological Survey Professional Paper 852, p. 128.
- , 1975b, Geologic map of the lower Conejos River canyon area, southeastern San Juan Mountains, Colorado, U.S. Geological Survey Miscellaneous Investigations Map I-901, scale 1:48,000.
- , 1979, The Taos Plateau volcanic field, northern Rio Grande rift, New Mexico, *in* Riecker, R.E., ed., *Rio Grande Rift: Tectonics and Magmatism*: Washington, D.C., American Geophysical Union, p. 289-311.
- , 1983, The Miocene Questa caldera, northern New Mexico: relationship to batholith emplacement and associated molybdenum mineralization: *The Genesis of Rocky Mountain Ore Deposits: Changes with Time and Tectonics: Proceedings of the Denver Region Exploration Geologists Society Symposium*, p. 133-149.
- , 2007, Incremental assembly and prolonged consolidation of Cordilleran magma chambers: evidence from the Southern Rocky mountain volcanic field: *Geosphere*, v. 3, p. 42-70.
- Lipman, P.W., and Mehnert, H.H., 1975, Late Cenozoic basaltic volcanism and development of the Rio Grande depression in the southern Rocky Mountains, *in* Curtis, B.F., ed., *Cenozoic History of the Southern Rocky Mountains: Geological Society of America Memoir 144*, p. 119-154.
- Lipman, P.W., Mehnert, H.H., and Naeser, C.W., 1986, Evolution of the Latir volcanic field, northern New Mexico, and its relation to the Rio Grande rift, as indicated by potassium-argon and fission track dating: *Journal of Geophysical Research*, v. 91, p. 6329-6345.
- Lipman, P.W., and Reed, J.C., Jr., 1989, Geologic map of the Latir Volcanic Field, and adjacent areas, northern New Mexico, U.S. Geological Survey Miscellaneous Investigations Map I-1907, scale 1:48,000.

- Machette, M.N., Thompson, R.A., and Drenth, B.J., 2008, Geologic map of the San Luis Quadrangle, Costilla County, Colorado: U.S. Geological Survey Scientific Investigations Map 2008-2963, 1:24,000 scale map.
- Morel, J., and Watkins, T.A., 1997, More data point to potential in S. Colorado sub-basin: *Oil and Gas Journal*, v. 95, p. 78-80.
- Personius, S.F., and Machette, M.N., 1984, Quaternary and Pliocene faulting in the Taos Plateau region, northern New Mexico, *New Mexico Geological Society Guidebook, 35th Field Conference, Rio Grande Rift: Northern New Mexico*, p. 83-90.
- Phillips, J.D., 2000, Locating magnetic contacts: a comparison of the horizontal gradient, analytic signal, and local wavenumber methods: 2000 Technical Program Expanded Abstracts, 70th Annual Meeting, Society of Exploration Geophysicists, p. 402-405.
- , 2007, Geosoft eXecutables (GX's) developed by the U.S. Geological Survey, version 2.0, with notes on GX development from Fortran code, U.S. Geological Survey Open-File Report 2007-1355, 111 p.
- Phillips, J.D., Hansen, R.O., and Blakely, R.J., 2007, The use of curvature in potential-field interpretation: *Exploration Geophysics*, v. 38, p. 111-119.
- Plouff, D., and Pakiser, L.C., 1972, Gravity study of the San Juan Mountains, Colorado: U.S. Geological Survey Professional Paper 800-B, p. 183-190.
- Quezada, O., Andronicos, C., and Keller, G.R., 2004, Structure of the Sangre de Cristo Mountains between Taos and Mora based on an integrated geophysical analysis, *in* Brister, B.S., Bauer, P.W., Read, A.S., and Lueth, V.W., eds., *New Mexico Geological Society Guidebook, 55th Field Conference, Geology of the Taos Region*, p. 257-263.
- Ruleman, C., and Machette, M.N., 2007, An overview of the Sangre de Cristo fault system and new insights to interactions between Quaternary faults in the Northern Rio Grande rift, *in* Machette, M.N., Coates, M.M., and Johnson, M.L., eds., 2007 *Rocky Mountain Section Friends of the Pleistocene Field Trip- Quaternary*

Geology of the San Luis Basin of Colorado and New Mexico, September 7-9, 2007: U.S. Geological Survey Open-File Report 2007-1193, p. 187-197.

Sales, J.K., 1983, Collapse of Rocky Mountain basement uplifts, *in* Lowell, J.D., ed., Rocky Mountain Foreland Basins and Uplifts: Denver, CO, Rocky Mountains Association of Geologists, p. 79-97.

Shirley, K., 1995, An oil find that was good as gold; utilizing several geophysical techniques helps: American Association of Petroleum Geologists Explorer, v. 16, p. 7-9.

Simpson, R.W., Jachens, R.W., Blakely, R.J., and Saltus, R.W., 1986, A new isostatic residual gravity map of the conterminous United States with a discussion on the significance of isostatic residual anomalies: Journal of Geophysical Research, v. 91, p. 8348-8372.

Smith, R.S., Thurston, J.B., Dai, T.-F., and MacLeod, I.N., 1998, iSPI™ -- the improved source parameter imaging method Geophysical Prospecting, v. 46, p. 141-151.

Steven, T.A., 1975, Middle Tertiary volcanic field in the southern Rocky Mountains, *in* Curtis, B.F., ed., Cenozoic History of the Southern Rocky Mountains, Geological Society of America Memoir 144, p. 75-94.

Telford, W.M., Geldart, L.P., and Sheriff, R.E., 1990, Applied Geophysics, 2nd Ed., Cambridge University Press, 770 p.

Thompson, R.A., and Dungan, M.A., 1985, The petrology and geochemistry of the Handkerchief Mesa mixed magma complex, San Juan Mountains, Colorado: Journal of Volcanology and Geothermal Research, v. 26, p. 251-274.

Thompson, R.A., Johnson, C.M., and Mehnert, H.H., 1991, Oligocene basaltic volcanism of the northern Rio Grande rift: San Luis Hills, Colorado: Journal of Geophysical Research, v. 96.

Thompson, R.A., and Lipman, P.W., 1994, Geologic map of the Los Pinos quadrangle, Rio Arriba and Taos Counties, New Mexico, and Conejos County, Colorado, U.S. Geological Survey Map GQ-1749, scale 1:24,000.

- Thompson, R.A., and Machette, M.N., 1989, Geologic map of the San Luis Hills area, Conejos and Costilla Counties, Colorado, U.S. Geological Survey Miscellaneous Investigations Map I-1906, scale 1:50,000.
- Thompson, R.A., Machette, M.N., and Drenth, B.J., 2007a, Preliminary geologic map of the Sanchez Reservoir Quadrangle and eastern part of the Garcia Quadrangle, Costilla County, Colorado: U.S. Geological Survey Open-File Report 2007-1074, 1:24,000 scale map.
- Thompson, R.A., Machette, M.N., Shroba, R., and Ruleman, C., 2007b, Geology of Mesita volcano, Colorado -- eruptive history and implications for basin sedimentation during the Quaternary, *in* Machette, M.N., Coates, M.M., and Johnson, M.L., eds., 2007 Rocky Mountain Section Friends of the Pleistocene Field Trip- Quaternary Geology of the San Luis Basin of Colorado and New Mexico, September 7-9, 2007: U.S. Geological Survey Open-File Report 2007-1193, p. 169-179.
- Thurston, J.B., and Smith, R.S., 1997, Automatic conversion of magnetic data to depth, dip, and susceptibility contrast using the SPI method: *Geophysics*, v. 62, p. 807-813.
- Topper, R., Spray, K.L., Bellis, W.H., Hamilton, J.L., and Barkmann, P.E., 2003, Ground Water Atlas of Colorado, Colorado Geological Survey, Special Publication 53, 210 p.
- Trevino, L., Keller, G.R., Andronicos, C., and Quezada, O., 2004, Rootless mountains and gravity lows in the Sangre de Cristo Mountains, southern Colorado-northern New Mexico, *in* Brister, B.S., Bauer, P.W., Read, A.S., and Lueth, V.W., eds., New Mexico Geological Society Guidebook, 55th Field Conference, Geology of the Taos Region, p. 264-271.
- Tweto, O., 1979a, Geologic Map Of Colorado, U.S. Geological Survey, 1:500,000 scale map.
- , 1979b, The Rio Grande rift system in Colorado, *in* Riecker, R.E., ed., Rio Grande Rift: Tectonics and Magmatism: Washington, D.C., American Geophysical Union, p. 33-56.

- Uitti, P.B., 1980, Interpretation of seismic reflection data from southern San Luis Valley, south-central Colorado: Golden, CO, Colorado School of Mines, M.S. thesis, 49 p.
- Upson, J.E., 1939, Physiographic subdivisions of the San Luis Valley, southern Colorado: *Journal of Geology*, v. 47, p. 721-736.
- Wallace, A.R., 2004, Evolution of the southeastern San Luis basin margin and the Culebra embayment, Rio Grande rift, southern Colorado, *in* Brister, B.S., Bauer, P.W., Read, A.S., and Lueth, V.W., eds., *New Mexico Geological Society Guidebook, 55th Field Conference, Geology of the Taos Region*, p. 181-192.
- Watkins, T.A., Belcher, J.S., Gries, R.R., and Longacre, M.B., 1995, "Black gold" leads to new structural interpretation, northern Sangre de Cristo Mountains/northeast San Luis basin: *American Association of Petroleum Bulletin Abstract no. 6, Rocky Mountain section meeting*, v. 79, p. 926.

A Geophysical Study of the San Juan Mountains Batholith, Southwestern Colorado

ABSTRACT

One of the largest and most pronounced gravity lows over North America lies over the rugged San Juan Mountains in southwestern Colorado. The mountain range is coincident with the San Juan Volcanic Field (SJVF), the largest erosional remnant of a widespread Oligocene volcanic field that covered much of the southern Rocky Mountains. A buried, low-density silicic batholith related to the volcanic field has been the accepted interpretation of the source of the gravity low since the 1970s. However, this interpretation was based on gravity data processed with standard techniques that break down in the SJVF region due to extreme topographic relief and densities of extrusive rocks in the volcanic field that are much lower than the standard reduction density (2670 kg/m^3) normally assumed for gravity data processing. The combined effects of high-relief topography, topography with low densities, and the use of a common reduction density of 2670 kg/m^3 produce spurious large-amplitude gravity lows that may mask or distort the geophysical signature of deeper features such as a batholith complex. Here, we apply an unconventional processing procedure that uses geologically appropriate densities for the uppermost crust and digital topography to mostly remove the effect of the low density units that underlie the topography associated with the SJVF. This approach results in a gravity map that provides an improved representation of deeper sources, including a reduced amplitude for the anomaly attributed to a batholith complex. We also reinterpret vintage seismic refraction data that indicate the presence of a low-

velocity zone under the SJVF. Assuming that the source of the gravity low on the improved gravity anomaly map is the same as the source of the low seismic velocities, integrated modeling corroborates the interpretation of a batholith complex and then defines the dimensions and overall density contrast of the complex. Models show that the thickness of the batholith complex varies significantly laterally, with the greatest thickness (~20 km) under the western SJVF, and lesser thicknesses (< 10 km) under the eastern SJVF. The largest group of nested calderas on the surface of the SJVF, the central caldera cluster, is not correlated with the thickest part of the batholith complex. This result is consistent with petrologic interpretations from recent studies that the batholith complex continued to be modified after cessation of volcanism and therefore is not necessarily representative of synvolcanic magma chambers. The total volume of the batholith complex is estimated to be 82,000 to 130,000 km³. Thus, residuum of considerably greater volume was produced and could be present in the lower crust or uppermost mantle. The interpreted density contrast (-60 to -110 kg/m³), density (2590-2640 kg/m³), and seismic expression of the batholith complex are consistent with results of geophysical studies of other large batholiths in the western U.S.

INTRODUCTION

The rugged San Juan Mountains of southwestern Colorado are the highest range of the southern Rocky Mountain region, lying north of the San Juan basin and between the San Luis basin of the Rio Grande rift and Colorado Plateau (Fig. B1). The voluminous Oligocene San Juan volcanic field (SJVF) constitutes most of the range (Fig. B2). One of the largest and most pronounced Bouguer gravity lows over North America

is spatially correlated with the San Juan Mountains (Fig. B3). The accepted interpretation for this anomaly has been the effect of a low density, upper-crustal granitic batholith, related to the overlying volcanic field and caldera complex (Plouff and Pakiser, 1972). Whereas the interpretation of a batholith is reasonable, processing of the gravity data that was standard for the time produces problems that can be resolved with a more modern approach. Specifically, the complex upper crustal density structure has not been adequately taken into account in terms of Bouguer and terrain corrections. The goals of this study are to reprocess and interpret gravity data and vintage seismic refraction data (Prodehl and Pakiser, 1980) to examine the lateral and depth extents of the batholith assumed to be present and its possible relationships to the overlying volcanic field. Our analyses were undertaken in the context of recent interpretations of underlying mantle structure (Roy et al., 2004) and petrologic evolution of the SJVF (Lipman, 2007).

We employed a new three-dimensional forward modeling approach to analyze the gravity signal of the region with density constraints from previous studies and topographic relief represented by digital elevation data. The purpose of this modeling was to derive a geologically appropriate Bouguer/terrain correction model, which we then used to create a new “Bouguer-like” map of the region to be interpreted in terms of the upper crustal architecture of the SJVF. The main goal of the subsequent modeling was to test and refine the interpretation of a batholith complex. Seismic refraction data (Prodehl and Pakiser, 1980) were used to constrain the gravity interpretation, and this integration of different geophysical datasets allowed us to confirm that a batholith complex was present, to produce reasonable end members of the batholith complex’s thickness and

volume, and to examine the implications of these results for the crustal evolution of the region.

GEOLOGIC BACKGROUND

The SJVF is a 25,000 km² erosional remnant of a volcanic province that was active across the southern Rocky Mountains during the Tertiary (Steven, 1975), between areas of outcropping Precambrian rocks on the north and southwest (Gunnison uplift and Needle mountains, respectively, Fig. B2). The oldest exposed Precambrian rocks in the study area, schists, gneisses, and metavolcanic rocks (included in undiff. Precambrian rocks, Fig. B2), are part of the 1.8-1.7 Ga Yavapai province accreted to the southern boundary of older North America (Karlstrom et al., 2004). The northeast-trending southern margin of this province may lie within the SJVF region but is poorly located (Shaw and Karlstrom, 1999). Episodes of significant tectonism and granitic intrusion at ~1.7 Ga and ~1.4 Ga left behind large plutons in the region, including those in the Needle mountains and Gunnison uplift (units Xg and Yg, Fig. B2) (Tweto, 1979; Bickford and Anderson, 1993; Anderson and Cullers, 1999; Karlstrom et al., 2004; Gonzales and Van Schmus, 2007). These plutons may be volumetrically significant in the subsurface, and may represent batholiths, although their subsurface extents are unknown.

A number of tectonic events since the Precambrian have affected the SJVF region. Cambrian rifting in Oklahoma, left behind as the southern Oklahoma aulacogen, may have extended into and through southern Colorado, including the SJVF region (Larsen et al., 1985; Casillas, 2004). Rocks associated with rifting include mafic and ultramafic intrusions that crop out immediately north of the SJVF (Fig. B2). Phanerozoic

sedimentary rocks of the Colorado Plateau lie along the western margin of the San Juan Mountains, and the region was affected by the Ancestral Rocky Mountain orogeny (Kluth and Coney, 1981; Kluth, 1986), including the Uncompahgre uplift that extends to the northwest of the SJVF (Casillas, 2004). The Laramide orogeny was responsible for uplift of the Needle dome and Gunnison uplift (Kelley, 1955; Tweto, 1975; Cather, 2004), and formation of the San Juan sag, a northward extension of the San Juan basin into the eastern SJVF region filled with up to ~2 km of sedimentary rocks (Gries, 1985; Brister and Chapin, 1994).

Oligocene volcanism began about 35 Ma, with eruption of andesitic and dacitic lavas of the Conejos Formation from stratovolcanoes until about 30 Ma, when eruption of silicic ash-flow tuffs from numerous calderas began (Lipman et al., 1970). These units account for about two thirds of the total volume of the volcanic field (unit Tpl, Fig. B2) (Lipman et al., 1970).

The younger caldera complexes formed within and around clusters of these stratovolcanoes (Steven and Lipman, 1976). Silicic ignimbrites (unit Taf, Fig. B2) erupted from approximately 18 different calderas, vary in volume from 25 to 5000 km³ (Lipman, 2000, 2007; Lipman and McIntosh, 2008), and individual eruptions are thought to be some of the most violently explosive events in Earth's history (Mason et al., 2004). The first eruptions, from 33.7 to 29.8 Ma, occurred in the northeastern portion of the SJVF, followed by eruptions from 29.4 to 28.8 Ma at the Platoro and Summitville calderas in the southeast SJVF. Volcanic activity then shifted to the western caldera cluster with formation of five calderas between 28.6 and 27.6 Ma. The massive La Garita caldera erupted at 27.8 Ma, the first of seven nested calderas to form in the central

cluster, ending with the Creede caldera at 26.9 Ma (Lipman, 2000, 2006). Eruptions of andesites similar to the Conejos Formation continued throughout the stage of ignimbrite volcanism, such that these rocks are interbedded with the ignimbrites. Caldera-centered eruptions of ignimbrites continued until ~26 Ma, when volcanism changed to a volumetrically minor assemblage of basalts and rhyolites, related to the formation of the Rio Grande rift (Steven and Lipman, 1976; Lipman, 2000, 2007). The Lake City caldera formed at 23 Ma as part of this latter episode within the preexisting western caldera cluster. The ignimbrites (including those of the Lake City caldera) account for about one third of the original total volume of the SJVF (Lipman et al., 1970), but have been eroded to the point that they may now only represent about one sixth the total volume (P. Lipman, written comm., 2007). The total volume of volcanic rocks erupted in the SJVF, including both the Conejos Formation and ignimbrites, is about 40,000 km³.

A large-amplitude gravity low occurs over the SJVF, and has been interpreted to reflect a low density, composite granitic batholith in the upper crust (Plouff and Pakiser, 1972). This interpretation is discussed in greater detail below, but has been accepted in a broad sense by subsequent studies in the region. Such a batholith could be considered the accumulated remnants of magma chambers that magma erupted from in caldera-forming eruptions (Lipman, 1984). However, a more recent interpretation holds that batholith growth continued incrementally after caldera subsidence ended, as recorded by ages and compositions of localized, shallow intrusions (Bachmann et al., 2007; Lipman, 2007). A number of granitic intrusions crop out in the SJVF region (unit Tmi, Fig. B2), and are associated with the ignimbrite stage of volcanism. They are as much as millions of years younger than the volcanic units at the corresponding calderas, and tend to be more mafic

in composition than the volcanic rocks, especially those that are significantly younger than the ignimbrites (Bachmann et al., 2007; de Silva and Gosnold, 2007; Lipman, 2007). A subvolcanic batholith remaining behind today isn't necessarily compositionally or volumetrically representative of large magma chambers that existed during or immediately following volcanism. It follows that a batholith would not be expected to be compositionally uniform, because it would have been assembled over a long period of time of magmas with differing compositions, with the possibility of relatively mafic lower portions (Bachmann et al., 2007; de Silva and Gosnold, 2007; Lipman, 2007). Thus, we refer to the batholith here as a "batholith complex."

Oligocene magmatism that produced the SJVF is interpreted to have originated as a thermal anomaly that originated in the upper mantle, possibly related to complex subduction processes underneath the western U.S. (Lipman et al., 1978). Mixing of basaltic magmas with crustal rocks is inferred to be the source of the silicic products emplaced into and erupted from the upper crust (Lipman et al., 1978). The possible amount of mafic residuum left behind in the upper mantle and lower crust has not been studied from a petrologic perspective, yet there may be a significant amount of these rocks at depth based on analogy with other regions of the southwestern U.S. (Keller et al., 2005).

GRAVITY AND SEISMIC DATA

Gravity anomalies reflect lateral variations of density, with gravity highs occurring over regions of relatively high rock densities, and gravity lows occurring over large volumes of low-density rocks. Regional quality gravity data, with station spacings

of 1-10 km, were extracted from the PACES database that is maintained by the University of Texas at El Paso (<http://gis.utep.edu>) and supplemented with 323 stations recently acquired in the San Juan sag region (R. Gries, written comm., 2007). The PACES database consists of data collected over decades by many previous workers and was compiled as the result of a major cooperative effort between federal agencies and universities (Keller et al., 2006). For comparison to the nonstandard approach taken in this report, a standard Bouguer anomaly map was computed using conventional techniques (Telford et al., 1990; Blakely, 1995). Corrections included those for predicted gravitational attraction at the elevation and latitude of the gravity stations (theoretical and free air corrections), effects of tabular and homogenous rocks masses between the stations and sea level (Bouguer slab correction), and effects of topographic masses (terrain corrections). The standard reduction density of 2670 kg/m^3 , assumed to represent an average upper crustal density (Hinze, 2003), was used for the Bouguer and terrain corrections. Application of these corrections yields complete Bouguer anomalies (Fig. B3).

The wavelengths of gravity anomalies can be related to the depths of the causative sources, because deep and/or broad sources produce longer-wavelength anomalies than those caused by shallow and/or narrow sources. One method used to enhance the signature of deep/broad sources at the expense of shallow/narrow sources is upward continuation, in which the gravity anomalies measured on the ground surface are mathematically transformed to a higher measurement level (Blakely, 1995). Here, the effect of the gravity field was calculated at a level of 10 km above the ground, in order to enhance the signature of relatively deep/broad geologic features (Fig. B5).

Seismic refraction data indicate broad velocity structure of the crust and upper mantle. Whereas these datasets do not provide detailed images of lateral variations of velocities or of stratigraphic layering, they do give direct estimates of seismic P-wave velocity for geologic situations where velocity increases with depth. A profile was recorded over the eastern SJVF by the U.S. Geological Survey during 1965, with shotpoints on the south and north flanks of the SJVF (Fig. B1) (Prodehl and Pakiser, 1980). By modern standards these data are low-quality, with low signal to noise ratio, few receivers, and imprecise location of receivers, yet are still useful for studies of gross velocity structure. Seismic velocities typically increase with depth, although in the southern Rocky Mountain region anomalously low velocities have been observed in the crust and mantle, spatially correlated with granitic batholiths (Schneider and Keller, 1994).

PREVIOUS GEOPHYSICAL INTERPRETATIONS

Densities of igneous rocks vary as functions of both composition and texture. Silicic rocks have lower densities than mafic rocks, and for a given composition volcanic rocks typically have lower densities than their plutonic equivalents (Telford et al., 1990). Granitic plutons commonly have lower densities than the country rocks they intrude, producing gravity lows (Bott and Smithson, 1967). A number of gravity lows in the southern Rocky Mountain region have been interpreted to reflect low-density granitic batholiths and plutons, including an Oligocene batholith in central Colorado (Isaacson and Smithson, 1976), Oligocene and Precambrian plutons in the Sangre de Cristo Mountains (Cordell and Keller, 1984; Cordell et al., 1985; Grauch and Keller, 2004;

Quezada et al., 2004), and an Oligocene batholith under the Mogollon-Datil volcanic field (Schneider and Keller, 1994).

The gravity low associated with the SJVF has dimensions of about 100 by 150 km and laterally is contained nearly completely within the boundaries of the SJVF (Figs. B2 & B3). An upper crustal, composite, Oligocene granitic batholith has been interpreted as the source of the anomaly (Plouff and Pakiser, 1972). A number of lines of evidence support this conclusion (Plouff and Pakiser, 1972; Bachmann et al., 2007): First, the boundaries of the gravity low correlate well with the mapped extent of calderas (Fig. B2), which would be expected for a batholith complex that is related to surface manifestations of magmatism (Lipman, 1984). Second, low-density volcanic rocks of the SJVF extend well beyond the area of the gravity low and tend to have small density contrasts with surrounding sediments and sedimentary rocks of the Colorado Plateau, San Juan basin, and San Luis basin, meaning that the surficial rocks cannot be the main source of the anomaly. Third, whereas there is a profound inverse correlation between surface elevation and the complete Bouguer gravity anomaly values (Fig. B3), the gradients at the margins of the gravity low are too sharp to be caused by a source greater than about 15-20 km depth at most and probably 5 km or less on average (Plouff and Pakiser, 1972). This means that Airy-type isostatic compensation cannot be responsible for a significant portion of the gravity low, unlike anomalies observed over other mountain ranges. Finally, Precambrian granites exposed in the Needle Mountains and in the Gunnison region may be expected to contribute to the gravity low, as is the case in the southern Sangre de Cristo Mountains (Quezada et al., 2004). However, the gravity low does not extend over the entire Needle Mountains, only over its northern portion (Figs. B2 & B3),

and at local scale, the contacts of Precambrian granites there do not appear to correlate with gravity anomalies. This led Plouff and Pakiser (1972) to interpret that the batholith was intruded underneath the northern portion of the Needle Mountains. The gravity low also does not extend over granitic rocks in the Gunnison region. Whereas Precambrian granites may account for some of the gravity low and their presence under the SJVF cannot be ruled out, it seems unlikely from these observations that they are a significant source for the gravity low. For these reasons, we do not challenge the interpretation that the main source of the gravity low is a low-density batholith complex. Rather, we seek to refine this conclusion using more rigorous gravity data processing and quantitative modeling.

Individual calderas are not associated with gravity anomalies within the larger gravity low, indicating that the densities of rocks that fill the calderas are not significantly different from the surrounding volcanic rocks. The Cochetopa caldera is an exception, with a spatially associated gravity low (Figs. B2 & B3). The source of the low is unknown, but may be caused by a density contrast with relatively dense Precambrian rocks surrounding much of the caldera margin (Plouff and Pakiser, 1972).

Plouff and Pakiser (1972) approximately placed the margin of the batholith complex at the -300 mGal contour, an interpretation consistent with their quantitative modeling of the batholith. To investigate the possible thickness of the batholith, they used 2D modeling (close to profile A-A' of this study) and an assumed density contrast of 100 kg/m^3 to estimate a thickness of about 24 km (Plouff and Pakiser, 1972). They did not attempt to estimate batholith volume.

A gravity low with similar dimensions and magnitude occurs to the north of the SJVF, between Aspen and Gunnison. This also has been related to a low-density, silicic Tertiary batholith (Isaacson and Smithson, 1976; McCoy et al., 2005). Density measurements on outcropping Tertiary granites in the region of the gravity low indicated densities of 2620 to 2630 kg/m³ (Tweto and Case, 1972; Isaacson and Smithson, 1976). When contrasted against an assumed upper crustal background density of 2710 to 2760 kg/m³, this resulted in a body that occupied the upper ~20 km of the crust in 2D models (Isaacson and Smithson, 1976).

A regional gravity low, 400-500 km in wavelength and therefore encompassing the gravity low related to the batholith, lies over the region surrounding the SJVF (Fig. B5). Roy et al. (2004) has interpreted the source of this low as a low-density zone of low densities in the upper mantle, developed as a product of Tertiary magmatism by extraction of basaltic magmas from the mantle into the lower crust. One possible solution for the source of the long-wavelength gravity low is a ~300 km wide, ~200 km thick zone assuming a density contrast of -33 kg/m³ with surrounding mantle rocks, on the basis of a model that corresponds in location to profiled B-B' of this paper (Roy et al., 2004). The source would be thicker for a lower magnitude of density contrast. Low seismic velocities in the upper mantle can be associated with sources of gravity lows, and even though no seismic studies examining the details of the upper mantle beneath the SJVF region have been reported, upper mantle seismic velocities are known to be generally depressed under the entire Southern Rocky Mountain region (Lee and Grand, 1996; Lerner-Lam et al., 1998; Dueker et al., 2001).

Seismic low-velocity zones are also present in the upper crust of the SJVF and Aspen-Gunnison regions. Vintage seismic refraction data collected by the U.S. Geological Survey during the 1960s revealed significant thicknesses of relatively low-velocity rocks within the upper 20 km of the crust (Prodehl and Pakiser, 1980). Rapid terminations of upper-crustal refractions were interpreted to reflect two stacked and laterally extensive zones with velocities < 6 km/s between rocks with velocities > 6 km/s, including a small zone of high-velocity rocks between the low-velocity zones (Prodehl and Pakiser, 1980). Whereas the rocks associated with the low-velocity zones were interpreted to occupy the same upper ~ 20 km of the crust occupied by the batholith beneath the SJVF (Prodehl and Pakiser, 1980), no literature has commented on the possible relationship between the source of the seismic low-velocity zones and the source of the gravity low.

GEOPHYSICAL METHODS

Gravity data processing (or “reduction”) involves the removal of numerous effects that influence observed gravity values, with the ultimate goal of removing predictable effects and enhancing the signal to be investigated. As discussed above, Bouguer slab and terrain corrections attempt to account for the gravity effects of a homogenous crust from the topographic surface to the sea level datum, assuming typically 2670 kg/m^3 (Hinze, 2003).

Problems may arise in processing of gravity data when the densities of rocks above sea level differ from 2670 kg/m^3 . The Bouguer slab and terrain corrections are of special interest in this study, because the andesites and ignimbrites that compose the high

elevations (Figs. B2 & B4) of the SJVF are much less dense than the standard reduction density of 2670 kg/m^3 , and because the San Juan Mountains contain extremely rugged topography and therefore large-magnitude terrain corrections are required. The Bouguer slab correction is proportional in magnitude to the assumed density and algebraically negative in effect, meaning that calculated Bouguer anomalies will be inappropriately low for topographically high regions with lower densities than the standard value of 2670 kg/m^3 . Intermediate- and silicic-composition volcanic rocks, like those that compose the SJVF, normally have densities significantly less than 2670 kg/m^3 . This means that the gravity low over the SJVF (Fig. B3) is likely too low, and quantitative interpretation of the anomaly will result in models of the batholith complex that are incorrect.

In order to compute a more representative gravity anomaly map, we employed a method that allows variable surface densities to be used in conjunction with digital elevation data to calculate a more appropriate correction that combines the Bouguer slab and terrain corrections into one 3D calculation (WINGRAV program, M. Baker, K. Crain, personal comm., 2003-2005). This method works by calculating the gravitational effect of mass between two layers at each gravity station, where the layers are defined by digital elevation models. Different calculation methods, following those of Hammer (1974), are used depending on the distance from the gravity station to different masses, where boundaries between different masses are defined in terms of a grid of density values (Fig. B6). The edges of individual masses are treated as vertical boundaries, extending from the top of the upper layer to the top of the bottom layer (Crain, 2006). For masses greater than 500 km away from a gravity station a row mass approximation (Hammer, 1974) is used and for distances closer than 500 km to a gravity station vertical

line element approximations (M. Baker, written comm., 2003) are employed. Groups of gravity stations are combined, or “binned,” into groups of masses for ease of calculation, with the spatial extent of station bins depending on the distance to masses.

Density information for the model came from published data and typical values based on lithologies (Popenoe and Steven, 1969; Popenoe and Luedke, 1970; Grauch and Hudson, 1987; Jenkins, 1989; Telford et al., 1990), as well as information from borehole density logs (R. Gries, written comm., 2007). The most important density assignment is that used for the SJVF, because these volcanic rocks form most of the high topography in the study area. Andesites of the Conejos Formation, as well as andesites that continued to erupt during the ignimbrite phase of volcanism, have typical densities of 2500 kg/m^3 (R. Gries, written comm., 2007) and make up approximately 5/6 of the total SJVF volume. Ignimbrites make up 1/6 of the SJVF volume and have typical densities of 2200 kg/m^3 . A weighted average of 2450 kg/m^3 was used to represent the entire SJVF, because the subsurface distribution of the different volcanic rocks is not known well enough to be built into the model. Geologic units of small thickness, such as Rio Grande rift-age volcanic flows, were not included in the model because they are volumetrically insignificant. Density assignments are summarized in Table B1.

For this study, we ideally wanted to calculate the gravitational effect of all masses above the level of the batholith complex, so that this effect could be removed and the resulting gravity anomalies would not include density variations related to surficial rocks. In practice, however, the depth to the top of the batholith complex is not known, nor is the 3D distribution of densities above the complex. Also, adjacent to the SJVF lie a number of complex structures, including the San Juan and San Luis basins and San Juan

sag, that we did not attempt to model in three dimensions. Thus, we proceeded by assigning variable densities (Fig. B6) and calculating the gravitational effect of rocks only above an elevation of 7500 feet (2286 m), the approximate lowest surface elevation of the adjacent San Luis basin. The structure of basins and uplifts of Precambrian basement rocks around the margin of the SJVF were not built into the model. For simplicity we further assumed that all density boundaries modeled above 7500 feet extended vertically down to 7500 feet, such that no dipping contacts were used. All rocks beneath 7500 feet were assigned a density of 2670 kg/m^3 . The gravitational effect was calculated for this model, defined by 90 m SRTM (Shuttle Radar Topography Mission) digital elevation data. This effect was subtracted from the original Free Air gravity field (corrected for distance above the center of the Earth but not masses of rock), in order to yield a new “complete Bouguer anomaly-like” map (Fig. B7).

This map gives an improved representation of buried anomaly sources. It indicates lateral variations in density, although in a more complicated fashion than standard gravity anomaly maps, because it reflects variations from the density model (Fig. B6) for all rocks above 7500 feet and variations from 2670 kg/m^3 below 7500 feet. The excess “artifact signal” removed by this computation method, found by subtraction of the conventional gravity map (Fig. B8) from the new map, is as much as 10-15 mGal with the greatest difference occurring over the highest elevations of the SJVF region (Figs. B4 & B8). The cumulative error level within the new gravity map is estimated to reach ~ 3 mGal based on observations of solutions at single stations thought to be spurious, likely the combined result of using relatively coarse (90 m) digital elevation data and the inherent resolution of WINGRAV program using the chosen calculation

parameters. The map was therefore only interpreted in terms of broad sources that produce anomalies with amplitudes much greater than 3 mGal, and surficial sources were not studied.

What if, instead of using this complex approach with variable densities, a single appropriate (i.e., not 2670 kg/m^3) reduction density was simply used for the Bouguer slab and terrain corrections? This approach was tested using 2450 kg/m^3 for the reduction density, the weighted average value believed to be appropriate for the SJVF and thus most of the study area (Fig. B9a). Whereas appropriate for the SJVF, this map fails to account for the higher densities of Precambrian rocks, which were assigned densities of 2670 kg/m^3 for the variable density model (Table B1). The best example is the Needle Mountains, where these relatively dense Precambrian rocks lie at high elevations. To illustrate this effect, the complete Bouguer anomaly field calculated using a reduction density of 2450 kg/m^3 (Fig. B9a) was subtracted from the gravity field computed using variable densities (Fig. B7). This result (Fig. B9b) is negative in sign over areas where the field calculated using a single reduction density of 2450 kg/m^3 is probably too high (i.e., inappropriate for rocks with higher densities) and positive where rocks may be less dense than 2450 kg/m^3 . Negative values lie over the Needle Mountains, showing that the variable density approach is likely necessary to most appropriately represent the gravity field there *and* over the SJVF simultaneously. Positive values of significant amplitude ($>3 \text{ mGal}$) lie over regions where the topographic relief is high and may not be adequately represented by the 90 m digital elevation data used in the variable density calculation.

The location of the batholith complex margin was interpreted from the horizontal gradient magnitude (HGM) of the new gravity map. This method is based on the principle that for the case of vertical boundaries, the gravity field's largest-magnitude gradients in the horizontal direction are located over the edges of density contrasts (Cordell, 1979; Blakely and Simpson, 1986). The method is therefore useful for detecting geologic contacts. Here, the HGM was calculated from the new gravity map after upward continuation of 5 km, in order to attenuate effects of near-surface sources (Fig. B10). The batholith complex margin, assumed to be vertical, was interpreted from the result, and the location is similar to the previously interpreted extent for the western, southern, and northern portions of the complex (Fig. B3) (Plouff and Pakiser, 1972). However, the interpreted eastern margin of the batholith complex was extended significantly to the east, such that it nearly reaches the western margin of the San Luis Basin (compare Figs. B3 & B7). The interpreted area of the complex in map view is 8200 km².

SEISMIC & GRAVITY MODELING

The vintage, analog seismic refraction profiles (A-A', Fig. B1) were also reinterpreted in order to provide subsurface constraints on gravity models made from the new gravity map. First-break times were picked from analog paper records provided by C. Prodehl, and were modeled using MacRay (Luetgert, 1992), a ray-tracing forward modeling program (Fig. B11). The pick error is assumed to be 0.2-0.3 seconds, due to poor quality of the original records (by modern standards). Picks were not significantly different from those originally made by Prodehl and Pakiser (1980).

Gravity and seismic refraction data were modeled in an integrated fashion along profiles A-A', B-B', and C-C'. The fundamental assumption underlying the following discussion is that the source of the gravity low is the same as the source of the seismic low velocity zones. Whereas not specifically addressed by previous studies, this assumption makes sense, as the source body interpreted by gravity data analysis (Plouff and Pakiser, 1972) occupies the same portion of the upper crust occupied by the sources of seismic low velocity zones (Prodehl and Pakiser, 1980) and low seismic velocities are normally correlated with low densities. This common source is interpreted to be a silicic Oligocene-age batholith complex. Because seismic refraction is a useful method for detecting broad variations of velocity with depth, the seismic modeling was used to define the top and bottom of the complex, and the gravity HGM map (Fig. B10) was used to define its lateral boundaries in the models. Other assumptions used to make the models presented here are that the complex lies entirely below an elevation of 7500' (2286 m), which the seismic model supports (see below), and that its density contrast with upper crustal rocks remains constant with depth.

The first step was to develop a crustal P-wave velocity model that satisfied the first break picks made from the seismic data along profile A-A', a short distance to the east of the central caldera cluster (Fig. B7). This was done from the shallow subsurface downward, adjusting layer thicknesses and velocities of refractors until the observed data were fit in a broad sense (Fig. B11). It was not reasonably possible to fit the arrival time of every first break pick, although this was not necessarily desirable due to the low spatial resolution and large possible time errors inherent in the data. Velocities averaging 4.1 km/s were used extending from the surface to a depth corresponding roughly to sea level,

where a very high velocity (6.2 km/s) refractor is interpreted. This may indicate Precambrian rocks under the eastern margin of the central caldera cluster.

Two low velocity zones lie within the upper crust (0-20 km depth below sea level), shown by rapid terminations of refraction arrivals (Fig. B11). These zones were modeled using a variety of different velocities, and velocities ranging from 5.8 to 6.0 km/s were found to allow reasonable fits to the observed data. Attempts to model the low velocity zones with values outside of this range resulted in refractor crossover distances and times that were inconsistent with the observed data. Because the velocity of rocks composing the low-velocity zones cannot be uniquely determined, there is a tradeoff between velocity and low-velocity zone thickness such that higher velocities result in a larger required thickness and lower velocities result in smaller required thickness. This tradeoff is expressed in terms of different batholith complex thicknesses for different velocities (Table B2). The best fit and hence preferred seismic model uses a velocity of 5.9 km/s for the low velocity zones that are interpreted to define the complex (Fig. B11).

The low-velocity zones are separated by a refractor with a velocity of 6.3 km/s. The shallowest low velocity zone is apparent in reversed arrivals (e.g. shown by seismic arrivals from both north and south directions) and is therefore a robust feature of the model. The same is true of the 6.3 km/s refractor. However, the deeper low velocity zone is only detected in seismic data from the northern shot, due to a lack of receivers south of the southern shot (Fig. B11), and hence is a less robust feature despite providing a reasonable fit to the observed data. The gravity model along profile A-A' was constructed to match the upper crustal configuration indicated by the seismic model (see discussion below, Fig. B12).

For profile B-B', the first step of the gravity modeling was to define the regional field, because this profile is coincident in location with the model of Roy et al. (2004) where the regional field and interpreted source were first defined. The same source of low densities in the mantle is used here: a ~300 km wide, ~200 km thick zone with a density contrast of -33 kg/m^3 with surrounding mantle rocks. However, Roy et al. (2004) only defined the regional field in an east-west direction. The upward continued gravity data were used as a rough guide to extend the interpreted regional source to the south and northwest (Fig. B5) to profile C-C'. The northern extent of the regional source (end of A-A') is more difficult to define because the regional gravity low over the SJVF merges with a broader regional low over much of central Rocky Mountains of Colorado. The continuation of the low to the north of A-A' may be related to a number of different sources, including isostatic crustal thickening under the Rocky Mountains, and therefore does not necessarily indicate a continuation of low mantle densities north of A'. Given this uncertainty, the north edge of the low densities in the mantle was initially left loosely defined along A-A'.

The next step was to use the top and bottom contacts of the batholith interpreted by seismic modeling in the gravity model along A-A', using the lateral position of the batholith edges from the HGM analysis (Fig. B10). These contacts were extended to B-B' and C-C' (Fig. B12). Modeling of the three profiles together allowed an overall best fit density contrast for the batholith complex to be determined, as well as variations in thickness away from A-A'. Once the gravity signature of the complex was determined across all three profiles, the location of the northern edge of the mantle low density zone was adjusted until the model along A-A' fit the observed data as shown on Fig. B12. The

entire process of using the seismic model to constrain the gravity interpretation was repeated using the range of reasonable velocities for the batholith complex (Table B2), although only the preferred models are shown here (Fig. B12). The seismic refractor that lies between the two low velocity zones was included in all the gravity profiles because it is a robust feature of the seismic model, although this was not required by the gravity data.

For the preferred model, the computed density contrast was a value of 80 kg/m^3 , corresponding to a batholith complex density of 2620 kg/m^3 if a background upper crustal density of 2700 kg/m^3 is assumed (only the density contrast can be uniquely determined). This contrast could reasonably be varied from -60 to -110 kg/m^3 for seismic velocities of 6.0 and 5.8 km/s , respectively (Table B2). All modeling runs showed the batholith complex to be significantly thicker under the western portion of the SJVF than under the central and eastern portions (Fig. B12). The preferred model shows a maximum thickness of about 20 km under the western SJVF that decreases eastward to $< 10 \text{ km}$ under the eastern SJVF. The model that produced a maximum thickness of 23 km , corresponding to a density contrast of -80 kg/m^3 , is consistent with the thickness estimate of Plouff and Pakiser (1972). However, the thickness estimate range presented here is generally thinner than the previous estimate, due to the modeling approach taken here that resulted in a low-amplitude gravity low. Assuming an area of 8200 km^2 (from the HGM analysis, Fig. B10) and using thickness estimates from the gravity modeling, the volume of the complex was estimated to be $82,000$ to $130,000 \text{ km}^3$ (Table B2).

DISCUSSION

Assuming that the source of the gravity low is the same as the source of the seismic low velocity zones, and that the density of the interpreted batholith complex doesn't change significantly with lateral position, integrated modeling can be used to infer the batholith's dimensions. The thickest part (15-23 km, Table B2) of the complex lies under the western SJVF and the western caldera cluster, where there are four nested calderas on the surface. The complex is thinner under the central caldera cluster, with seven calderas, showing that there is not a direct relationship between batholith thickness and the number of calderas on the surface. This supports petrologic and chronologic interpretations that the batholith complex continued to accumulate after volcanism ended, and that the batholith remaining today is not necessarily representative of magma chambers that existed during volcanic eruptions and caldera formation (Lipman, 2007). A more direct relation between batholith thickness and caldera clustering would be expected if the complex represented fossil magma chambers that were tapped by surficial volcanism.

Despite the fact that the batholith complex is shown here to have constant physical properties and simple boundaries, it almost certainly was assembled over a long period of time (e.g., several million years), is composed of rocks emplaced in multiple episodes with different densities, and has complex boundaries. The simple models presented here are only approximations of its properties and dimensions, which were chosen to be consistent with the seismic model. For example, batholiths are thought to become more mafic in composition and thus denser with increasing depth, although with no constraints on increasing density with depth, any models with this characteristic would

be quantitatively arbitrary and were not attempted here. Also, the top and bottom of the complex may not correspond well to boundaries that would be picked based on petrologic analyses. Despite these limitations, the overall densities (2590-2640 kg/m³) determined for the batholith, assuming an upper-crustal background density of 2700 kg/m³, are consistent with published values for granite densities (Daly et al., 1966; Telford et al., 1990), as well as density measurements on outcropping granites of the SJVF (Popenoe and Steven, 1969; Popenoe and Luedke, 1970; Grauch and Hudson, 1987) and similar rocks thought to be the source of the large gravity low over the Aspen-Gunnison region (Tweto and Case, 1972; Isaacson and Smithson, 1976).

The interpreted density range of 2590-2640 kg/m³ assumes an overall upper-crustal density of 2700 kg/m³, a value that is commonly assumed for gravity studies but may or may not be valid in the SJVF region. The density contrast between the batholith complex and surrounding rocks, however, can be uniquely determined. The range of permissible values, -60 to -110 kg/m³, particularly the preferred value of -80 kg/m³, compares favorably to the few other studies that have examined the geophysical expressions of large batholiths and have included joint seismic and gravity modeling: The inferred batholith under the Mogollon-Datil volcanic field of New Mexico and Arizona (Fig. B1), was interpreted to have a density contrast of -100 kg/m³ (Schneider and Keller, 1994). The Boulder batholith of Montana, similar in dimensions and interpreted thickness to the SJVF batholith complex (Biehler and Bonini, 1969), was found by joint seismic reflection and gravity modeling to have a density contrast of -80 kg/m³ (Vejmelek and Smithson, 1995).

The main source of the gravity low is interpreted to be an Oligocene batholith complex. However, elsewhere in the southern Rocky Mountain region Precambrian granitic intrusions are interpreted to cause gravity lows (Quezada et al., 2004), and numerous Precambrian granites crop out on the northern and southwestern margins of the SJVF (Fig. B2). Therefore, possibly significant contributions to the gravity low from Precambrian granites buried under the SJVF cannot be ruled out, especially because their distribution at depth is not known.

Another assumption in the gravity modeling and the interpreted thickness distribution is that the density of the batholith complex does not vary vertically or laterally. As discussed above, although batholith density may be expected to vary vertically, it is difficult to model these variations in a meaningful way because nothing is known of the batholith at depth. Lateral density variations are also possible, as observed dramatically within the Sierra Nevada batholith in California (Oliver, 1977; Oliver et al., 1993). Such variations within the SJVF batholith would change the interpretation of lateral thickness patterns. However, this is difficult to address quantitatively because the batholith complex cannot be sampled for densities. Existing density measurements are confined to the western portion of the study area and further may not be representative of the petrology and density of the deeper batholith (Lipman, 2007).

The batholith complex underlying the SJVF is expressed seismically by relatively low velocities compared to surrounding upper crustal rocks. Numerous studies have interpreted seismic low-velocity zones indicate magma chambers under active caldera systems of similar scale to the SJVF (de Silva, 1989; Chmielowski et al., 1999; Zandt et al., 2003; de Silva et al., 2006; Bachmann et al., 2007), although this study is one of few

to interpret low velocities for a batholith. A similar interpretation was made for the batholith under the Mogollon-Datil volcanic field (Schneider and Keller, 1994), comparable in age to the SJVF and also along the western margin of the Rio Grande rift (Fig. B1). A 1-2 km thick refractor (e.g., high velocity zone) between two low velocity zones is found to be a robust feature of the seismic model along A-A'. The geologic significance of the refractor is unknown, although it has a higher velocity than low-velocity zones that lie above and below. Its presence and geometry are not constrained by the gravity data and modeling, although gravity models along B-B' and C-C' show it in order to maintain consistency with the models along A-A' (Fig. B12).

A relationship may exist between batholith complex thickness and the elevation of the overlying ground surface. The thickest part of the complex is interpreted to underlie the western SJVF, spatially coincident with the highest elevations of the San Juan Mountains (Figs. B4 & B12). Whereas not addressed quantitatively, this observation is consistent with a previous hypothesis that thick, low-density batholiths may cause uplift of overlying rocks on the order of hundreds to several hundreds of meters (Lipman, 1988, 2007).

The lower crust and upper mantle are not well imaged by the seismic refraction data, although an upper mantle low-density zone has been previously interpreted to lie under the SJVF (Roy et al., 2004). The source of the low densities is interpreted to be de-densified residuum left behind from extraction of basaltic melt into the lower crust, and the interpretation of this zone is herein extended from two dimensions to three.

CONCLUSIONS

A new approach to gravity data processing, one that uses geologically appropriate densities and digital topography to represent areas of high elevations, was used to compute a new “complete Bouguer anomaly-like” gravity map of the San Juan Mountains region. Traditional methods of gravity data processing break down there, due to high elevations composed of rocks of the San Juan volcanic field (SJVF) that have densities significantly lower than the standard Bouguer correction density (2670 kg/m^3). A large-amplitude gravity low over the region has long been interpreted to reflect a silicic Oligocene batholith complex that is related to the SJVF, although this anomaly was reduced in amplitude by 10-15 mGals by the processing approach used here.

The enhanced gravity expression of the interpreted batholith complex was modeled quantitatively in conjunction with reinterpreted seismic refraction data that image thick low-velocity zones in the upper crust beneath the SJVF. Assuming that the source of both the gravity low and the source of the low seismic velocities is an Oligocene batholith, a series of two-dimensional modeling runs indicated that the batholith has an overall density contrast of -60 to -110 kg/m^3 with surrounding upper crustal rocks, an overall density of 2590-2640 kg/m^3 , and an estimated volume of 82,000 to 130,000 km^3 . The interpreted density contrasts, densities, and inferred seismic expression of the batholith are consistent with other similar intrusions in the western U.S.

The batholith complex is thickest under the western SJVF, as much as ~ 20 km in the best-fit model, and thins to < 10 km under the eastern SJVF. The thickness pattern is not correlated with clustering of calderas on the surface, in that the largest caldera cluster does not overlie the thickest part of the complex. This is consistent with the latest

petrologic interpretations that the complex continued to be modified following cessation of volcanism, and therefore is not necessarily representative of syn-volcanic magma chambers. Batholith complex thickness is instead better correlated with areas of high elevation, implying that the batholith may have caused moderate amounts of surface uplift.

Thicknesses presented here are overall smaller than previously estimated (~24 km), due to the use of the enhanced gravity processing technique that reduced the amplitude of the gravity low over the SJVF.

Table B1. Surficial densities used to calculate new gravity map

<u>Geologic Unit</u>	<u>Density (kg/m³)*</u>
Oligocene volcanic rocks of San Juan volcanic field (SJVF)	2450
Intermediate composition plutons of SJVF	2550
Mafic plutons of Needle Mountains (small volumes)	2900
Default density for unassigned units and granitic plutons of Needle Mountains	2670

*Values from R. Gries, written comm. (2007), Grauch and Hudson (1987), Jenkins (1989), Popenoe and Luedke (1970), Popenoe and Steven (1969), and Telford et al. (1990)

Table B2. Range of reasonable batholith complex properties from joint seismic and gravity modeling

<u>Model</u>	Average A-A' thickness (km)	Minimum overall thickness (km)*	Maximum overall thickness (km)*	Total volume (km ³)**	Average density contrast (kg/m ³)	Density of batholith (kg/m ³)***
Seismic Model A-A', 5.8 km/s assigned to low-velocity zone	8.3	4.5	15.0	82,000	110	2590
Seismic Model A-A', 5.9 km/s assigned to low-velocity zone (preferred model)	9.8	7.6	19.9	110,000	80	2620
Seismic Model A-A', 6.0 km/s assigned to low-velocity zone	11.8	7.7	23.0	130,000	60	2640

*across all three gravity profile models

**based on interpreted total batholith area of 8200 km² and average of modeled thicknesses along gravity profiles

***assumes surrounding rocks have density of 2700 kg/m³

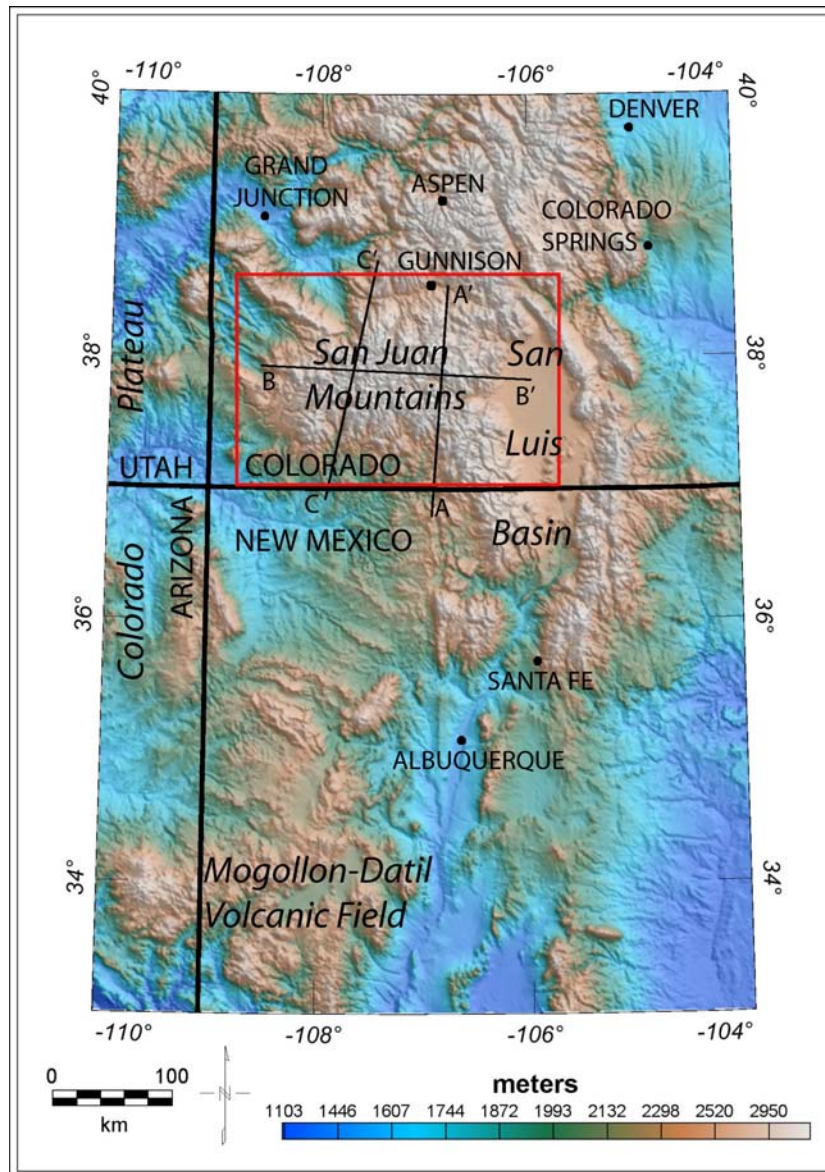


Figure B1: Physiography and geography of the San Juan Mountains region. Red box defines area of this study and subsequent figures. Locations of gravity profiles that were modeled are shown as A-A', B-B', and C-C'.

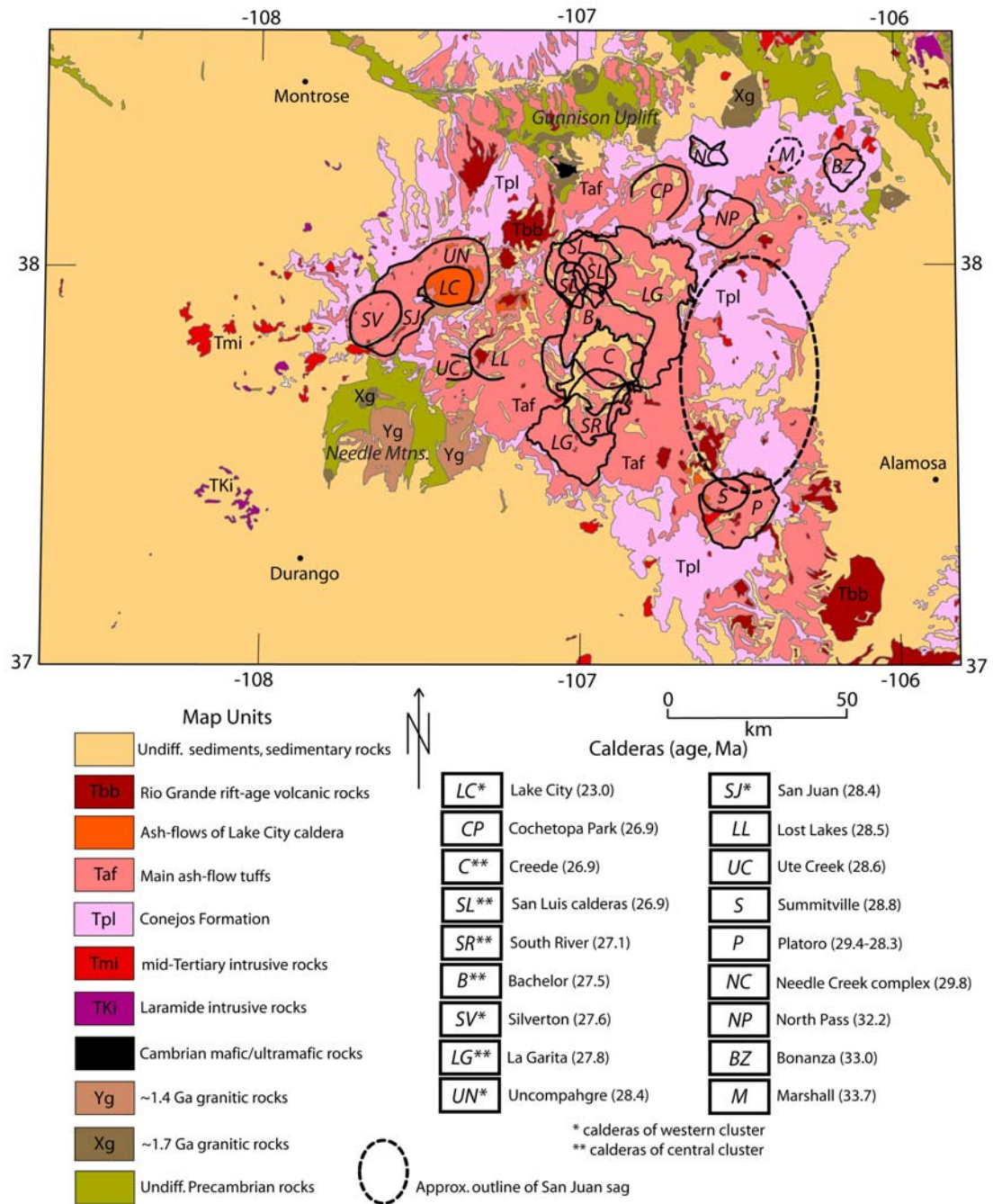


Figure B2: Simplified geology of the study area. Geology modified from Tweto (1979), Lipman (2000), Lipman (2006), and Lipman and McIntosh (2008). Approximate outline of San Juan sag after Brister and Chapin (1994).

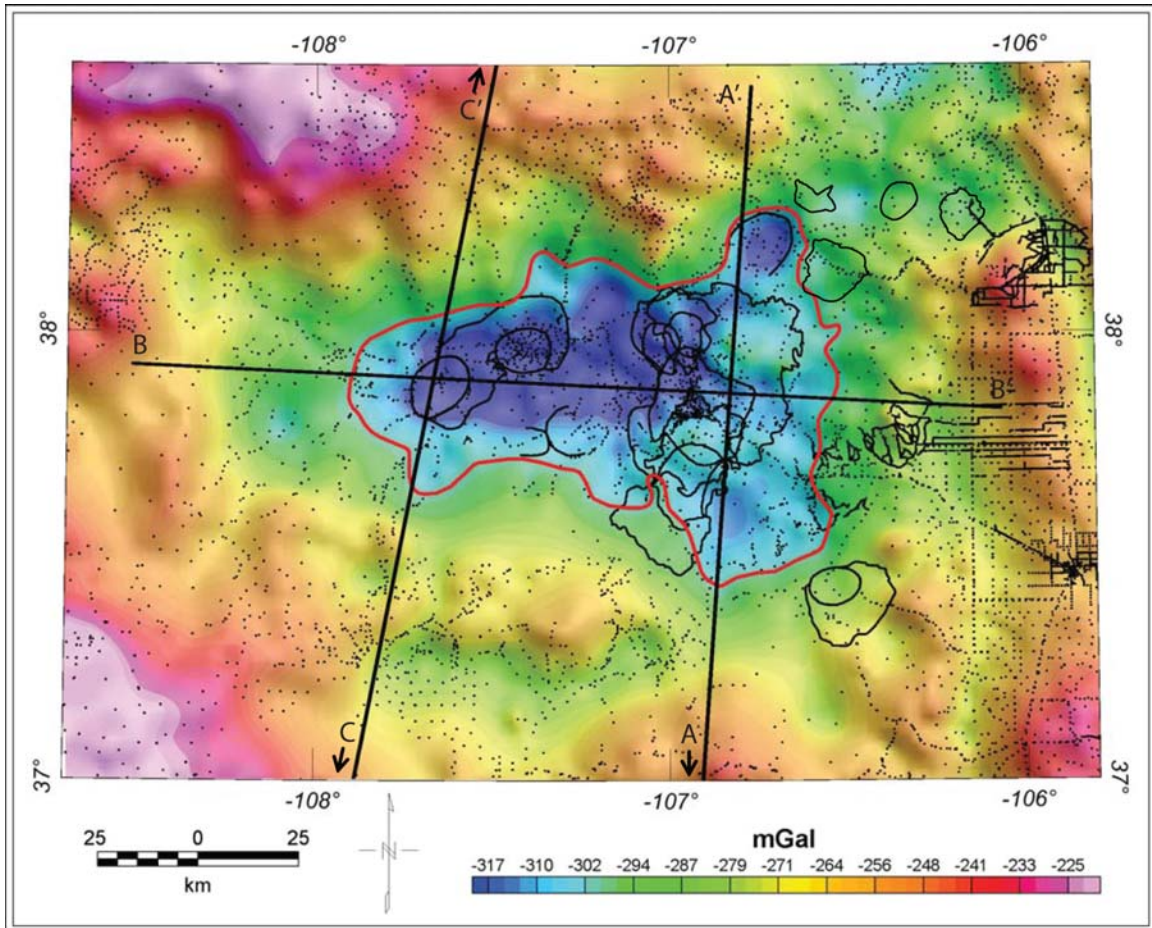


Figure B3: Conventional complete Bouguer anomaly map of the study area. Caldera outlines from Fig. B2 included for reference. Black dots are gravity stations. Locations of gravity profiles that were modeled are shown as A-A', B-B', and C-C'. Red polygon is interpreted extent of batholith from Plouff and Pakiser (1972).

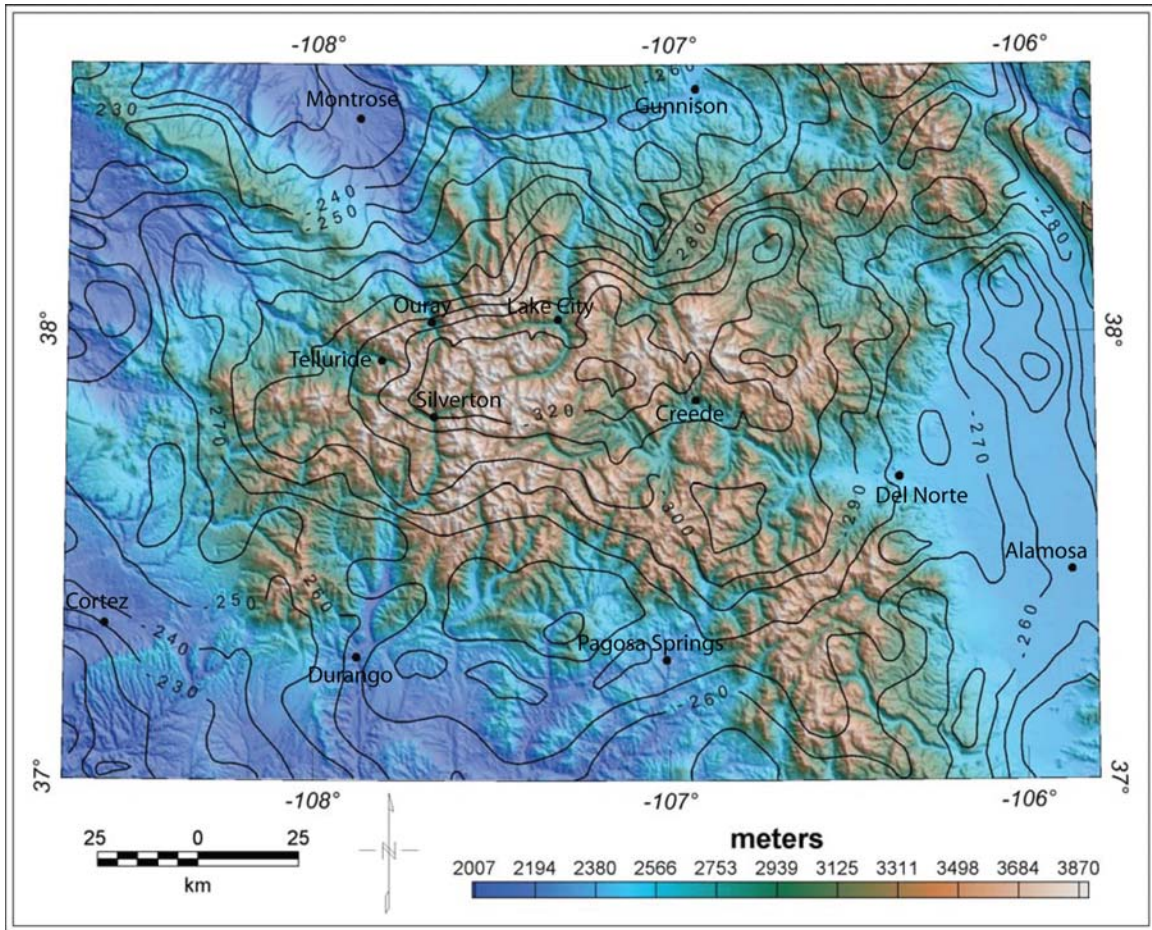


Figure B4: Elevation map of the study area. Cities are shown as black circles. Black contours are conventional complete Bouguer anomaly values in mGal.

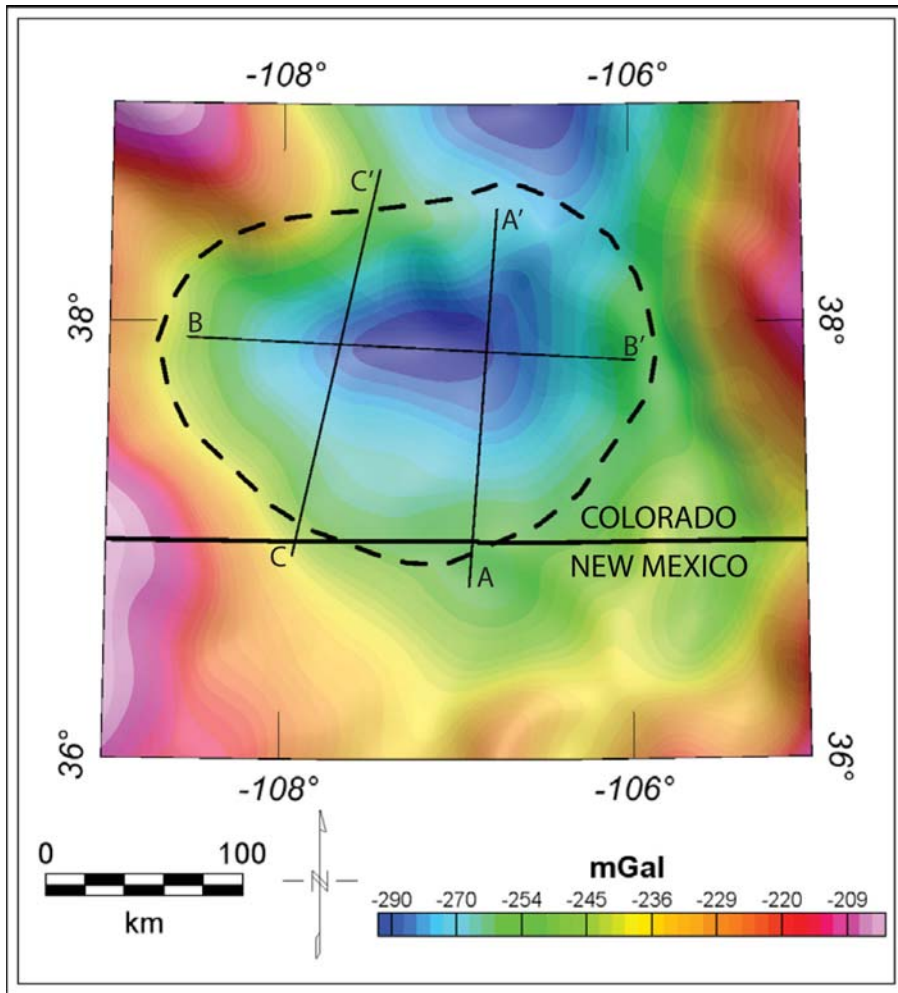


Figure B5: Upward-continued conventional complete Bouguer anomaly values for the SJVF region. Continuation distance 10 km. Locations of gravity profiles that were modeled are shown as A-A', B-B', and C-C'. Dashed polygon shows interpreted extent of source of long-wavelength gravity low.

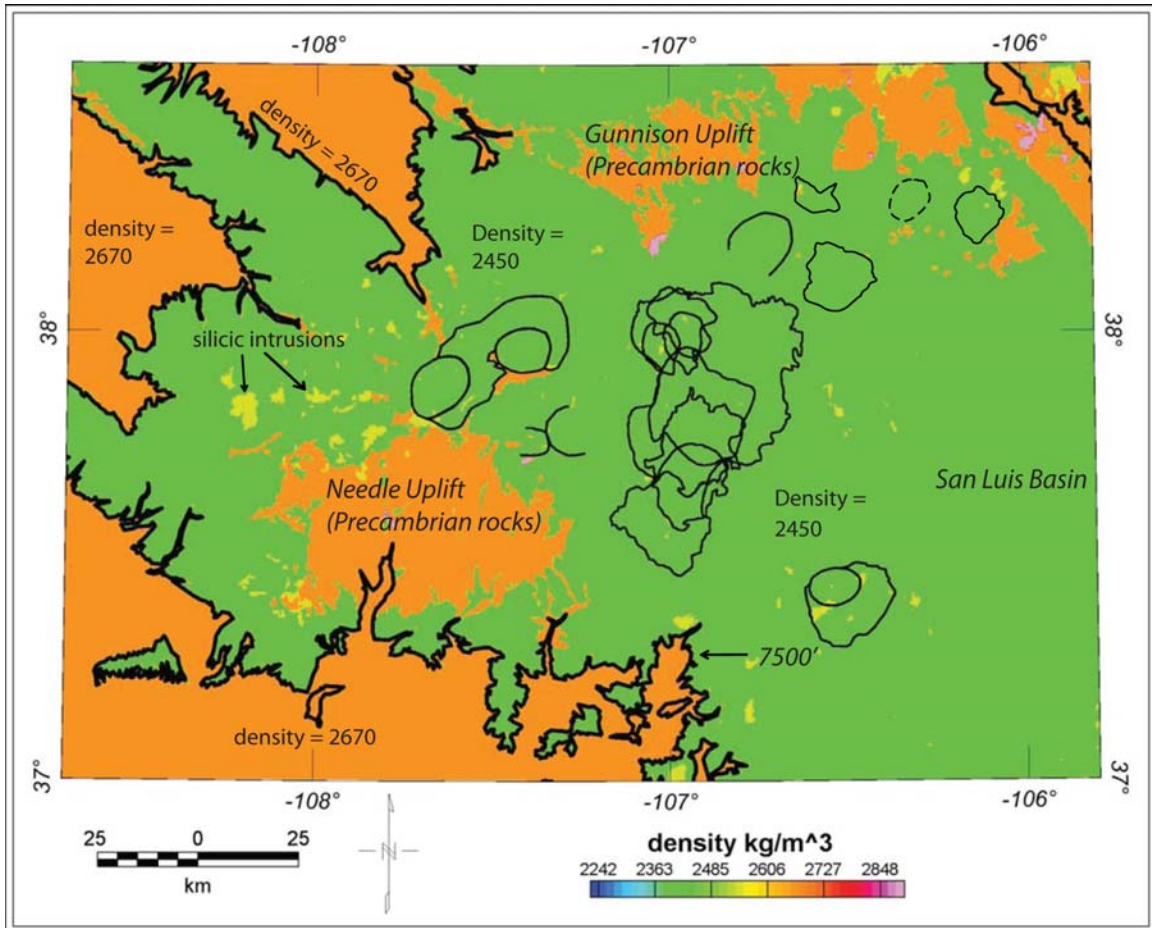


Figure B6: Density model used for all rocks above elevation of 7500 feet (2286 m). Heavy black line indicates 7500-foot elevation contour; all rocks below this level were assigned a standard density of 2670 kg/m³. The units for all densities are kg/m³. High and low densities, represented by extreme ends of the color scale, are small in extent (thus difficult to see) at the scale of this figure.

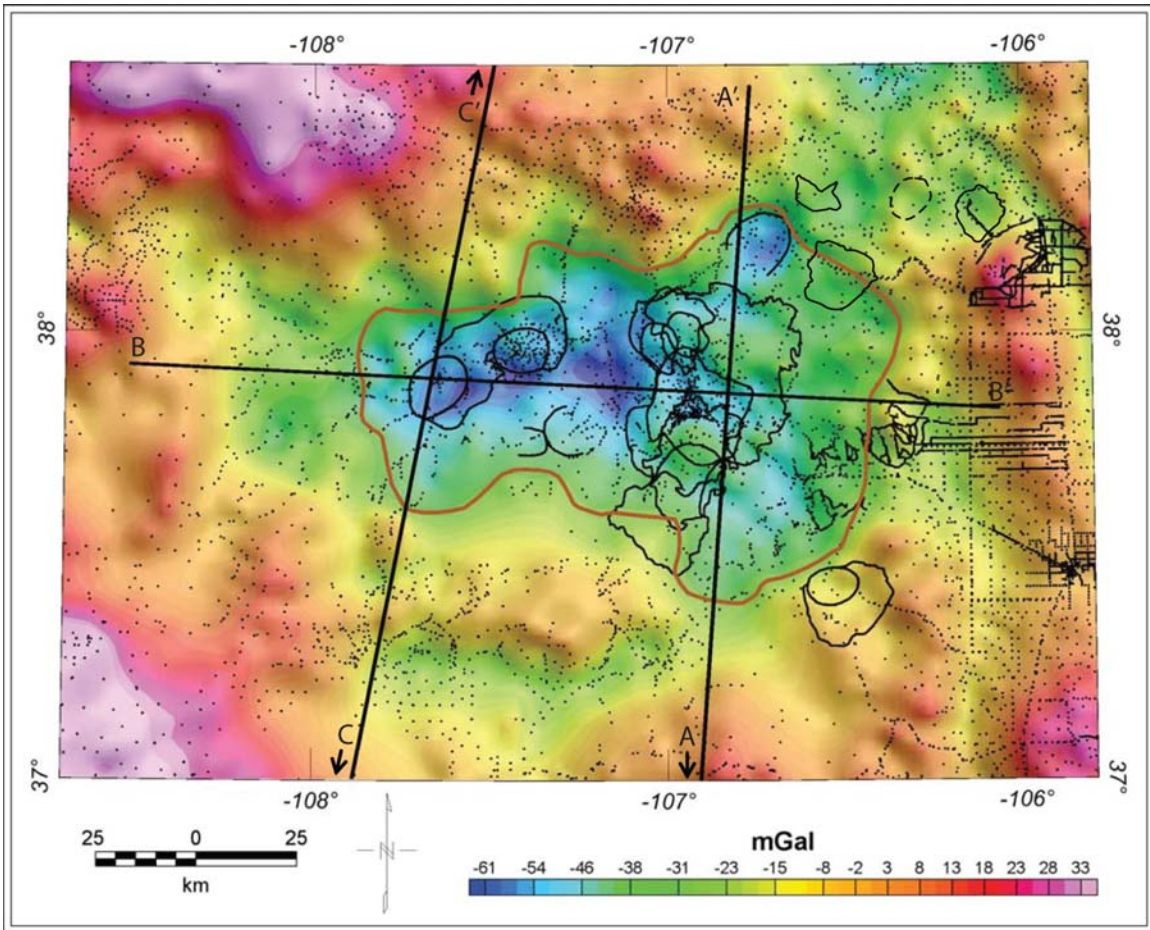


Figure B7: New “complete Bouguer anomaly-like” gravity anomaly map of the study area, Brown polygon is new interpretation of batholith margin based on horizontal gradient magnitude (HGM) trends (see Fig. B9).

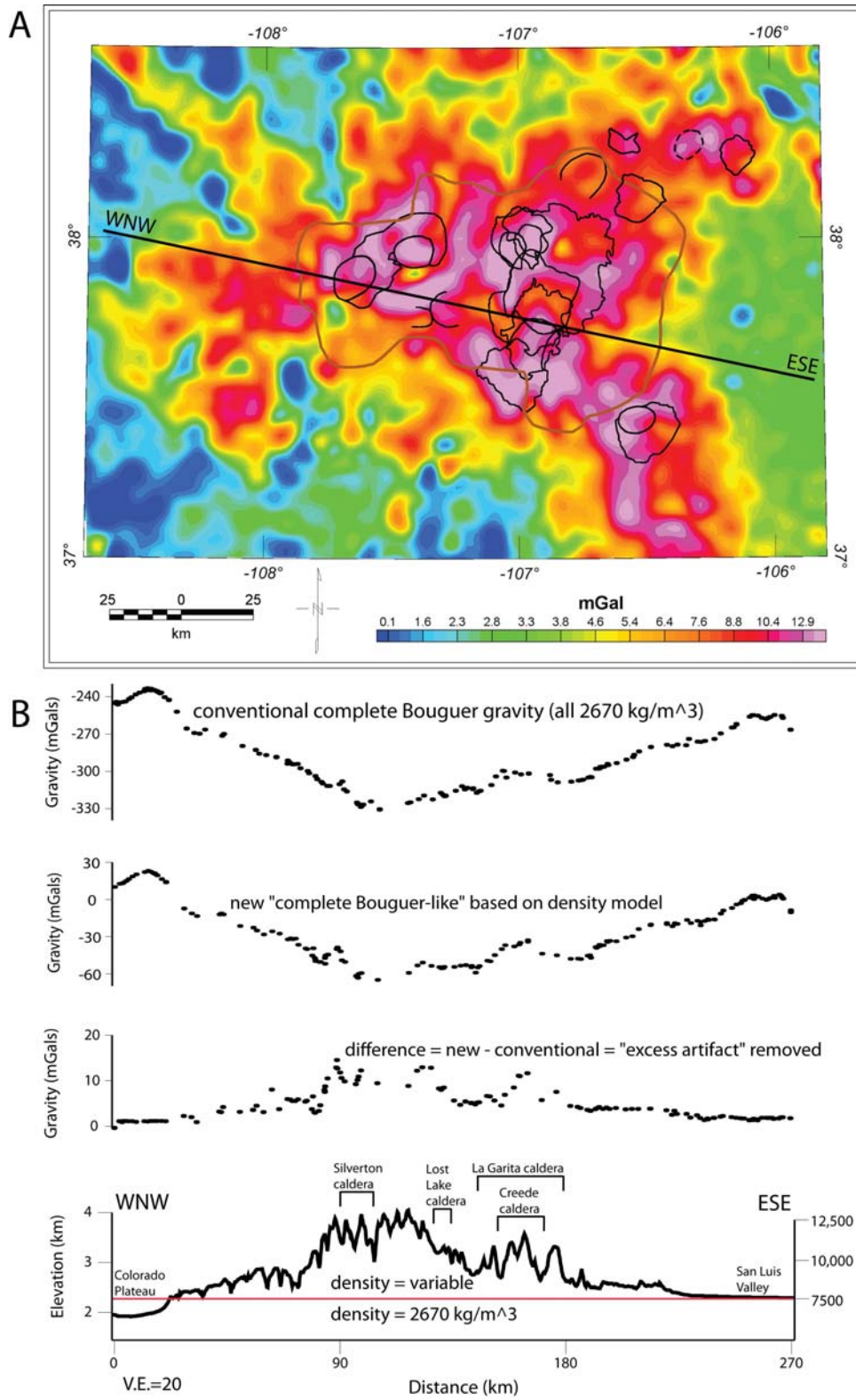


Figure B8: Difference between new and conventional gravity anomaly maps, in map form (A) and profile (B).

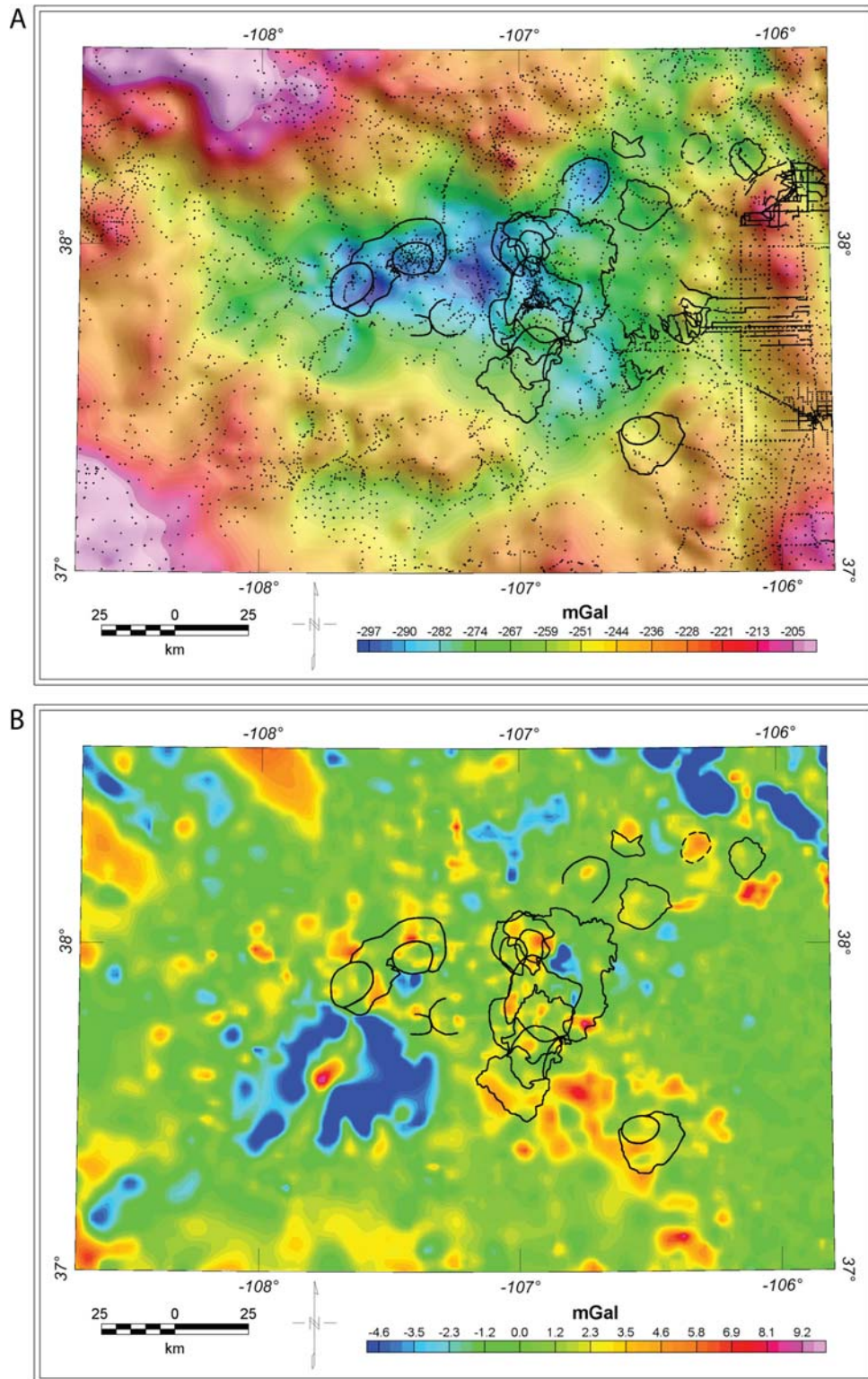


Figure B9: Complete Bouguer anomaly map using 2450 kg/m³ as the reduction density (A), and difference (B) with new “complete Bouguer anomaly-like” map (Fig. B7). Negative values on (B) indicate regions of higher density than 2450 kg/m³, and positive values indicate regions of lower density than 2450 kg/m³.

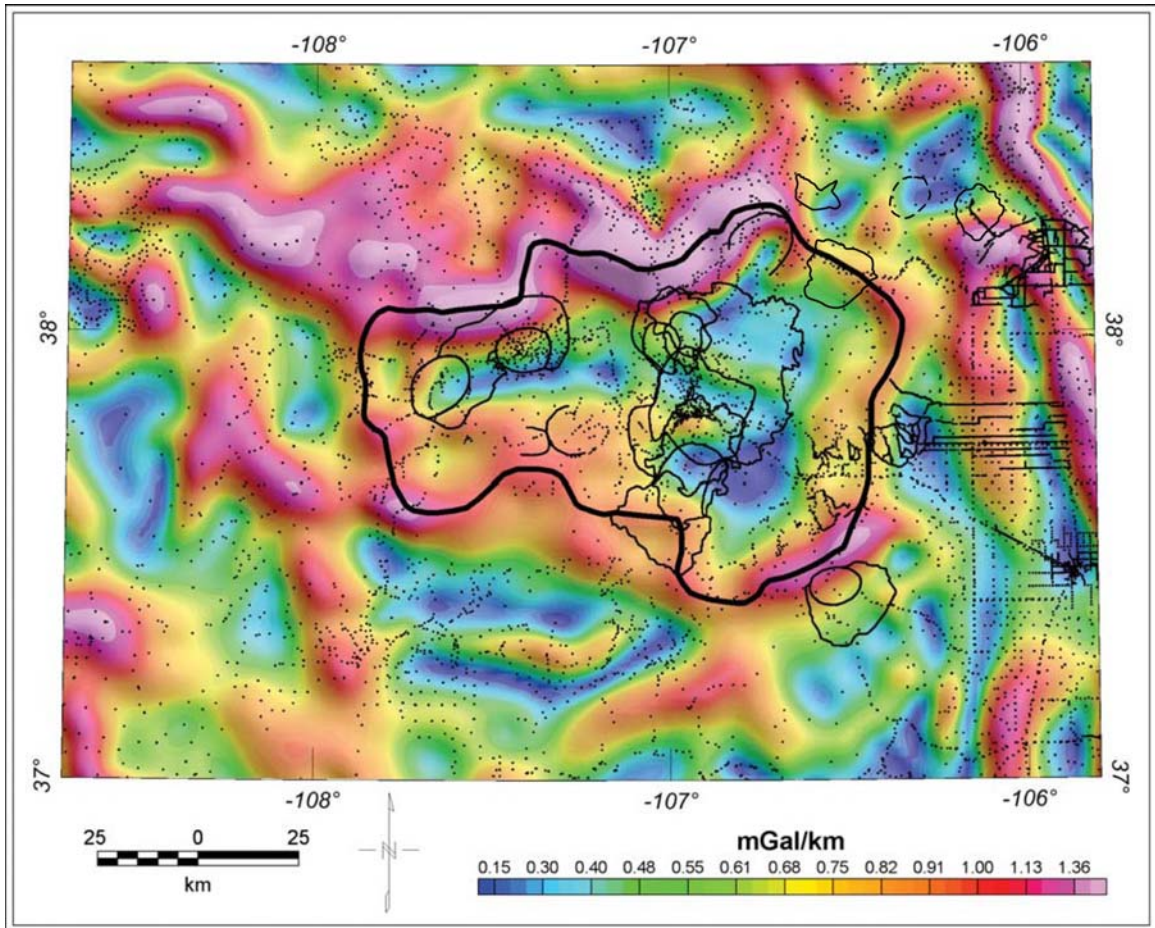


Figure B10: Horizontal gradient magnitude (HGM) of new gravity anomaly map (Fig. B7) after upward-continuation 5 km. Thick black line is the interpreted margin of the batholith complex.

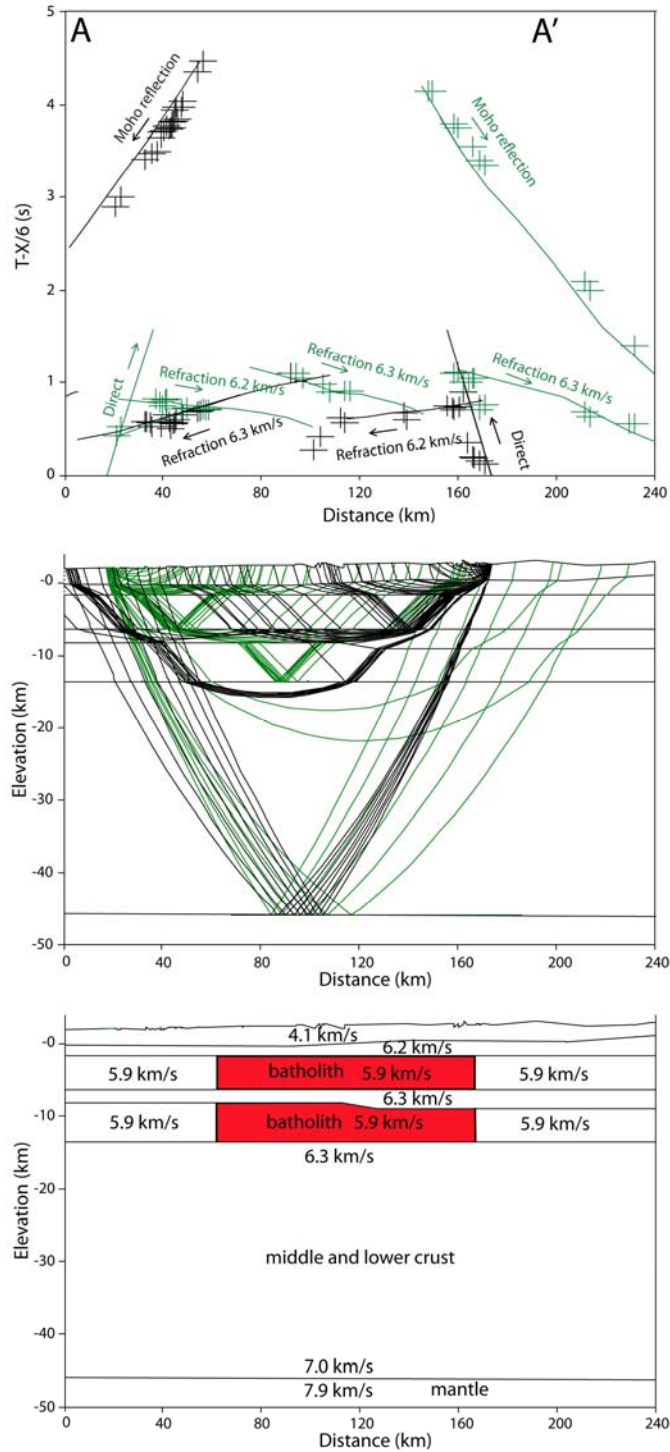


Figure B11: Seismic refraction first break picks and predicted response (top panel), ray paths through the model (middle panel), and interpretation of the best-fit seismic model (bottom panel). Black colors indicate northward-traveling seismic energy, green colors indicates southward-traveling seismic energy. Pick sizes chosen to represent amount of uncertainty. Zero elevation corresponds to sea level. Note that seismic model length is greater than A-A' length.

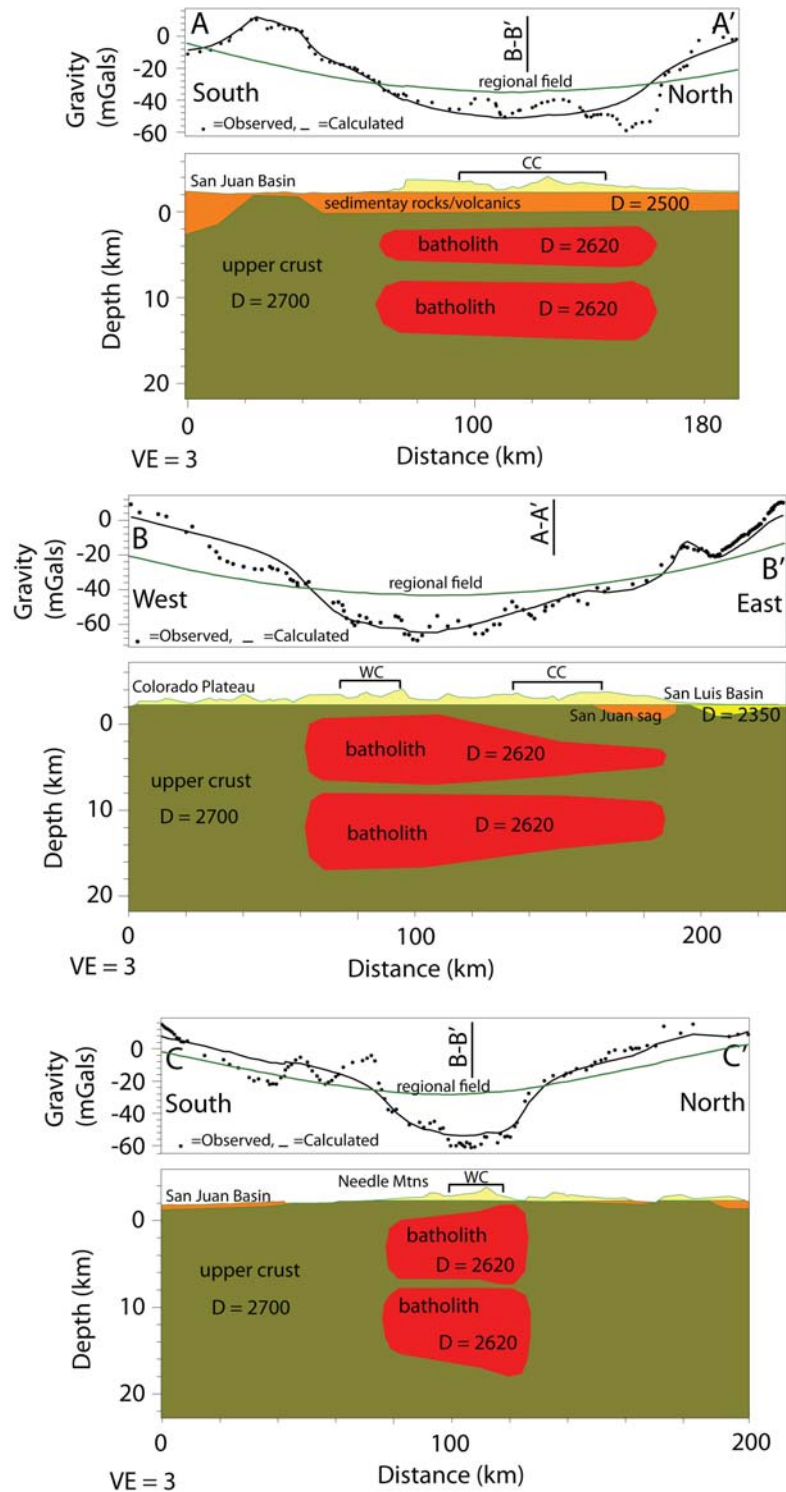


Figure B12: Gravity profile models along A-A' (top panel), B-B' (middle panel), and C-C' (bottom panel). The units for all densities (D) are kg/m^3 . Yellow regions indicate rocks above 7500-foot (2286 m) elevation. "WC" stands for western caldera cluster. "CC" stands for central caldera cluster. Green lines labeled "regional field" indicate the gravitational effect of a low-density zone within the upper mantle (see text).

REFERENCES

- Anderson, J.L., and Cullers, R.L., 1999, Paleo- and Mesoproterozoic granite plutonism of Colorado and Wyoming: *Rocky Mountain Geology*, v. 34, p. 149-164.
- Bachmann, O., Miller, C.F., and de Silva, S.L., 2007, The volcanic-plutonic connection as a stage for understanding crustal magmatism: *Journal of Volcanology and Geothermal Research*, v. 167, p. 1-23.
- Bickford, M.E., and Anderson, J.L., 1993, Middle Proterozoic magmatism, *in* Reed, J.C., Bickford, M.E., Houston, R.S., Link, P.K., Rankin, D.W., Sims, P.K., and Van Schmus, W.R., eds., *The Geology of North America v. C2*, Geological Society of America, p. 281-292.
- Biehler, S., and Bonini, W.E., 1969, A regional gravity study of the Boulder batholith, Montana, *Igneous and Metamorphic Geology: Geological Society of America Memoir 115*, p. 401-422.
- Blakely, R.J., 1995, *Potential Theory in Gravity and Magnetic Applications*: Cambridge University Press, 441 p.
- Blakely, R.J., and Simpson, R.W., 1986, Approximating edges of source bodies from magnetic or gravity anomalies: *Geophysics*, v. 51, p. 1494-1498.
- Bott, M.H.P., and Smithson, S.B., 1967, Gravity investigations of subsurface shape and mass distributions of granite batholiths: *Geological Society of America Bulletin*, v. 78, p. 859-878.
- Brister, B.S., and Chapin, C.E., 1994, Sedimentation and Tectonics of the Laramide San Juan sag, southwestern Colorado: *The Mountain Geologist*, v. 31, p. 2-18.
- Casillas, H., 2004, *An integrated geophysical study of the Uncompahgre uplift, Colorado and Utah [Master's thesis]*: The University of Texas at El Paso, 151 p.

- Cather, S.M., 2004, Laramide orogeny in central and northern New Mexico and southern Colorado, *in* Mack, G.H., and Giles, K.A., eds., *The Geology of New Mexico: A Geologic History*: New Mexico Geological Society Special Publication 11, p. 203-248.
- Chmielowski, J., Zandt, G., and Haberland, C.H., 1999, The central Andean Altiplano-Puna magma body: *Geophysical Research Letters*, v. 26, p. 783-786.
- Cordell, L., 1979, Gravimetric expression of graben faulting in Santa Fe country and the Espanola basin, New Mexico, *in* Ingersoll, R.V., ed., *Guidebook to Santa Fe Country*, 30th Field Conference, New Mexico Geological Society, p. 59-64.
- Cordell, L., and Keller, G.R., 1984, Regional structural trends inferred from gravity and aeromagnetic data in the New Mexico-Colorado border region: *New Mexico Geological Society Guidebook*, 35th Field Conference, Rio Grande Rift: Northern New Mexico, p. 21-23.
- Cordell, L., Long, C.L., and Jones, D.W., 1985, Geophysical expression of the batholith beneath Questa caldera, New Mexico: *Journal of Geophysical Research*, v. 90, p. 11263-11269.
- Crain, K.D., 2006, Three dimensional gravity inversion with a priori and statistical constraints [Ph.D. thesis]: The University of Texas at El Paso, 62 p.
- Daly, R.A., Manger, E., and Clark, S.P., 1966, Density of rocks, *in* Clark, S.P., ed., *Handbook of Physical Constants-- Revised Edition*, Geological Society of America Memoir 97, p. 19-26.
- de Silva, S.L., 1989, The origin and significance of crystal-rich inclusions in pumices from two Chilean ignimbrites: *Geological Magazine*, v. 126, p. 159-175.
- de Silva, S.L., and Gosnold, W.D., 2007, Episodic construction of batholiths: insights from the spatiotemporal development of an ignimbrite flare-up: *Journal of Volcanology and Geothermal Research*, v. 167, p. 320-335.

- de Silva, S.L., Zandt, G., Trumbull, R., and Viramonte, J., 2006, Large scale silicic volcanism - the result of thermal maturation of the crust, *in* Chen, Y.T., ed., *Advances in Geosciences*, World Scientific Press, p. 215-230.
- Dueker, K., Yuan, H., and Zureck, B., 2001, Thick-structured Proterozoic lithosphere of the Rocky Mountain region: *GSA Today*, v. 11, p. 4-9.
- Gonzales, D.A., and Van Schmus, W.R., 2007, Proterozoic history and crustal evolution in southwestern Colorado: Insight from U/Pb and Sm/Nd data: *Precambrian Research*, v. 154, p. 31-70.
- Grauch, V.J.S., and Hudson, M.R., 1987, Summary of natural remanent magnetization, magnetic susceptibility, and density measurements from the Lake City caldera area, San Juan Mountains, Colorado: U.S. Geological Survey Open-File Report 87-182, 23 p.
- Grauch, V.J.S., and Keller, G.R., 2004, Gravity and aeromagnetic expression of tectonic and volcanic elements of the southern San Luis Basin, New Mexico and Colorado, *in* Brister, B.S., Bauer, P.W., Read, A.S., and Lueth, V.W., eds., *New Mexico Geological Society Guidebook, 55th Field Conference, Geology of the Taos Region*, p. 230-243.
- Gries, R.R., 1985, San Juan sag: Cretaceous rocks in a volcanic-covered basin, south central Colorado: *The Mountain Geologist*, v. 22, p. 167-179.
- Hammer, S., 1974, Approximation in gravity interpretation calculations: *Geophysics*, v. 39, p. 205-222.
- Hinze, W.J., 2003, Bouguer reduction density: Why 2.67?: *Geophysics*, v. 68, p. 1559-1560.
- Isaacson, L.B., and Smithson, S.B., 1976, Gravity anomalies and granite emplacement in west-central Colorado: *Geological Society of America Bulletin*, v. 87, p. 22-28.
- Jenkins, R.D., 1989, An interpretation of basement structures from gravity anomalies in the central portion of the Colorado Plateau [M.S. thesis]: University of Texas at El Paso.

- Karlstrom, K.E., Amato, J.M., Williams, M.L., Heizler, M., Shaw, C.A., Read, A.S., and Bauer, P., 2004, Proterozoic tectonic evolution of the New Mexico region: a synthesis, *in* Mack, G.H., and Giles, K.A., eds., *The Geology of New Mexico: A Geologic History*, New Mexico Geological Society Special Publication 11, p. 1-34.
- Keller, G.R., Hildenbrand, T.G., Hinze, W.J., and Li, X., 2006, The quest for the perfect gravity anomaly: Part 2 -- Mass effects and anomaly inversion: Society of Exploration Geophysicists Technical Program Expanded Abstracts, v. 25, p. 864.
- Keller, G.R., Karlstrom, K.E., Williams, M.L., Miller, K.C., Andronicos, C., Levander, A.R., Snelson, C.M., and Prodehl, C., 2005, The dynamic nature of the continental crust-mantle boundary: Crustal evolution in the southern Rocky Mountain region as an example, *in* Karlstrom, K.E., and Keller, G.R., eds., *The Rocky Mountain Region: An Evolving Lithosphere: Tectonics, Geochemistry, and Geophysics: American Geophysical Union Geophysical Monograph 154*, p. 403-420.
- Kelley, V.C., 1955, Regional tectonics of the Colorado Plateau and relationships to the origin and distribution of uranium: University of New Mexico Publications in Geology no. 5, 120 p.
- Kluth, C.F., 1986, Plate tectonics of the Ancestral Rocky Mountains, *in* Peterson, J.A., ed., *Paleotectonics and Sedimentation in the Rocky Mountain Region, United States: American Association of Petroleum Geologists Memoir 41*, p. 353-369.
- Kluth, C.F., and Coney, P.J., 1981, Plate tectonics of the Ancestral Rocky Mountains: *Geology*, v. 9, p. 10-15.
- Larsen, E.E., Patterson, P.E., Curtis, G., Drake, R., and Mutschler, F.E., 1985, Petrologic, paleomagnetic, and structural evidence of a Paleozoic rift system in Oklahoma, New Mexico, Colorado, and Utah: *Geological Society of America Bulletin*, v. 96, p. 1364-1372.
- Lee, D.K., and Grand, S.P., 1996, Upper mantle shear structure beneath the Colorado Rocky Mountains: *Journal of Geophysical Research*, v. 101, p. 22,233-22,244.

- Lerner-Lam, A.L., Sheehan, A., Grand, S., Humphreys, E., Dueker, K., Hessler, E., Guo, H., Lee, D., and Savage, M., 1998, Deep structure beneath the Southern Rocky Mountains from the Rocky Mountain Front Broadband Seismic Experiment: *Rocky Mountain Geology*, v. 33, p. 199-216.
- Lipman, P.W., 1984, The roots of ash-flow calderas in North America: Windows into the tops of granitic batholiths: *Journal of Geophysical Research*, v. 89, p. 8801-8841.
- , 1988, Evolution of silicic magma in the upper crust: The mid-Tertiary Latir volcanic field and its cogenetic granitic batholith, northern New Mexico, U.S.A.: *Transactions of the Royal Society of Edinburgh, Earth Sciences*, v. 79, p. 265-288.
- , 2000, Central San Juan caldera cluster: Regional volcanic framework, *in* Bethke, P.M., and Hay, R.L., eds., *Ancient Lake Creede: Its Volcano-Tectonic Setting, History of Sedimentation, and Relation to Mineralization in the Creede Mining District*: Geological Society of America Special Paper 346, p. 9-69.
- , 2006, Geologic map of the central San Juan caldera cluster, southwestern Colorado: U.S. Geological Survey Geologic Investigations Series I-2799, 1:50,000 scale.
- , 2007, Incremental assembly and prolonged consolidation of Cordilleran magma chambers: evidence from the Southern Rocky mountain volcanic field: *Geosphere*, v. 3, p. 42-70.
- Lipman, P.W., Doe, B.R., Hedge, C.E., and Steven, T.A., 1978, Petrologic evolution of the San Juan volcanic field, southwestern Colorado: Pb and Sr isotope evidence: *Geological Society of America Bulletin*, v. 89, p. 59-82.
- Lipman, P.W., and McIntosh, W.C., 2008, Eruptive and noneruptive calderas, northeastern San Juan Mountains, Colorado: Where did the ignimbrites come from?: *Geological Society of America Bulletin*, v. 120, p. 771-795.
- Lipman, P.W., Steven, T.A., and Mehnert, H.H., 1970, Volcanic history of the San Juan Mountains, Colorado, as indicated by potassium-argon dating: *Geological Society of America Bulletin*, v. 81, p. 2327-2352.

- Luetgert, J.H., 1992, MacRay; interactive two-dimensional seismic raytracing for the Macintosh: U.S. Geological Survey Open-File Report 92-356, 45 p.
- Mason, B.G., Pyle, D.M., and Oppenheimer, C., 2004, The size and frequency of the largest explosive eruptions on Earth: *Bulletin of Volcanology*, v. 66, p. 735-748.
- McCoy, A.M., Roy, M., Trevino, L., and Keller, G.R., 2005, Gravity modeling of the Colorado Mineral Belt, *in* Karlstrom, K.E., and Keller, G.R., eds., *The Rocky Mountain Region: An Evolving Lithosphere: Tectonics, Geochemistry, and Geophysics: American Geophysical Union Geophysical Monograph 154*, p. 99-106.
- Oliver, H.W., 1977, Gravity and magnetic investigations of the Sierra Nevada batholith, California: *Geological Society of America Bulletin*, v. 88, p. 445-461.
- Oliver, H.W., Moore, J.G., and Sikora, R.F., 1993, Internal structure of the Sierra Nevada batholith based on specific gravity and gravity measurements: *Geophysical Research Letters*, v. 20, p. 2179-2182.
- Plouff, D., and Pakiser, L.C., 1972, Gravity study of the San Juan Mountains, Colorado: U.S. Geological Survey Professional Paper 800-B, p. 183-190.
- Popenoe, P., and Luedke, R.G., 1970, Interpretation of the aeromagnetic pattern of the Uncompahgre primitive area, San Juan Mountains, Colorado: U.S. Geological Survey Open-File Report 70-266, 26 p.
- Popenoe, P., and Steven, T.A., 1969, Interpretation of the aeromagnetic pattern of the San Juan primitive area, Colorado: U.S. Geological Survey Open-File Report 69-211, 7 p.
- Prodehl, C.P., and Pakiser, L.C., 1980, Crustal structure of the southern Rocky Mountains from seismic measurements: *Geological Society of America Bulletin*, v. 91, p. 147-155.
- Quezada, O., Andronicos, C., and Keller, G.R., 2004, Structure of the Sangre de Cristo Mountains between Taos and Mora based on an integrated geophysical analysis,

in Brister, B.S., Bauer, P.W., Read, A.S., and Lueth, V.W., eds., New Mexico Geological Society Guidebook, 55th Field Conference, Geology of the Taos Region, p. 257-263.

Roy, M., Kelley, S., Pazzaglia, F., Cather, S.M., and House, M., 2004, Middle Tertiary buoyancy modification and its relationship to rock exhumation, cooling, and subsequent extension at the eastern margin of the Colorado Plateau: *Geology*, v. 32, p. 925-928.

Schneider, R.V., and Keller, G.R., 1994, Crustal structure of the western margin of the Rio Grande rift and Mogollon-Datil volcanic field, southwestern New Mexico and southeastern Arizona, *in* Keller, G.R., and Cather, S.M., eds., Basins of the Rio Grande Rift: Structure, Stratigraphy, and Tectonic Setting: Boulder, Colorado, Geological Society of America Special Paper 291, p. 207-226.

Shaw, C.A., and Karlstrom, K.E., 1999, The Yavapai-Mazatzal crustal boundary in the southern Rocky Mountains: *Rocky Mountain Geology*, v. 34, p. 37-52.

Steven, T.A., 1975, Middle Tertiary volcanic field in the southern Rocky Mountains, *in* Curtis, B.F., ed., Cenozoic History of the Southern Rocky Mountains, Geological Society of America Memoir 144, p. 75-94.

Steven, T.A., and Lipman, P.W., 1976, Calderas of the San Juan volcanic field, southwestern Colorado, U.S. Geological Survey Professional Paper 958, 35 p.

Telford, W.M., Geldart, L.P., Sheriff, R.E., and Keys, D.A., 1990, *Applied Geophysics*, 2nd Ed., Cambridge University Press, 770 p.

Tweto, O., 1975, Laramide (late Cretaceous-early Tertiary) orogeny in the southern Rocky Mountains, *in* Curtis, B.F., ed., Cenozoic History of the Southern Rocky Mountains, Geological Society of America Memoir 144, p. 1-44.

—, 1979, Geologic map of Colorado, U.S. Geological Survey, 1:500,000 scale map.

Tweto, O., and Case, J.E., 1972, Gravity and magnetic features as related to geology in the Leadville 30-minute quadrangle, Colorado: U.S. Geological Survey Professional Paper 726-C, 31 p.

Vejmelek, L., and Smithson, S.B., 1995, Seismic reflection profiling in the Boulder batholith, Montana: *Geology*, v. 23, p. 811-814.

Zandt, G., Leidig, M., Chmielowski, J., Baumont, D., and Yuan, X., 2003, Seismic detection and characterization of the Altiplano-Puna magma body, central Andes: *Pure and Applied Geophysics*, v. 160, p. 789-807.

Chapter C: Geophysical Expression of Intrusions and Tectonic Blocks of Southern and Western Afghanistan

ABSTRACT

Southern and western Afghanistan are mostly part of the Afghan block, a series of Gondwanan terranes that lie between the Eurasian and Indian plates. The tectonic history of the Afghan block is dramatically expressed in space-time patterns of magmatism and deformation related to Mesozoic terrane collisions and the ongoing Himalayan orogeny. However, the tectonic history is very poorly constrained, and studies on the ground by western geologists have not been possible since the Soviet invasion in 1979. In this study, recently acquired regional aeromagnetic and aerogravity datasets were used to examine the geophysical expressions of plutons related to magmatic arcs, major tectonic blocks within the broader Afghan block, Himalayan deformation, and the Helmand basin. Numerous plutons are reflected as aeromagnetic highs, allowing the plutons to be mapped in areas where they do not crop out. Dating of these rocks would provide critical new constraints on the magmatic history of the region, which can be related directly to the history of subduction. The Farah and Helmand blocks have distinctive geophysical expressions that separate them from the adjacent Eurasian and Indian plates. The Farah block is shown to have relatively weakly magnetized and dense upper crust, and the Helmand block is characterized by many strongly magnetized intrusions and a large gravity low that may reflect the presence of a large batholith. West-southwestward crustal extrusion, an effect of the Himalayan orogeny, is indicated to have occurred with greater displacement along the Farah block than along the Helmand Block. Patterns of

smaller-scale Himalayan deformation are expressed as east-west to northeast-southwest trending aeromagnetic lineaments. Estimates to the depth of magnetic sources under the Helmand basin are generally <3 km, and high-amplitude aeromagnetic anomalies are interpreted to reflect several large buried intrusions, suggesting that the basin has low potential for significant petroleum reserves.

INTRODUCTION

Southern and western Afghanistan is broadly coincident with the Afghan block, defined as the region between the Chaman fault on the southeast and Herat (also known as Hari Rud) fault on the north (Fig. C1), and is thought to be composed of tectonostratigraphic terranes that originated as parts of Gondwana. The North Afghan block lies north of the Herat fault and has long been a stable portion of the Eurasian plate. Amalgamation of Gondwanan terranes to the Eurasian plate during Mesozoic time was part of a series of tectonic events that affected essentially all of southern Eurasia, known as the Cimmeride orogeny (Tapponnier et al., 1981; Sengor, 1984; Boulin, 1988; Sengor et al., 1988; Boulin, 1990; Sengor and Natal'in, 1996). The Himalayan orogeny followed from the late Mesozoic to the present day, triggering emplacement of numerous mineralized intrusions, causing widespread deformation, and continues to define the modern tectonic environment of Afghanistan (Treloar and Izatt, 1993; Wheeler et al., 2005; Ruleman et al., 2007; Wheeler and Rukstales, 2007).

The geology and tectonic history of Afghanistan has not been studied in detail by western geoscientists since the Soviet invasion in 1979, and ground access is presently severely hampered by security concerns. As a consequence, the details of the tectonic

history of Afghanistan are very poorly understood and remain controversial. Many first-order geologic observations and interpretations are lacking or poorly developed, such as the distribution and age of plutonic belts related to past and present subduction events, the tectonic history of the accreted terranes that comprise the Afghan block, and the effects of the Himalayan orogeny. Further complications are that very few reliable subsurface constraints (e.g., information on deep boreholes) exist, and that only a handful of geologic mapping studies undertaken prior to 1979 incorporated concepts of plate tectonics.

This study brings recently acquired regional aeromagnetic and aerogravity datasets to bear on this overall question: How are the main tectonic elements of southern and western Afghanistan expressed geophysically, and what do these observations indicate about the region's tectonic history? In order to address these questions in detail, we examine the geophysical signature of major plutonic belts and map their distribution, compare the boundaries of inferred accreted terranes mapped from surface geology to their geophysically-derived boundaries, highlight the geophysical expression of Himalayan deformation, and address the subsurface nature of the unexplored Helmand basin.

GEOLOGIC BACKGROUND

Afghanistan lies within the Mesozoic collision zone between Eurasia and Gondwana, and the Afghan block is generally assumed to be composed of two separate accreted terranes, the Farah and Helmand blocks (Figs. C1 & C2). These are separated by the Waser (also known in scientific literature as Panjao, Penjaw, Waras, and Khash

Rud) suture zone. Each block originated as parts of Gondwana that separated from that continent, drifted northward, and finally collided with Eurasia (e.g. Sengor and Natal'in, 1996). The Himalayan orogeny can be thought of as the final event in this series of collisions of Gondwana fragments with Eurasia and closing of the Tethyan oceans.

The few elements of the generally accepted pre-Himalayan tectonic interpretation that are known to likely be robust include the following: The interpretation that the Farah and Helmand blocks originated as parts of Gondwana is based on observations of Paleozoic biostratigraphy, which clearly shows a Gondwanan affinity, and the fact that the blocks were not deformed by Paleozoic orogenies that affected Eurasia (e.g. Tapponnier et al., 1981, and references therein). The timing of accretion of the Farah block to Eurasia and the accretion of the Helmand block to the Farah block are constrained to be pre-Early Cretaceous and pre-Mid Cretaceous, respectively, based on geologically-mapped fabrics within inferred suture zones, local relationships with overlying sedimentary rocks, and regional interpretations of sedimentary rock distribution (Tapponnier et al., 1981; Sengor, 1984; Girardeau et al., 1989). Finally, plutonic belts are thought to represent magmatic arcs that formed on overlying plates during subduction episodes, an interpretation consistent with their generally I-type composition (see discussion below) (Debon et al., 1987).

The generally accepted tectonic interpretation of the Afghan block includes several assumptions that are plausible, yet are very poorly constrained. The first is that northward-dipping subduction was the rule prior to accretion of the Farah and Helmand blocks, as well as during subduction that preceded accretion of the Indian plate during the Himalayan orogeny. This interpretation is based on a small number of K-Ar and Rb-Sr

ages (Debon et al., 1987) of dubious quality on plutonic belts that appear to record a consistent pattern of magmatism along the southern margins of the northern plates prior to terrane accretion (e.g., Treloar and Izatt, 1993). However, Debon et al. (1987) recognized that the quality of the pluton ages they reported was not sufficient to constrain subduction zone polarity.

The second major assumption is that what has been mapped as the >500 km-long Waser suture zone (Blaise et al., 1978; Tapponnier et al., 1981) represents the tectonic boundary between the Farah and Helmand blocks. This assumption has a good chance of being valid, given that it contains an ophiolitic *mélange* as much as 60 km wide, indicating that a significant ocean existed there. Mafic/ultramafic volcanic rocks that may include oceanic crust (too small to show at scale of Fig. C2) crop out along the southeastern margin of the suture zone. However, the precise style of emplacement of the *mélanges* is difficult to address, since they have been severely deformed into steeply dipping, northeast trending slices (Tapponnier et al., 1981).

The third and final major assumption is that the locations of Mesozoic suture zones are reflected today by major strike-slip faults related to the Himalayan orogeny (see below). This hypothesis appears to generally work well in the vicinity of the Waser suture zone, where there is evidence for major strike-slip faulting on either side of the suture zone that includes a significant component of Quaternary displacement (Ruleman et al., 2007). However, this hypothesis may need to be refined along the Herat fault, now a major right-lateral strike slip fault with Quaternary displacement (Ruleman et al., 2007), that is assumed to represent the location of the suture zone between the Farah block and the Eurasian plate. Little supporting geologic evidence for a suture zone has

been found within the study area, as ophiolitic remnants and other indicators of suturing are scarce to nonexistent (Tapponnier et al., 1981; R. Bohannon, personal comm., 2009).

The Himalayan orogeny is responsible for large amounts of deformation within the Farah and Helmand blocks, with the most intense folding occurring within the Helmand block. Fold axes and faults generally trend parallel to local margins of tectonic blocks, ranging from east-west near the Herat fault to northeast-southwest near the Chaman fault. Timing of the collision between India and the Afghan block is not well-constrained, but related compression within the Afghan block, and presumably uplift of the Hindu Kush (Figs. C1 & C3), is interpreted to be post-Miocene based on ages of deformed rocks (e.g., Treloar and Izatt, 1993). The active, left lateral strike-slip Chaman fault is commonly assumed to represent the boundary between the Afghan block and the Indian plate. Southeast of the Chaman fault is the Katawaz basin, a thick wedge of mostly marine(?) sediments, strongly folded internally. Depths to basement are estimated to be ~15 km under the Katawaz basin (Jadoon and Khurshid, 1996).

One of the variably accepted, broad effects of the Himalayan orogeny appears to be westward or southwestward extrusion of the Afghan block between the Chaman and Herat faults, analogous to the “escape tectonics” demonstrated for much of Tibet (Molnar and Tapponnier, 1975; Tapponnier and Molnar, 1976). This interpretation was rejected at one point based on the incorrect assumption that the Herat fault was not active following the collision of the Indian plate (Treloar and Izatt, 1993), although the recent demonstration of Quaternary offset (Ruleman et al., 2007) has revived the extrusion hypothesis. Shortening of the eastern portions of the Farah and Helmand blocks during the Himalayan orogeny, as well as west-southwestward extrusion, may have triggered

extension in the western portion of the Afghan block (Treloar and Izatt, 1993), forming the Helmand basin.

Several plutonic belts crop out on or near the Afghan block, and have been related to individual subduction events that preceded terrane accretion (Debon et al., 1987) (Fig. C2). Most plutons are granitic, and many of them can be classified as I-type (Chappell and White, 1974) or magnetite-series (Ishihara, 1977) in composition (Debon et al., 1987). This association is important for a number of reasons. First, these types of granitoids are normally associated with and used as evidence for the subduction of oceanic crust beneath continental margins. Second, they are typically correlated with porphyry copper deposits (Ishihara, 1981), a major potential source of mineral wealth for Afghanistan (Peters et al., 2007). Third, they are normally ferromagnetic and therefore frequently important sources of aeromagnetic anomalies (Maniar and Piccoli, 1989; Clark, 1999). Other types of granitoids that are normally weakly magnetized include S-type (Chappell and White, 1974) and ilmenite-series (Ishihara, 1977) rocks; these are also present in the Afghan block (Debon et al., 1987) and in some cases are associated with tin mineralization (Clark, 1999; Peters et al., 2007).

The ages of intrusions on and near the Afghan block are poorly constrained by very small numbers of possibly unreliable K-Ar and Rb-Sr dates, although these poor constraints have not prevented interpretations of the tectonic significance of the plutonic belts from being made. The following listing of recognized plutonic belts/magmatic arcs is based on published dates (Debon et al., 1987), classifications (Debon et al., 1987), and interpretations (Debon et al., 1987; Treloar and Izatt, 1993) consistent with the generally accepted tectonic history of the Afghan block.

The Feroz Koh (FK, Fig. C2) belt lies immediately north of the Herat fault and displays Triassic ages, and thus has been interpreted to represent the magmatic arc resulting from north-dipping subduction of oceanic crust beneath Eurasia that preceded accretion of the Farah block. However, several Eocene and Oligocene ages have also been reported, and have an ambiguous tectonic association. The Farah Rud (FR) and Band-E Bayan (BEB) plutons display Cretaceous to Oligocene ages, and therefore have tentatively been interpreted in terms of north- or northwest-dipping subduction of oceanic crust beneath the Afghan block prior to the collision of India. An alternative is that these rocks are related to extrusion and extension of the western Afghan block in response to the Himalayan orogeny. The Arghandab (ARG) plutonic belt/batholith appears to be entirely Cretaceous. It and the Spin Boldak (SB) belt (~59 Ma) are interpreted to reflect subduction prior to collision of India. Oligocene and younger plutons of the Chagai Hills (CH) are part of the magmatic arc associated with north-dipping subduction along the Makran coast of southwestern Pakistan (Fig. 1) (Arthurton et al., 1982; Peters et al., 2007). The Helmand (HEL) plutonic belt is likely much older than the tectonic events that formed the Afghan block, possibly related to Cambrian-Ordovician rifting. Notably absent from this generally accepted interpretation of magmatic patterns are plutons related to subduction that preceded accretion of the Helmand block. These rocks, if they exist, have not been located/recognized.

Rocks and structures characteristic of the Helmand block have been assumed to extend into the subsurface under the Helmand basin, covered by Cenozoic sediments. However, the precise nature of the subsurface pre-Cenozoic rocks and the geometry of the Helmand basin are poorly understood. On the basis of high-amplitude aeromagnetic

anomalies, the floor of the Helmand basin was originally interpreted to be a Precambrian basement shield province (Bosum et al., 1968). However, this interpretation was made prior to the discovery of a Quaternary carbonatite (Vikhter et al., 1976; Alkhazov et al., 1978; Vikhter et al., 1978) (Fig. C2) that correlates spatially with one of the high-amplitude aeromagnetic anomalies (Peters et al., 2007).

GEOPHYSICAL DATA AND METHODS

Aeromagnetic anomalies reflect spatial variations of total magnetization, the vector sum of induced and remanent magnetizations. Induced magnetization, an instantaneous property, is proportional to magnetic susceptibility and has the same direction as the present-day ambient field (inclination of 48 degrees, declination of 2 degrees in the study area). Remanent magnetization is a long-lived property, is related to a rock's formation and geologic history, and may be directed in a different direction than the induced magnetization. Large-magnitude components of remanent magnetization are common in volcanic rocks but rare in silicic- and intermediate-composition plutons (Clark, 1999).

Data from two vintage total-field aeromagnetic (100 meters to 1 km above the ground) surveys acquired during the 1960s (Bosum et al., 1968; Sweeney et al., 2006a, b) were continued to a surface 5 km above the ground and merged with regional-scale aeromagnetic data collected during 2006 to create an aeromagnetic map of the study area (Ashan et al., 2007). A reduction-to-pole transformation, a standard geophysical technique to center anomalies over their sources, was applied to the aeromagnetic data using an inclination of 48 degrees and declination of 2 degrees (Fig. C4) (Baranov and

Naudy, 1964; Blakely, 1995). A magnetic potential, or “pseudogravity”, transformation was also applied to the aeromagnetic data (Fig. C5). This technique also centers anomalies over their sources, but further transforms magnetic anomalies to a mathematical form that makes them comparable to gravity anomalies (Baranov, 1957; Blakely, 1995). Compared to aeromagnetic anomalies (Fig. C4), the long-wavelength portions of the field are enhanced at the expense of short-wavelength anomalies. Thus, the magnetic potential field emphasizes the effect of relatively deep and/or broad geologic features (Fig. C5).

Aerogravity anomalies reflect lateral variations of density, with aerogravity highs occurring over regions of relatively high densities, such as crustal blocks that include dense basement, and aerogravity lows occurring over large volumes of low-density materials, such as sedimentary basins and silicic intrusions.

Regional aerogravity data were acquired with a 4 km line spacing during 2006, continued to a surface 7 km above the ground, and merged (Ashan et al., 2008) with vintage ground gravity data (McGinnis, 1971). Standard techniques for aerogravity processing (Parker, 1972; Blakely, 1995; Ashan et al., 2008) were used to process the data and calculate complete Bouguer anomalies, including corrections for predicted gravitational attraction at the elevation and latitude of the observation point (theoretical and free air corrections), effects of homogeneous masses underneath (Bouguer correction), and effects of topographic masses (terrain corrections). The standard reduction density of 2670 kg/m^3 (Hinze, 2003) was used for the Bouguer and terrain corrections, in order to compute complete Bouguer anomalies (Fig. C6). Errors in the final data are likely to be on the order of a few mGals. Complete Bouguer gravity

anomaly maps are often dominated by long-wavelength anomalies inversely correlated with regional topography, an effect of Airy-type isostasy that causes gravity lows over mountain belts. An additional step of computing isostatic residual anomalies was performed, in order to remove the effect of long-wavelength anomalies that correlate with regional topography. This method is only one possible way of removing a regional field and results in an aerogravity anomaly map (Fig. C7) that is a better representation of upper-crustal density variations than a more standard complete Bouguer anomaly map (Simpson et al., 1986). Computation of isostatic residual anomalies requires estimates of crustal thickness and Moho density contrast, but these values do not need to be accurate to yield useful results. For this study, we used parameters that gave the least correlation between isostatic residual anomalies and regional terrain, including a Moho density contrast of 330 kg/m^3 and a normal (assuming ground surface at sea level) crustal thickness of 30 km.

In order to objectively define the extents of geologic sources of geophysical anomalies over the large study area, two related techniques were used. The first is the horizontal gradient magnitude (HGM) of the aeromagnetic and aerogravity anomalies. This method is based on the principle that for the case of vertical boundaries, the measured field's largest-magnitude gradients in the horizontal direction are located over the edges of magnetization or density contrasts (Cordell, 1979; Cordell and Grauch, 1985; Grauch and Cordell, 1987). The method is therefore useful for detecting geologic contacts and faults. The relationship between a density contrast, its corresponding aerogravity anomaly (Telford et al., 1990), and the peak of the HGM function is illustrated in Fig. C8. In this example, a low-density body has a contrast of -100 kg/m^3 ,

and represents a hypothetical sedimentary basin or granitic intrusion with a simple vertical contact. An aerogravity low (measured at an altitude of 7 km above the ground surface) occurs over the low-density material, and the HGM of the aerogravity field reaches a peak value over the edge of the geologic source.

The second technique is terracing, a method that transforms the measured magnetic or gravity data into a field of domains with uniform properties surrounded by sharp boundaries that separate different domains (Cordell and McCafferty, 1989). This is done by iteratively “steepening” the gradients at the margins of anomalies, until anomalies are “flattened” and reflect the physical properties within each domain. The boundaries of the domains are defined by the peaks of the HGM of the measured magnetic or gravity field. In the example presented here (Fig. C8), terracing results in two domains, one reflecting the gravity field over the low-density source and one over the adjacent high-density material. The boundary between the domains occurs at the location of the HGM peak. Terracing was applied to the reduced-to-pole aeromagnetic field (Fig. C9) and the isostatic residual aerogravity field (Fig. C10).

The depths to the tops of magnetic sources can be estimated from low-altitude aeromagnetic anomalies, and here were calculated from a vintage dataset (Bosum et al., 1968; Sweeney et al., 2006a). Using Euler’s homogeneity relation and assuming a simple magnetic source type, the lateral and vertical gradients and Hilbert transforms of the aeromagnetic anomalies can be uniquely related to the horizontal and vertical positions of the source (Thompson, 1982; Reid et al., 1990; Mushayandebvu et al., 2001; Nabighian and Hansen, 2001; Phillips, 2002) (Fig. C11). Good clustering of solutions indicates that a source location is well resolved, and poor clustering indicates solutions that should be

ignored (Reid et al., 1990). The choice of source model, or structural index, is critical for reasonable results and is defined in terms of the rate the field decreases with distance from the source. The use of an improper index will yield solutions that are scattered and have inaccurate depths. Tests were performed using different structural indices, and an index of zero was found to give the most accurate locations of magnetic sources where their locations were known. An index of zero theoretically gives depths to the tops of magnetization contrasts that have large depth extents, such as high-throw faults.

DISCUSSION

Correlations between geophysical anomalies, the geophysical derivative maps, mapped geology, and inferred crustal blocks were used to interpret the extents and types of plutons, define the geophysical expression of tectonic blocks, illuminate patterns of deformation associated with the Himalayan orogeny, and define the broad subsurface nature of the Helmand basin. These interpretations, related hypotheses, and questions raised are discussed in detail below.

Plutons Belts-Magmatic Arcs

Aeromagnetic highs correlate well spatially with the mapped extents of many plutons and plutonic belts (Fig. C4). This observation is consistent with the I-type compositions of many of the plutons, and shows that aeromagnetic anomalies can be used to map the extents of plutons into the subsurface. Using aeromagnetic highs to locate intrusions and the terraced map (Fig. C9) to define their extents, a new map of strongly

magnetized plutons was developed (Fig. C13) within the classification framework of Debon et al. (1987).

Tectonic associations originally based partially on outcropping intrusions can be extended using the new map, and the extents of plutons of the Feroz Koh, Farah Rud, Arghandab, and Spin Boldak belts/arcs are significantly increased. Perhaps the best way to develop better constraints on the tectonic history of the Farah and Helmand blocks is to develop better constraints on the ages of plutons that are representative of magmatic arcs formed during subduction episodes, and this map shows where to look to find relevant plutons. For example, there are currently no known plutons that can be correlated spatially and temporally with subduction that preceded accretion of the Helmand block. If the presence of these rocks can be demonstrated, then polarity of the long-disappeared subduction zone may be interpreted based on which block the magmatic arc is found to lie within (i.e., if found to be on the Farah block, then north- or northwestward-dipping subduction is indicated). If no plutons can be found that are between pre-Early Cretaceous (interpreted age of accretion of Farah block) and pre-Mid Cretaceous (interpreted age of accretion of Helmand block), then the currently accepted tectonic history of the Helmand block must be reevaluated.

Outcropping portions of the Arghandab plutonic belt are correlated with aeromagnetic highs and an aerogravity low that extends far to the southwest over the center of the Helmand basin (Figs. C4 & C7). Measurements of magnetic properties on the Arghandab plutons indicate that it is strongly magnetized (Bosum et al., 1968), and granitic bodies often produce gravity lows (Bott and Smithson, 1967). A model (Fig. C12) was constructed along profile A-A' to demonstrate the plausibility of the batholith

producing both aeromagnetic highs and an aerogravity low. This is not meant to be a quantitatively rigorous model, since there are no independent subsurface constraints. The modeled density of the batholith (2600 kg/m^3) is on the low end of permissible densities for granite (Telford et al., 1990), meaning that the interpreted thickness of $\sim 6 \text{ km}$ at A-A' is close to a minimum value. The aerogravity low over the Arghandab batholith extends over 200 km to the southwest of A-A' (Fig. C7), suggesting that the batholith may extend into the subsurface of the Helmand basin. However, a basin with thick sediments may also produce an aerogravity low, and no independent constraints exist for the Helmand basin. An additional possibility is that sedimentary rocks that crop out between the batholith and the Waser suture zone (Fig. C2) contribute to the gravity low. The possibility of thick accumulations of sediments contributing to the aerogravity low is addressed below.

Numerous plutons of unknown tectonic associations are interpreted to lie under younger sediments, particularly in the Helmand basin region. Many of these produce high-amplitude aeromagnetic highs (Fig. C4), including an WSW-ENE-trending anomaly that is spatially associated with an outcropping carbonatite (note #1, Fig. C13) (Vikhter et al., 1976; Alkhazov et al., 1978; Vikhter et al., 1978; Peters et al., 2007). This anomaly and another with similar shape and amplitude to its immediate north were originally interpreted to reflect a buried Precambrian shield, since high-amplitude aeromagnetic highs are commonly observed over basement terranes (Bosum et al., 1968). However, this interpretation was made prior to the discovery of the carbonatite, and carbonatites frequently occur with very strongly magnetized and dense mafic and ultramafic rocks, such as pyroxenites (Clark, 1999). Therefore, it is possible that these aeromagnetic

anomalies are caused by a buried ultramafic or mafic igneous complex. However, there is no associated aerogravity high (Fig. C7), so that such a complex must not have a significant thickness (i.e., likely not more than ~1.5 km).

A high-amplitude aeromagnetic anomaly along the western margin of the Helmand basin (Figs. C4 & C13, note #2) has also been interpreted to be caused by a strongly magnetized (6-20 A/m) pluton buried >1 km with a thickness of 3-10 km (Bosum et al., 1968). The source of this anomaly has a strong component of magnetic remanence that is not collinear with the ambient field and thus has a total magnetization direction different from the ambient direction. The direction of total magnetization has been estimated to have an inclination of 1 degree and a declination of 22 degrees (Phillips, 2005), although the direction of the remanent magnetization alone and the age information it carries cannot be determined due to a likely large magnetic susceptibility and induced magnetization. It is rare for plutons to carry strong remanent magnetization, except for mafic or ultramafic lithologies (Clark, 1999). Based on this observation and the interpretation of aeromagnetic anomalies in the region of the carbonatite, there is a strong possibility that more of the aeromagnetic anomalies over the Helmand basin (Fig. C4) are caused by mafic/ultramafic plutons (Fig. C13). If this is correct, these rocks may represent the expression of hypothesized Himalayan-age extension in the western Afghan block (Treloar and Izatt, 1993).

Aeromagnetic and aerogravity highs lie over the southeastern margin of the Waser suture zone, near the Helmand fault (Figs. C4-C6). The source of these anomalies is ambiguous, as there are outcropping Precambrian rocks near the Helmand fault (Fig. C2), as well as possibly a large thickness of oceanic crust wedged into the southern part

of the suture zone (Tapponnier et al., 1981); both rock types may carry strong magnetizations and high densities. The model presented here (Fig. C12) displays this source in terms of wedge of oceanic mafic rocks that thickens with depth, consistent with the interpretation of Tapponnier et al. (1981), but this does not rule out the possibility that Precambrian rocks are contributing sources to the geophysical anomalies.

Geophysical Expression of Major Tectonic Blocks

In general, there are strong geophysical differences between the inferred tectonostratigraphic terranes in southern and western Afghanistan, and thus broad geophysical support for the first-order tectonic divisions interpreted by geological studies. This discussion highlights the major geophysical trends and their possible implications.

The southern portion of the Eurasian plate is bounded on the south by aeromagnetic and aerogravity gradients that correspond in location to the Herat fault (Figs. C4-C7). The Eurasian plate is locally more strongly magnetic and denser than the Farah block to its south. Aeromagnetic highs arise from near-surface plutons (Figs. C4 & C13), as well as a broader, possibly deeper-seated area of strongly magnetized upper crust (Figs. C4 & C5) that also correlates partially with an aerogravity high (Figs. C6 & C7).

Most of the Farah block correlates spatially with a broad magnetic potential low (Fig. C5), reflecting a lack of strongly magnetized plutons (Fig. 13) and very deep and/or weakly magnetized basement (Bosum et al., 1968). The western Farah block appears to be more weakly magnetized than the main part. The southwestern part of the block includes a large, batholith-scale pluton ~250 km long along a north-northeast trend and

~50 km wide. Isostatic residual aerogravity anomalies (Fig. C7) reach relatively high values throughout the Farah block, showing that the upper crust of the block is generally denser than surrounding blocks. Short-wavelength (<30 km) aerogravity anomalies may reflect variations of basement depth under the sedimentary section, but no borehole or other geologic constraints exist that would allow this hypothesis to be tested in a meaningful way.

The Waser suture zone is well-expressed geophysically along the length that it crops out. A strong gradient of the magnetic potential field lies over its center, marking a boundary between the generally low-amplitude regional magnetic field observed over the Farah block versus the higher-amplitude regional field over the Helmand block. Aeromagnetic (Fig. C4) and aerogravity (Fig. C7) highs correlate spatially with oceanic crust and/or structurally high Precambrian rocks along the southeastern margin of the suture zone. The isostatic residual aerogravity high in particular may permit extension of the mapped southeastern suture zone margin ~100 km into the subsurface to the southwest (Fig. C7), although beyond this distance the clear geophysical signature is lost. Other rocks of the suture zone, mainly ophiolitic sediments, do not appear to have a strong geophysical signature beyond the presence of northeast-southwest-trending aeromagnetic lineaments (Fig. C9).

The Helmand block is characterized by generally much higher magnetic potential values and lower isostatic residual aerogravity values than the Farah block (Figs. C5 & C7), indicating relatively strongly magnetized and low-density upper crust. These effects result at least in part from the large number of strongly magnetized plutons and the possibilities of an extensive low-density Arghandab batholith and sub-basins (see

discussion below) (Fig. C13). Aerogravity values reach a maximum in the region of the Spin Boldak plutonic belt (Fig. C7), where the upper crust is especially strongly magnetized (Fig. C6). However, these aerogravity highs are not as pronounced in amplitude and areal extent as those observed over the Farah Block.

What is the significance the large number of strongly magnetized plutons within the Helmand block, with so many fewer to the north on the Farah block? Most of the (poorly) known ages of plutons in the Helmand block correspond to the expected age of subduction that preceded the Himalayan collision, suggesting that the Helmand block was simply affected to a larger degree by magmatism related to subduction prior to the Himalayan orogeny. However, given the large uncertainties in age relationships and number of plutons with uncertain tectonic significance buried under the Helmand basin (Fig. C13), and the lack of a known magmatic arc that can be correlated with subduction prior to accretion of the Helmand block, the possibility that many of the plutons existed prior to accretion of the Helmand block cannot be ruled out.

The Chaman fault corresponds to perhaps the most profound geophysical boundary in the study area. Strongly magnetized and dense rocks of the southeastern Helmand block are juxtaposed against a thick section of sediments in the Katawaz basin, and geophysical lineaments lie along the boundary (Figs. C4-C7, C9-C11). The lack of aeromagnetic anomalies over the basin is consistent with very deeply buried basement (Jadoon and Khurshid, 1996). The source of a mid-basin aerogravity high (Fig. C7) is poorly understood.

Geophysical Expression of Himalayan Deformation

Complete Bouguer gravity anomalies are typically strongly influenced by variations in crustal thickness that correlate with surface elevations, with lows occurring over mountain belts. This can be understood in the context of Airy-type isostasy, as gravity lows over thick crust reflect the relatively large distance from the surface to dense mantle rocks. Correspondingly, the isostatic root of the Hindu Kush is likely responsible for the deep complete Bouguer gravity low (Fig. C6) over the highest ground elevations (Fig. C3).

Bouguer aerogravity lows are also correlated with ground elevations at the scale of individual tectonic blocks, with a deeper aerogravity low over the Farah block than over the Helmand and a sharp boundary between the two regimes at the Waser suture zone (compare smoothed topography, Fig. C14, to Fig. C6). This suggests a deeper isostatic root (i.e., thicker crust) under the Farah block, but how did this sharp boundary develop? One possibility is that it is inherited from the original nature of the Farah block, and therefore is a Mesozoic structure. However, this seems unlikely given that it corresponds spatially to the much younger (late Tertiary?) uplift of the Hindu Kush. A more likely possibility is that the high elevation of and Bouguer aerogravity low over the Farah block reflect late Tertiary or younger crustal thickening, and that the Farah block has been subsequently extruded to the west-southwest a greater distance than the Helmand block (Fig. C14). In this hypothesis, left-lateral strike-slip faulting along the approximate location of the Waser suture zone accommodated greater extrusion displacement of the Farah block. Offset is estimated to be 100-250 km, based on the distances that the gravity anomaly and high elevations are offset. Quaternary left-lateral

strike-slip faulting is observed on the surface near the margins of and along the same trend as the Waser suture zone (Ruleman et al., 2007), supporting the hypothesis. This suggests mechanical decoupling of the Farah and Helmand blocks in addition to the previously hypothesized west-southwest extrusion of the Afghan block as a whole (Molnar and Tapponnier, 1975; Tapponnier and Molnar, 1976), which may be testable with GPS velocity measurements.

Quaternary faulting on the Afghan block can be regarded as an expression of Himalayan deformation (Ruleman et al., 2007) and its interaction with previously existing structures. Comparison of these faults with the HGM transformation of the aeromagnetic anomalies (Fig. C15) shows that magnetic boundaries correlate well both in location and trend. Thus, the HGM map may be used to infer trends of Himalayan-age deformation as it is expressed in terms of magnetic contrasts. As discussed above, magnetic lineaments correspond very well with interpreted boundaries between different terranes, including along the Herat and Chaman faults and Waser suture zone. The general northeast-southwest trending fabric that is apparent on geologic (Fig. C2) and fault maps within individual terranes is also reflected as magnetic lineaments. For example, trends of Himalayan deformation affect the magnetic basement where covered by young sediments, as shown for the Helmand basin.

Helmand basin

The thickness of sediments that fill the Helmand basin has long been a subject of interest, due to the possibility of petroleum resources there. However, no deep boreholes have been drilled, and very little is known of the subsurface. The possible thickness distribution of sediments may be studied in two different ways: aerogravity anomalies

(Fig. C7), and estimates of depth to magnetic sources (Fig. C11). An aerogravity low may reflect a structural depression filled with low-density sediments, and high-amplitude aeromagnetic anomalies are often assumed to arise from “basement” rocks under the base of sediments or sedimentary rocks. However, complications to these simple cases often arise, because aerogravity lows may also reflect silicic igneous rocks, and aeromagnetic anomaly sources may lie above the base of sediments, which would be the case if the sedimentary section had been intruded by a strongly magnetized pluton. Therefore, a closed sedimentary sub-basin was only interpreted where aerogravity lows coincided in location with relatively deep magnetic source depth estimates, as shown on Figs. C7 & C11. These may not be the only closed sub-basins within the broader Helmand basin, although the depth estimates show that magnetic sources (presumably igneous rocks) are mostly buried at depths <3 km, and few large areas exist with depths >3 km (Fig. C11). The lack of evidence for a broad, deep basin, combined with evidence for numerous plutons at depth (Fig. C13), means that the Helmand basin is an unlikely target for petroleum exploration.

One possible exception to this conclusion is the largest of the interpreted sub-basins, in the Lashkar Gah region. Depth estimates show depths of 6 km to strongly magnetized rocks (Fig. C11) over an area ~ 150 km wide, and a large aerogravity low (Fig. C7) may indicate a thick accumulation of sediments/sedimentary rocks of unknown lithology. This aerogravity low can alternatively be interpreted in terms of a southwestward extension of the Arghandab batholith (Fig. C13, see discussion above).

CONCLUSIONS

Recently acquired aeromagnetic and aerogravity data facilitate new interpretations of the extents of plutons, and the geophysical expressions of major tectonic blocks, the Himalayan orogeny, and the Helmand basin in southern and western Afghanistan. The major plutonic belts can be identified by the strongly magnetized nature of their constituent intrusions, a legacy of their genesis by subduction-related processes. The pluton map presented here gives new insights into the possible locations of magmatic arcs that may be related by dating to subduction and orogenic episodes, and the polarities of long-disappeared subduction zones. There is broad geophysical support for the generally assumed subdivision of major tectonic blocks, with the Farah and Helmand blocks displaying distinctive geophysical signatures that separate them from the Eurasian and Indian plates. New evidence is presented for westward extrusion of the Farah block at a greater rate since the formation of the Hindu Kush than for the Helmand block, and left-lateral strike slip offset of 100-250 km in the region of the Waser suture zone. Patterns of smaller-scale deformation throughout southern and western Afghanistan related to the Himalayan orogeny are clearly indicated by aeromagnetic gradients. Finally, the Helmand basin is shown to have relatively small thicknesses (generally <3 km) of sediments overlying a large number of plutons, indicating that it may not be a lucrative target for petroleum exploration.

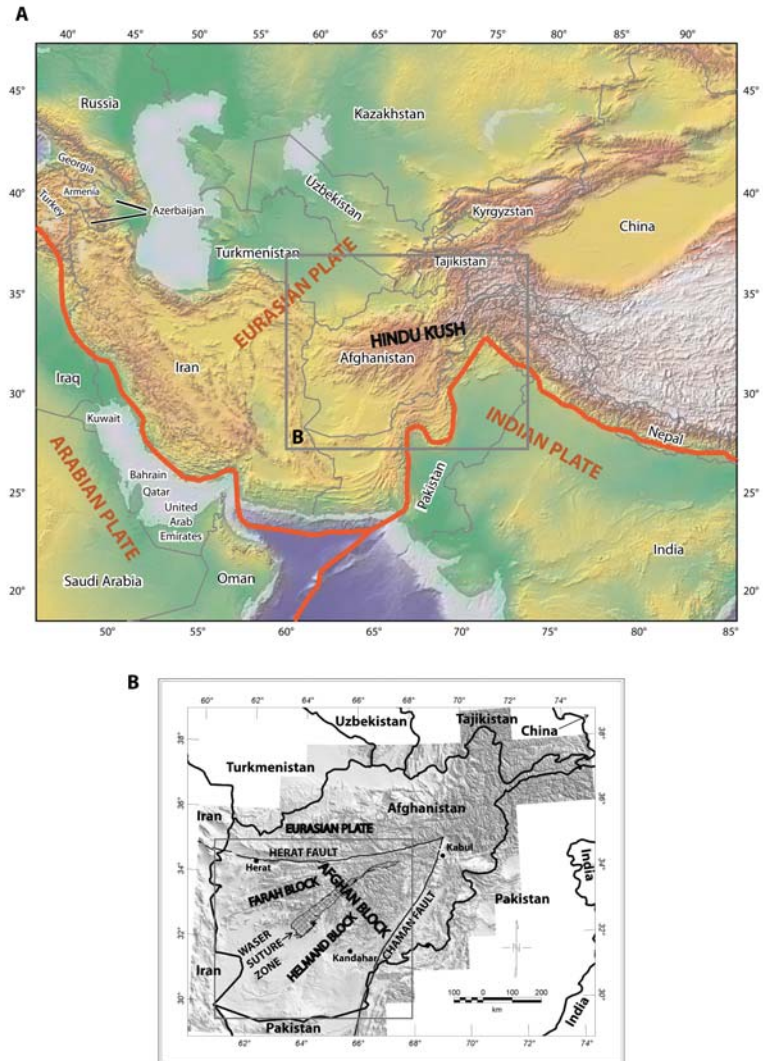
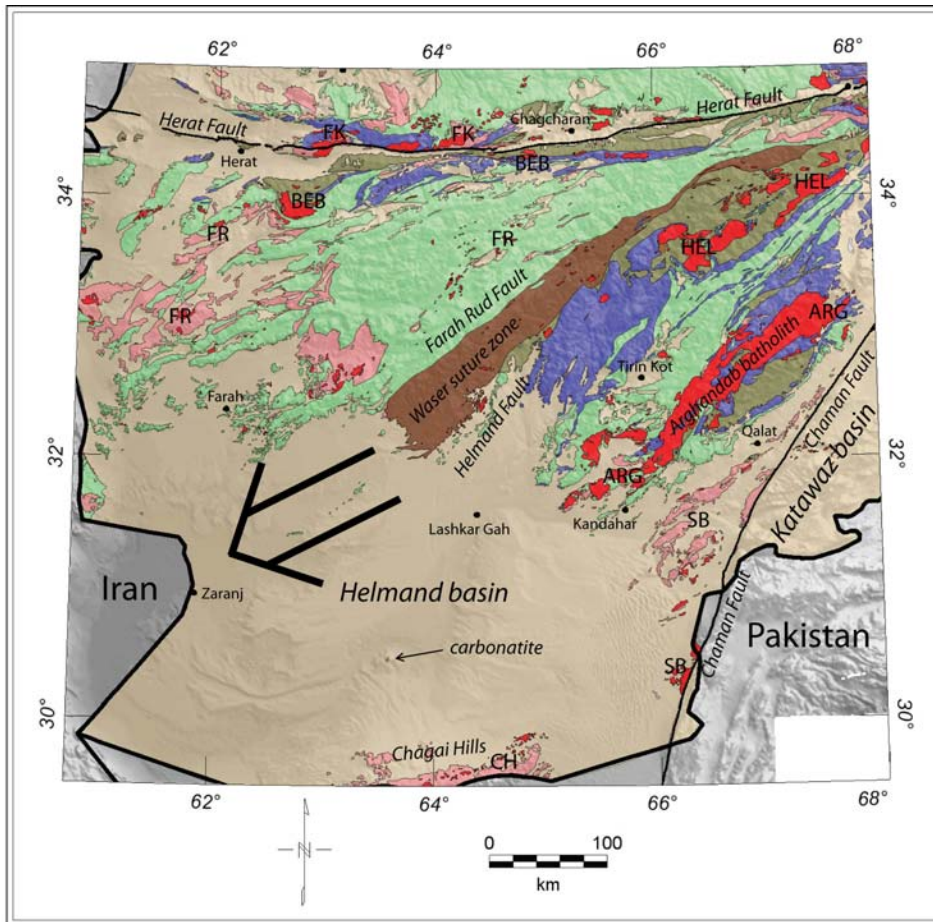











Figure C1: A: Regional geography and tectonics of south Asia. B: Physiography, geography, and selected tectonic features of the Afghanistan region. Gray box defines area of this study and subsequent figures.



General Explanation

	Cenozoic sediments and sedimentary rocks
	undifferentiated volcanic rocks
	plutonic rocks
	Mesozoic sedimentary rocks
	Mesozoic sedimentary rocks of Waser suture zone
	Paleozoic sedimentary rocks
	Precambrian rocks
	major fault
	Provincial Capital

Major Plutonic Belts

<i>name</i>	<i>symbol</i>	<i>age (Ma if known)</i>
Chagai	CH	Oligocene(?) and younger?
Feroz Koh	FK	~37 and Triassic
Spin Boldak	SB	~59
Farah Rud	FR	Cretaceous to Paleogene(?)
Band-E Bayan	BEB	Cretaceous to Oligocene(?)
Arghandab	ARG	110-106
Helmand	HEL	~500(?) and Mid- to Upper Cretaceous

Figure C2: Simplified geology of the study area. Geology modified from Doebrich et al (2006). Plutonic belt classifications from Debon et al. (1987). Large arrow indicates hypothesized west-southwestward extrusion of Afghan block between Herat and Chaman faults.

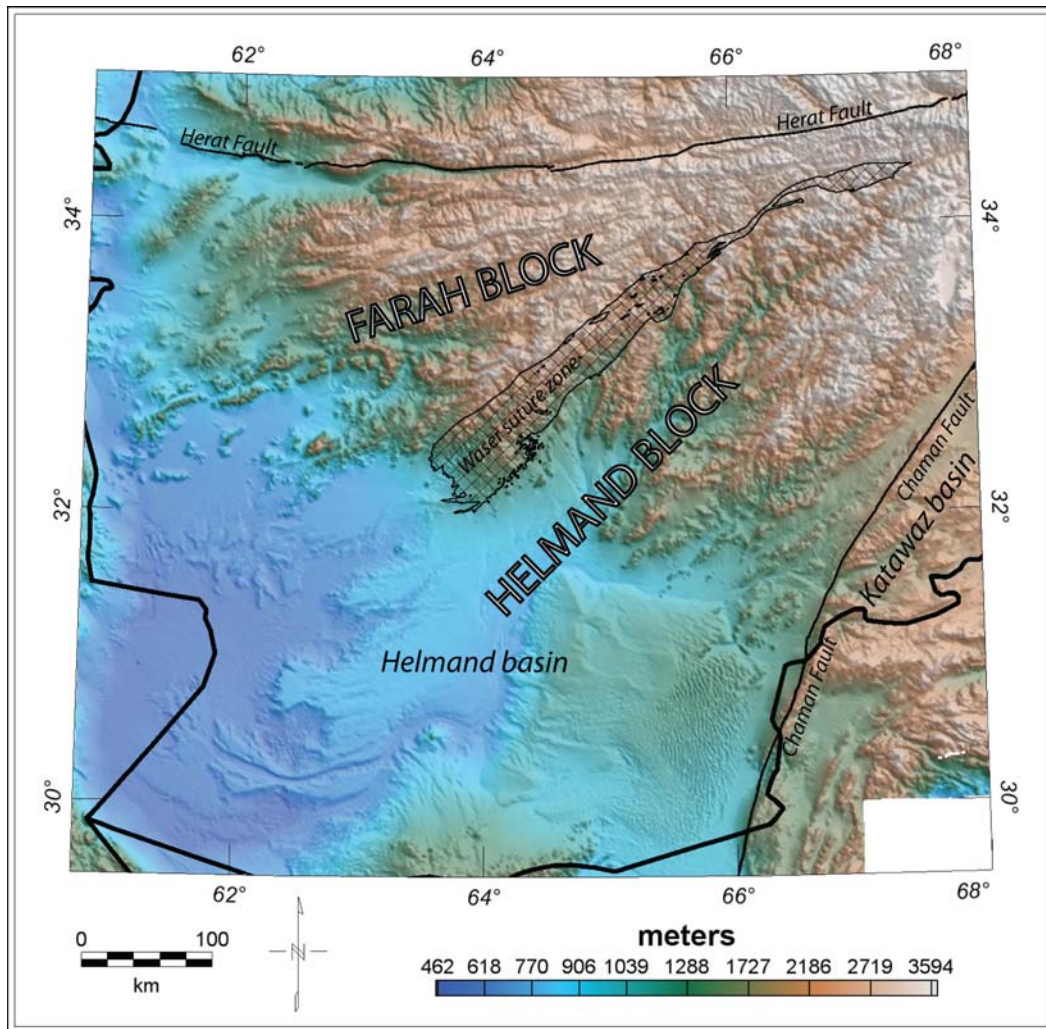


Figure C3: Elevation map of the study area, major tectonic blocks labeled.

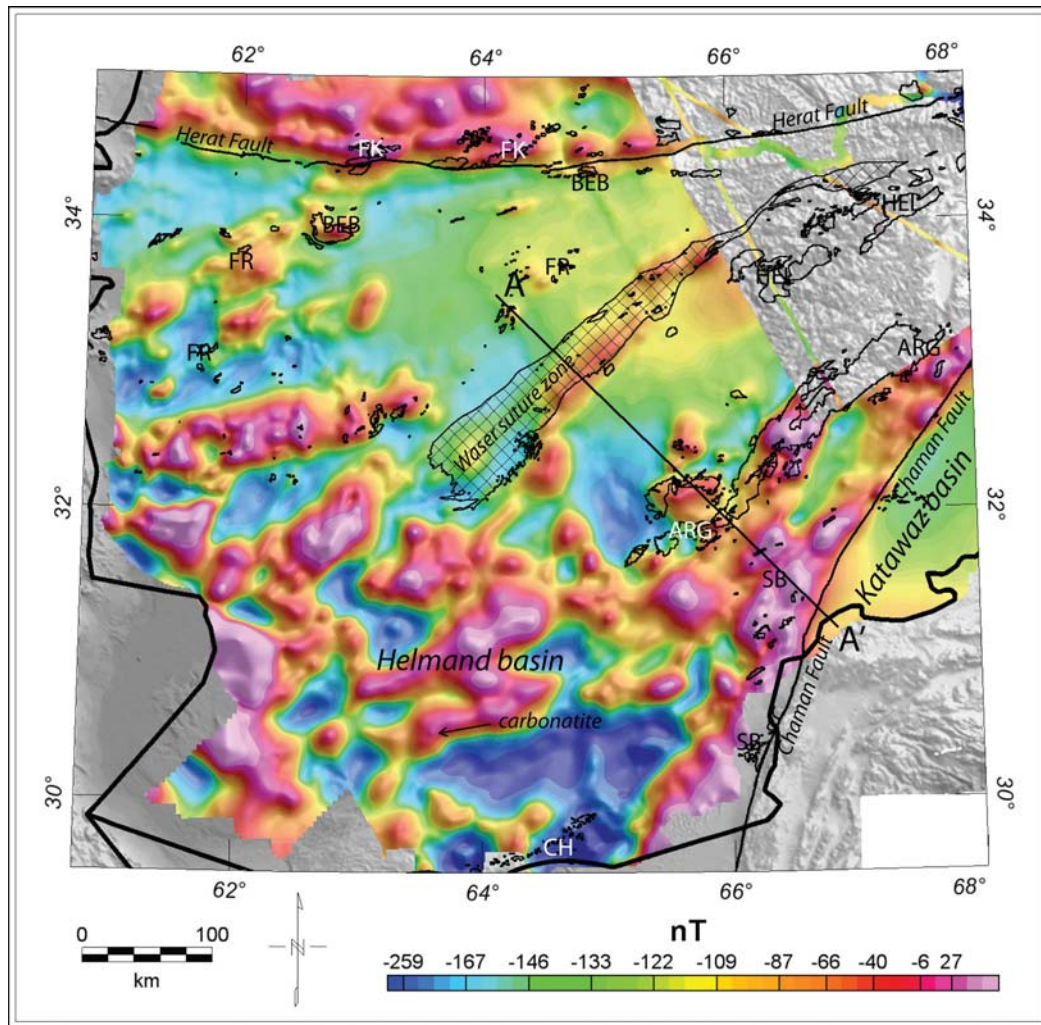


Figure C4: Reduced-to-pole aeromagnetic anomalies draped at 5 km above the ground. Location of profile A-A' shown. Black polygons and labels show outcropping intrusions, after Fig. C2.

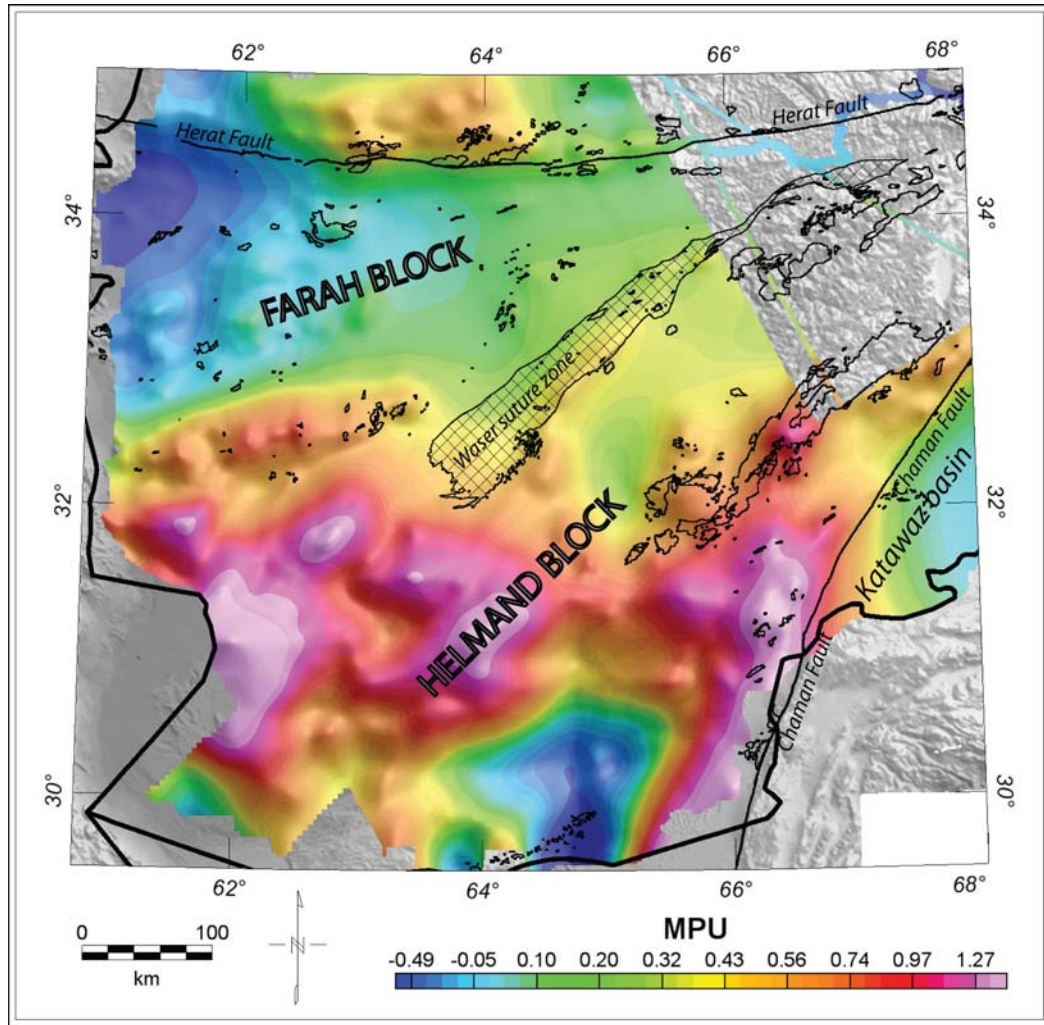


Figure C5: Magnetic potential anomalies (MPU: magnetic potential units). Black polygons show outcropping intrusions, major tectonic blocks labeled.

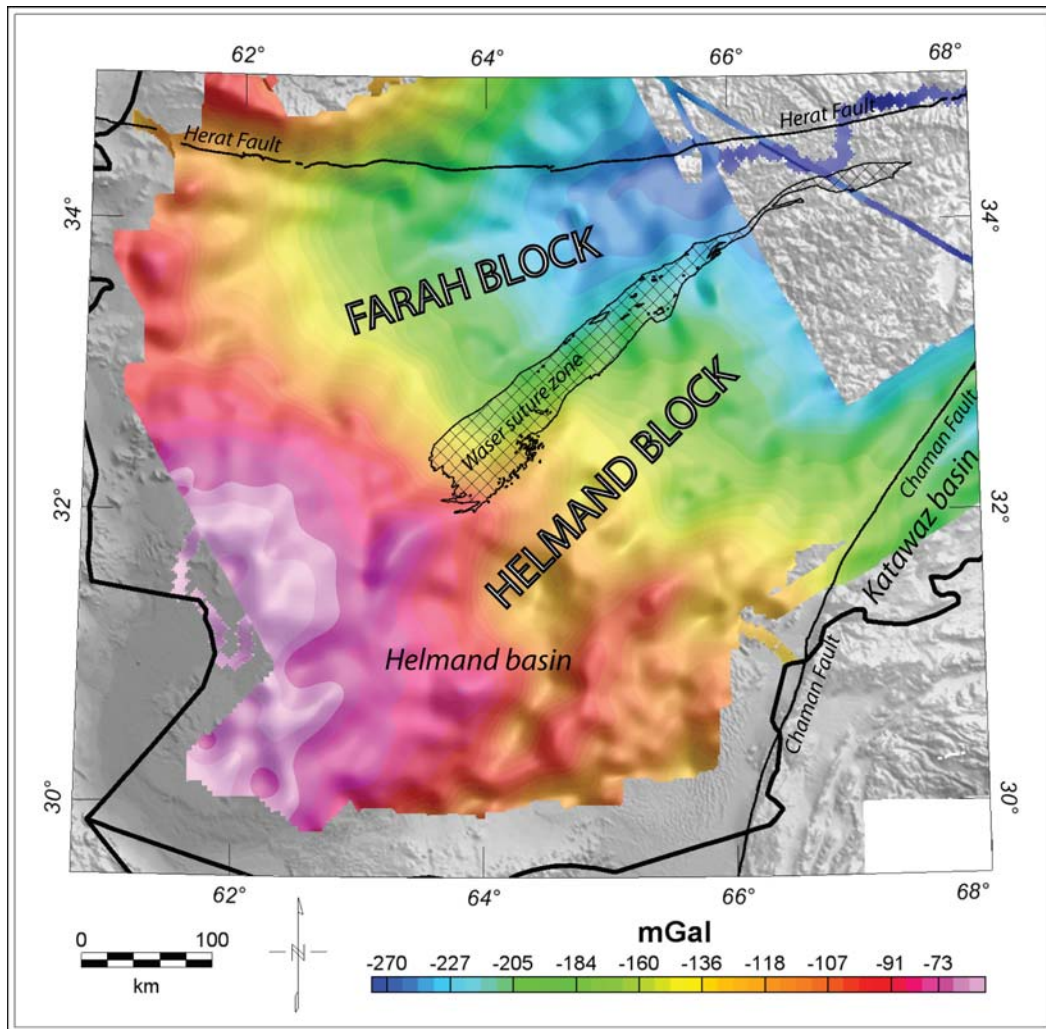


Figure C6: Complete Bouguer aerogravity anomaly map, major tectonic blocks labeled.

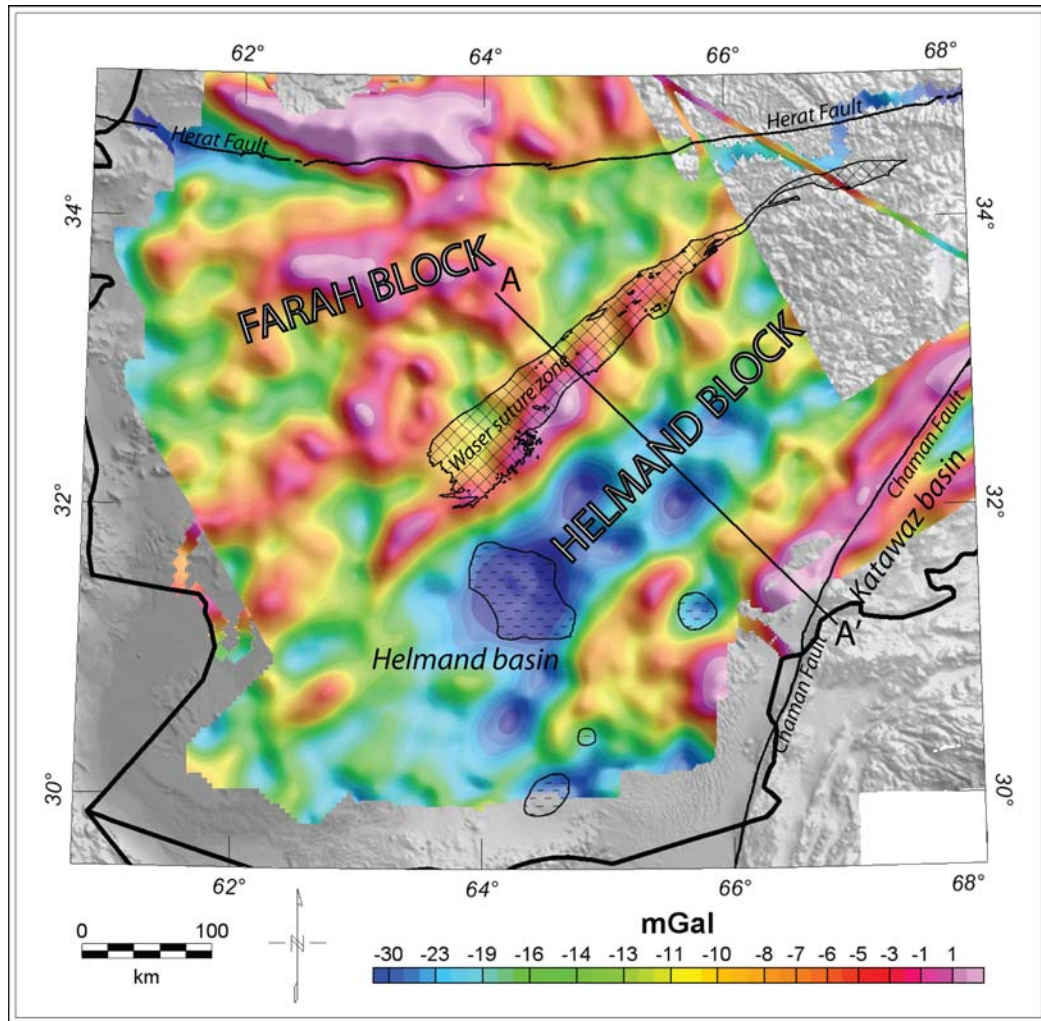


Figure C7: Isostatic residual aerogravity anomalies at 7 km above the ground. Location of profile A-A' shown. Major tectonic blocks labeled. Polygons within the Helmand block indicate possible basin areas with > 3 km sedimentary thickness.

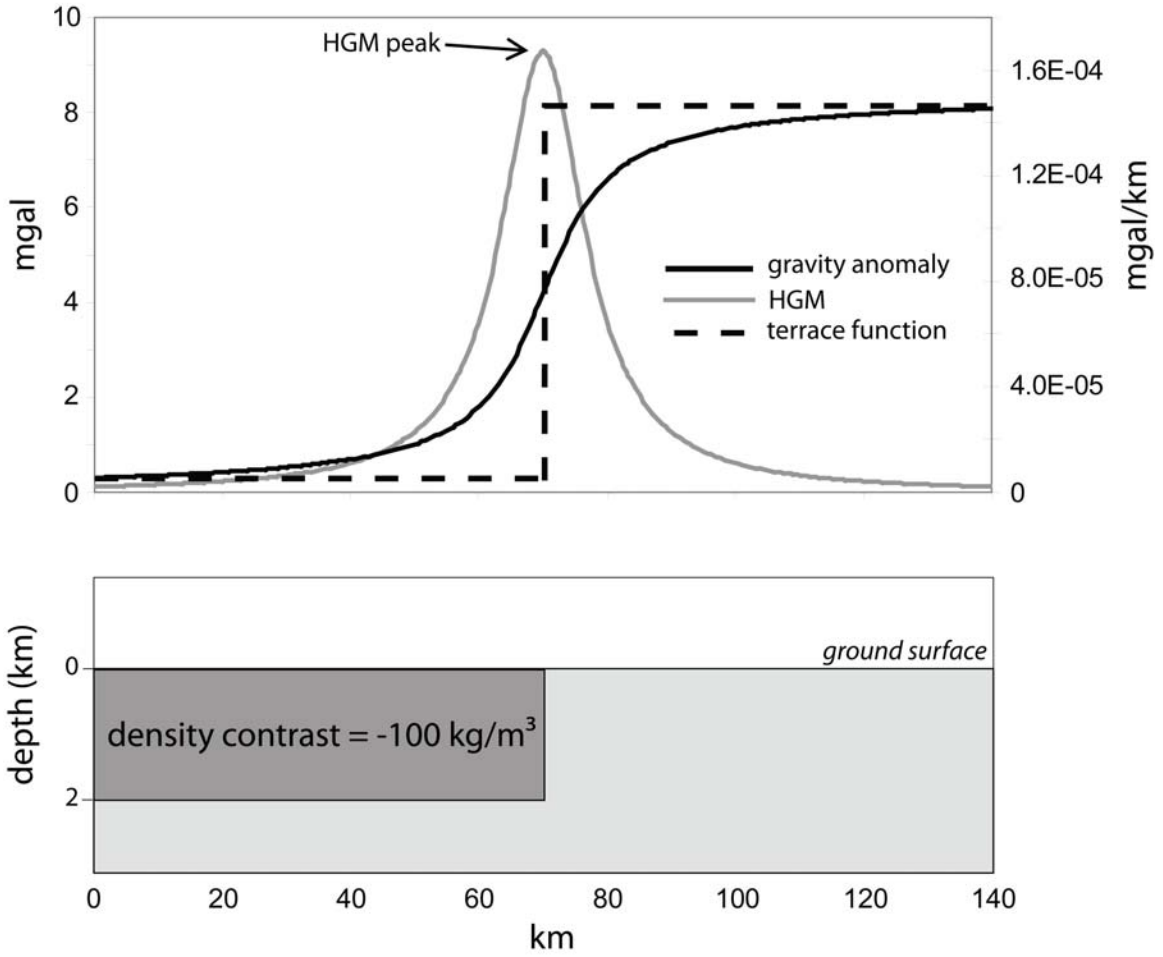


Figure C8: Synthetic data example showing gravity anomaly, horizontal gradient magnitude (HGM) function, and terrace function over a hypothetical density boundary. Gravity anomaly calculated using equation 2.70 of Telford et al. (1990).

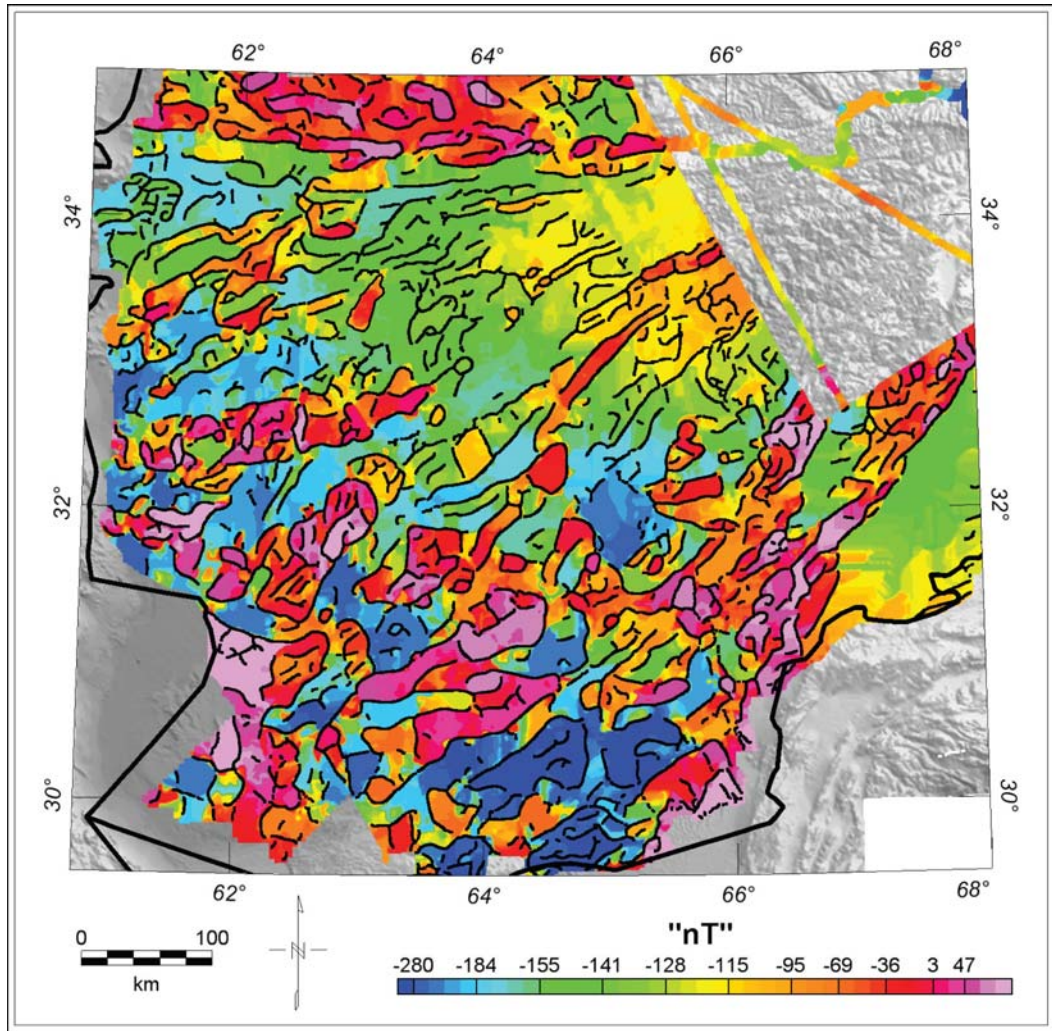


Figure C9: “Terraced” version of reduced-to-pole aeromagnetic anomalies (Fig. C4). Black lines show locations of HGM peaks.

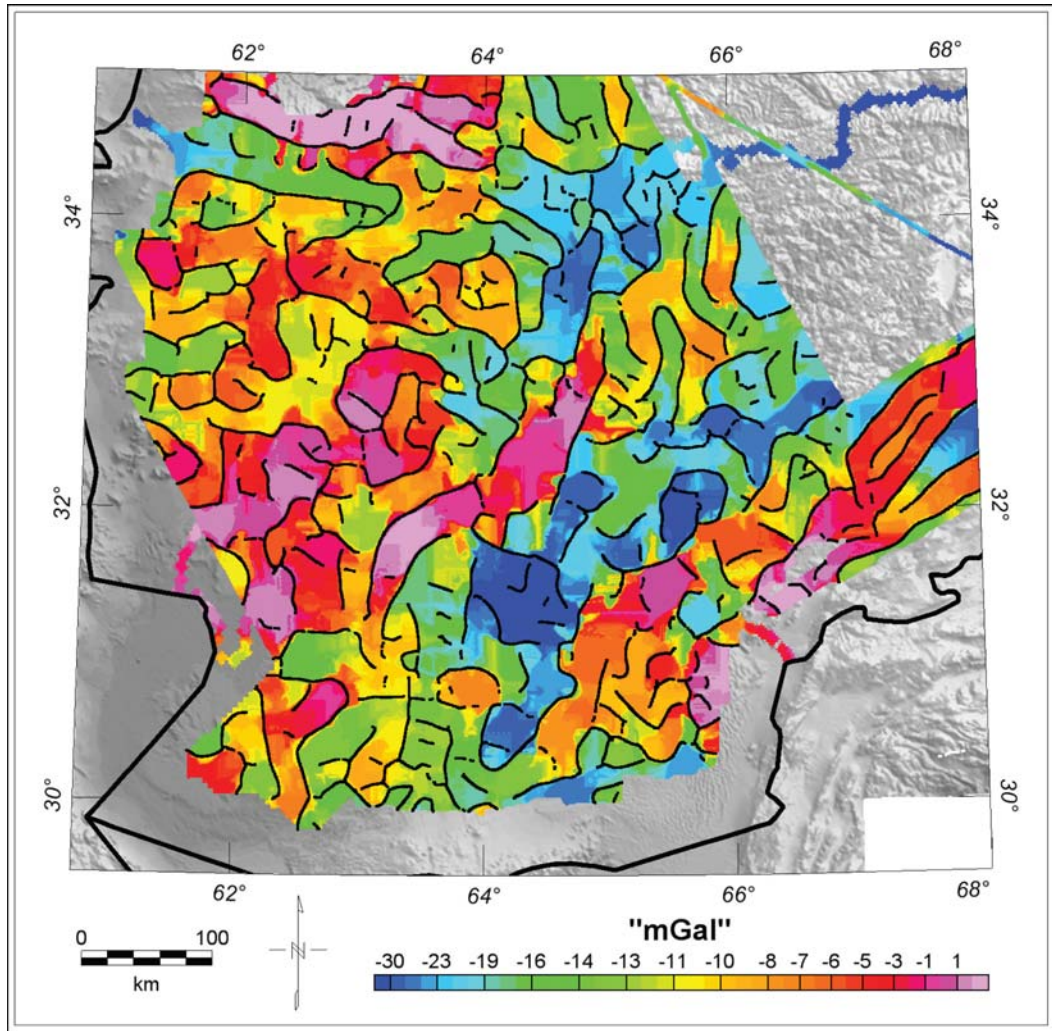


Figure C10: “Terraced” version of isostatic residual aerogravity anomalies (Fig. C6). Black lines show locations of HGM peaks.

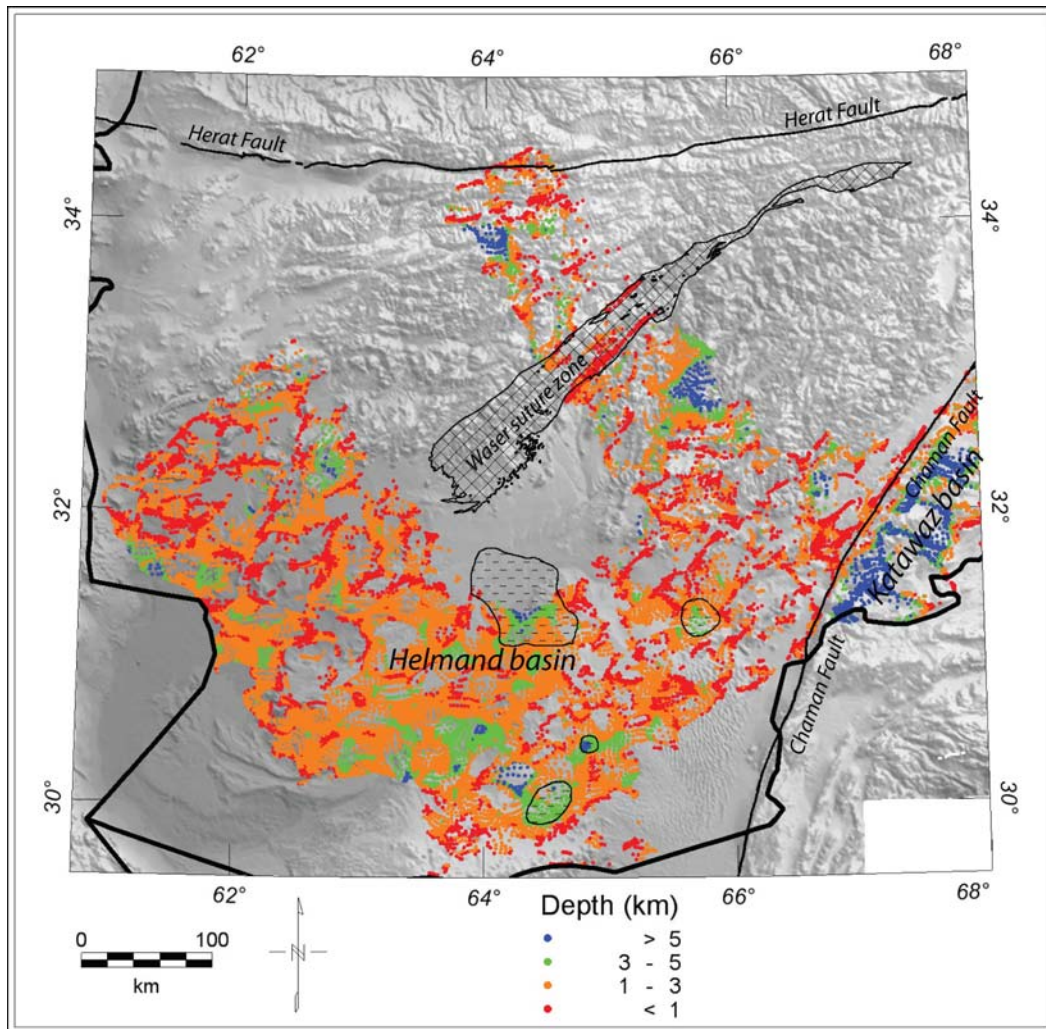


Figure C11: Depth estimates from extended Euler deconvolution (Mushayandebvu et al., 2001; Nabighian and Hansen, 2001; Phillips, 2002) assuming a structural index of 0. Calculated using a vintage aeromagnetic dataset over the Helmand basin region (Bosum et al., 1968; Sweeney et al., 2006). Depths in kilometers from the ground surface.

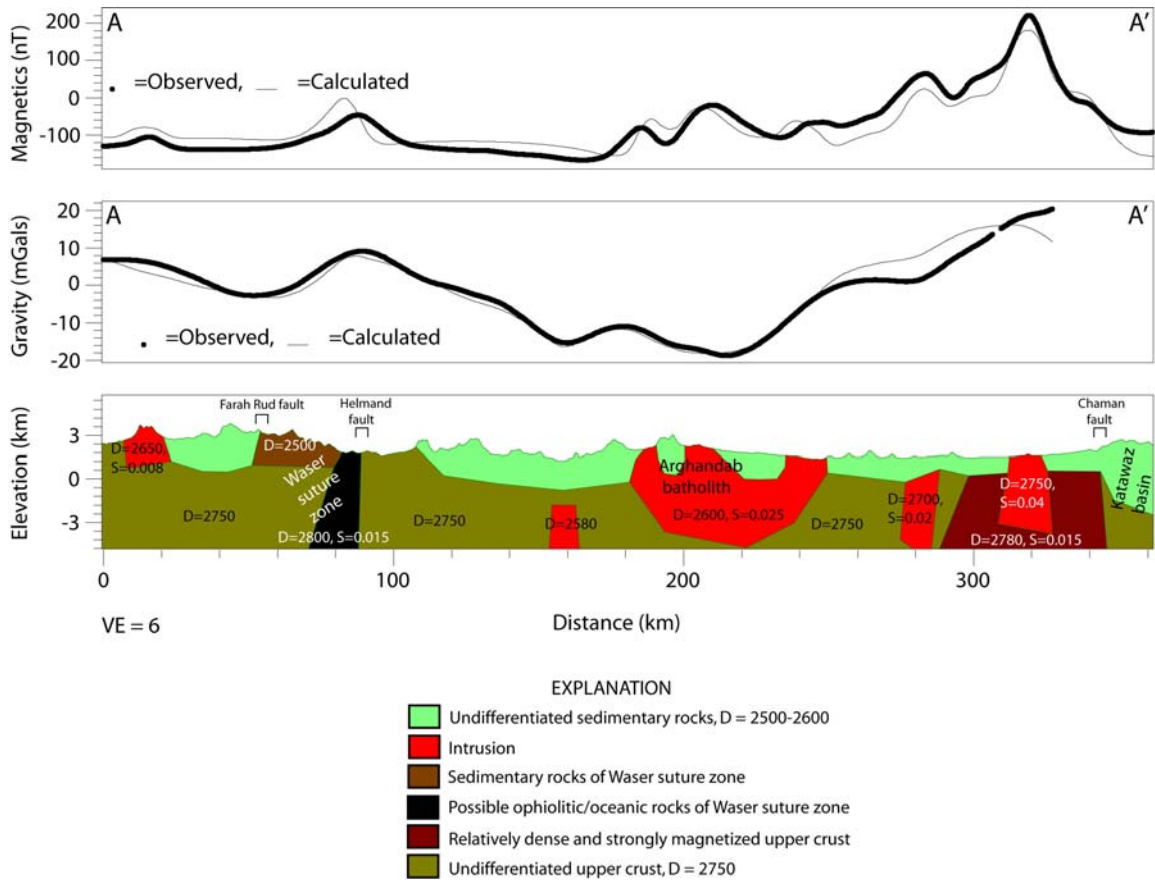
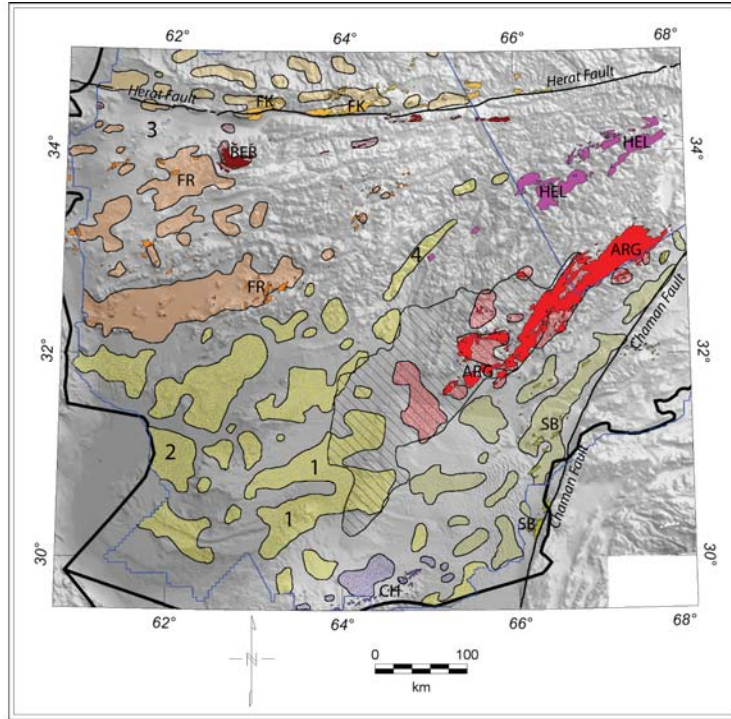


Figure C12: Geophysical profiles along A-A' (Figs. C3 & C5). Densities in geologic model are in kg/m^3 (D) and magnetic susceptibilities in SI units (S). Units lacking susceptibility value were modeled with any magnetic properties (i.e. were interpreted to be weakly magnetized). Vertically exaggerated 6 times.



Plutonic Belts

<i>plutonic belt name</i>	<i>symbol (solid where outcropping)</i>	<i>age</i>	<i>inferred tectonic environment(s)</i>
Chagai	CH	Oligocene(?) and younger?	subduction along Makran coast
Feroz Koh	FK	Eocene and Triassic	accretion of Farah and Helmand(?) blocks, Himalayan orogeny?
Spin Boldak	SB	Paleocene	Himalayan orogeny
Farah Rud	FR	Cretaceous to Paleogene(?)	accretion of Helmand block(?), Himalayan orogeny
Band-E Bayan	BEB	Cretaceous to Oligocene(?)	accretion of Helmand block(?), Himalayan orogeny
Arghandab	ARG	Cretaceous	Himalayan orogeny
Helmand	HEL	Cambrian(?), Mid- to Upper Cretaceous	unknown, pre-assembly of Afghan block, Himalayan orogeny?
buried intrusions, unknown association	(hatched pattern)		

Symbols

- major fault
- geophysical data extent
- ▨ maximum possible extent of Arghandab batholith, based on gravity data

Notes

- 1: spatially associated with Quaternary carbonatites, previously interpreted as rocks of Precambrian shield (Bosum et al., 1968)
- 2: total magnetization direction: inclination 1 degree, declination 22 degrees (using method of Phillips, 2005)
- 3: uncertain boundary between Band-E Bayan and Farah Rud plutonic belts
- 4: may be oceanic mafic rocks associated with Waser suture zone/ophiolite

Figure C13: Interpreted distribution of strongly-magnetized intrusions, based on interpretation of aeromagnetic and aerogravity anomalies. Plutonic belt classifications from Debon et al. (1987). Boundaries taken from terraced maps (Figs. C9 & C10).

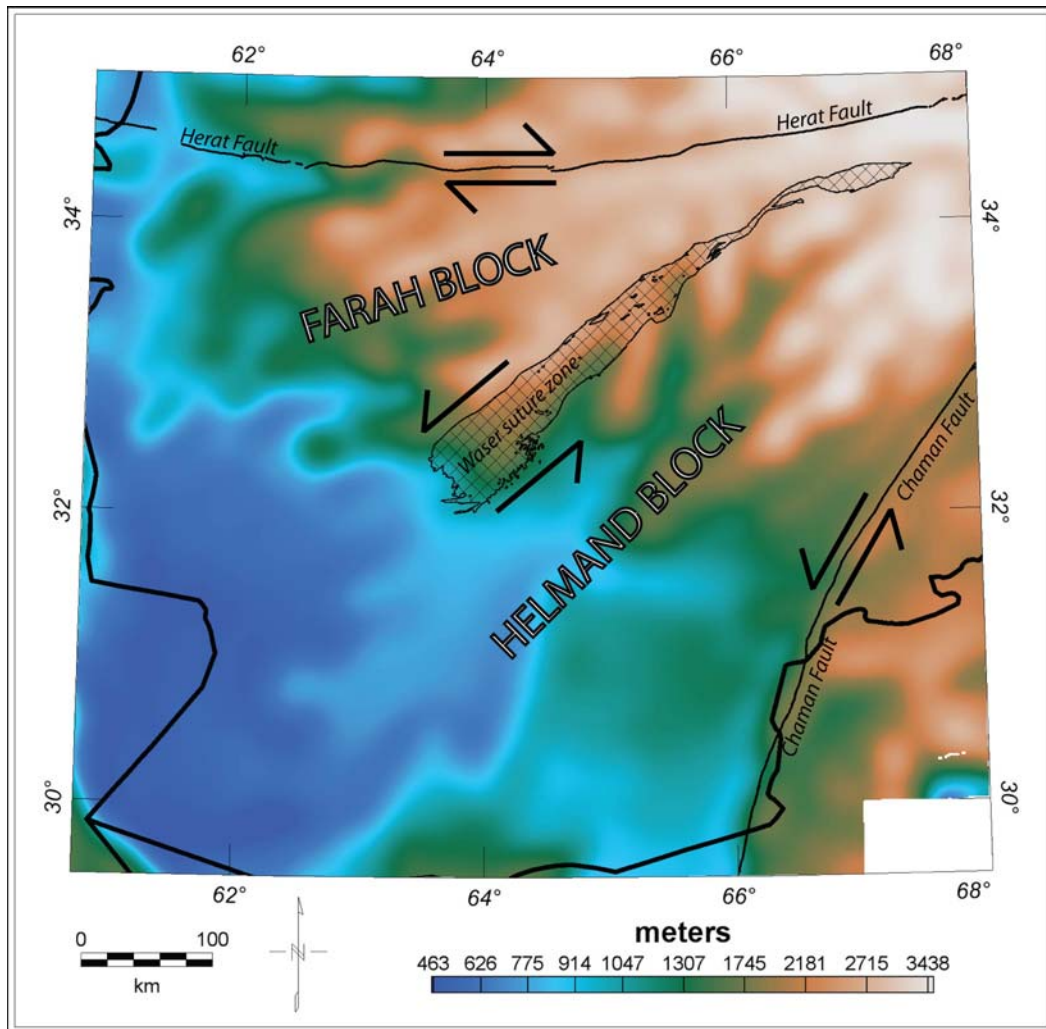


Figure C14: Smoothed elevation map, topographic features less than 40 km wide removed. Shear-sense arrows indicate hypothesized pattern of crustal extrusion, enhanced from existing model (Molnar and Tapponnier, 1975; Tapponnier and Molnar, 1976). Compare to Figs. C3 and C6.

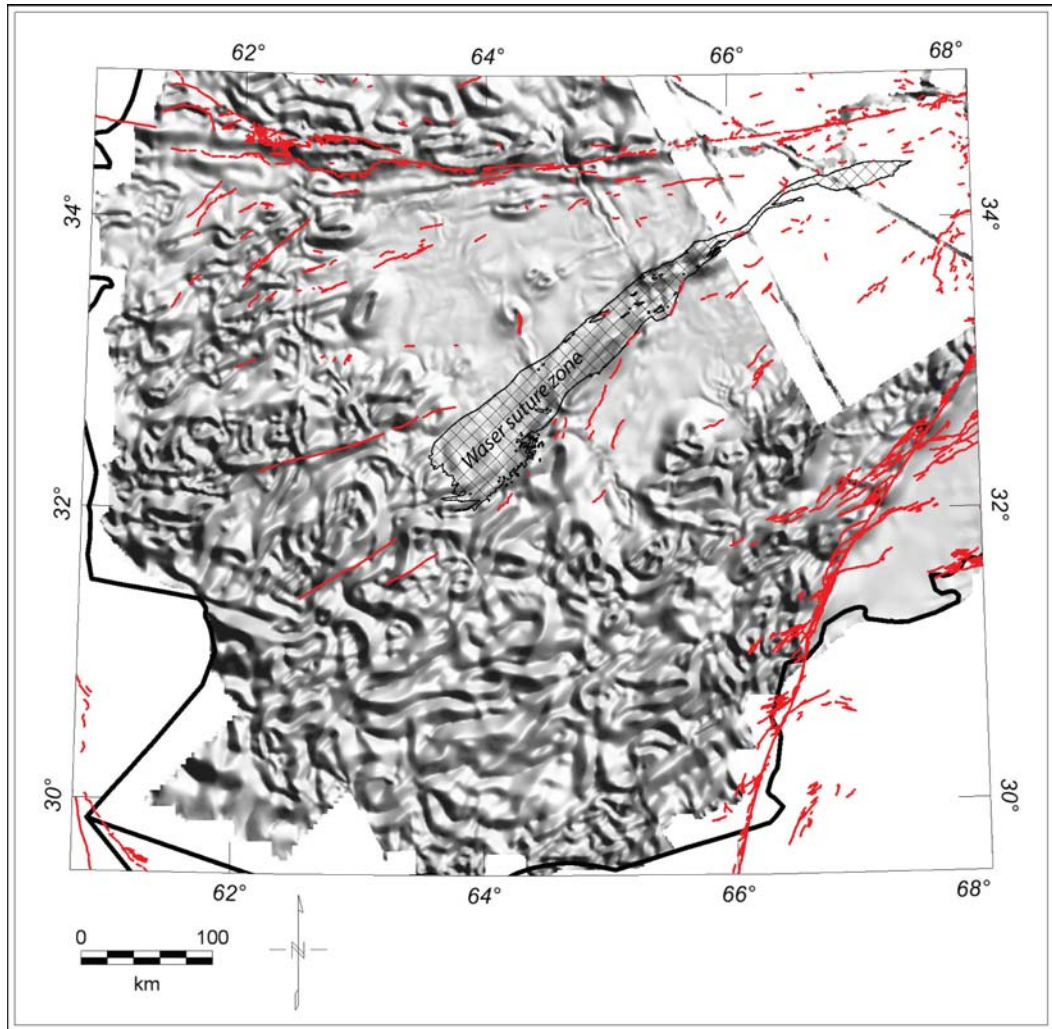


Figure C15: Grayscale representation of the HGM of the reduced-to-pole aeromagnetic anomalies. Red lines are Quaternary faults mapped by Ruleman et al. (2007).

REFERENCES

- Alkhazov, V.Y., Atakishiyev, Z.M., and Azimi, N.A., 1978, Geology and mineral resources of the early Quaternary Khanneshin carbonatite volcano (Southern Afghanistan): *International Geology Review*, v. 20, p. 281-285.
- Arthurton, R.S., Farah, A., and Ahmed, W., 1982, The late Cretaceous-Cenozoic history of western Baluchistan Pakistan-the northern margin of the Makran subduction complex, *in* Leggett, J.K., ed., *Trench Forearc Geology: sedimentation and tectonics on modern and ancient active plate margins*: Geological Society Special Publication, Volume 10, p. 373-385.
- Ashan, S., Hussain, S., Kohistany, A.H., Shenwary, G.S., Mutty, A.S., Daud, M.A., Abraham, J.D., Anderson, E.D., Drenth, B.J., Finn, C.A., Kucks, R.P., Lindsay, C.R., Phillips, J.D., Sweeney, R.E., Brozena, J.M., Ball, D.C., Childers, V.A., Gardner, J.M., Jarvis, J.L., and Liang, R.T., 2007, Aeromagnetic survey in Afghanistan, U.S. Geological Survey Open-File Report 2007-1247.
- Ashan, S., Hussain, S., Kohistany, A.H., Shenwary, G.S., Mutty, A.S., Daud, M.A., Brozena, J.M., Ball, D.C., Childers, V.A., Gardner, J.M., Jarvis, J.L., Liang, R.T., Abraham, J.D., Anderson, E.D., Drenth, B.J., Finn, C.A., Kucks, R.P., Lindsay, C.R., Phillips, J.D., and Sweeney, R.E., 2008, Airborne gravity survey and ground gravity in Afghanistan, U.S. Geological Survey Open-File Report 2008-1089.
- Baranov, V., 1957, A new method for interpretation of aeromagnetic maps: pseudo-gravimetric anomalies: *Geophysics*, v. 22, p. 359-383.
- Baranov, V., and Naudy, H., 1964, Numerical calculation of the formula of reduction to the magnetic pole: *Geophysics*, v. 29, p. 67-79.
- Blaise, J., Bordet, P., Carbonnel, J.P., and Montenat, C., 1978, Flyschs et ophiolites dans la region de Panjaw: une suture neocimmerienne en Afghanistan central: *Bulletin de la Société Géologique de France*, v. 20, p. 795-798.
- Blakely, R.J., 1995, *Potential Theory in Gravity and Magnetic Applications*, Cambridge University Press, 441 p.

- Bosum, W., Hahn, A., Kind, E.G., and Weippert, D., 1968, Aeromagnetic Survey in Afghanistan 1968, Bundesanstalt für Bodenforschung, 49 p.
- Bott, M.H.P., and Smithson, S.B., 1967, Gravity investigations of subsurface shape and mass distributions of granite batholiths: Geological Society of America Bulletin, v. 78, p. 859-878.
- Boulin, J., 1988, Hercynian and Eocimmerian events in Afghanistan and adjoining regions: Tectonophysics, v. 148, p. 253-278.
- , 1990, Neocimmerian events in Central and Western Afghanistan: Tectonophysics, v. 175, p. 285-315.
- Chappell, B.W., and White, A.J.R., 1974, Two contrasting granite types: Pacific Geology, v. 8, p. 173-174.
- Clark, D.A., 1999, Magnetic petrology of igneous intrusions: implications for exploration and magnetic interpretation: Exploration Geophysics, v. 30, p. 5-26.
- Cordell, L., 1979, Gravimetric expression of graben faulting in Santa Fe country and the Espanola basin, New Mexico, *in* Ingersoll, R.V., ed., Guidebook to Santa Fe Country, 30th Field Conference, New Mexico Geological Society, p. 59-64.
- Cordell, L., and Grauch, V.J.S., 1985, Mapping basement magnetization zones from aeromagnetic data in the San Juan basin, New Mexico, *in* Hinze, W.J., ed., The Utility of Regional Gravity and Magnetic Anomaly Maps, Society of Exploration Geophysicists, p. 181-197.
- Cordell, L., and McCafferty, A.E., 1989, A terracing operator for physical property mapping with potential field data: Geophysics, v. 54, p. 621-634.
- Debon, F., Afzali, H., Le Fort, P., and Sonet, J., 1987, Major intrusive stages in Afghanistan: typology, age and geodynamic setting: Geologische Rundschau, v. 76, p. 245-264.

- Girardeau, J., Marcoux, J., and Montenat, C., 1989, The Neo-Cimmerian ophiolite belt in Afghanistan and Tibet: comparison and evolution, *in* Sengor, A.M.C., ed., Tectonic Evolution of the Tethyan Region, Kluwer Academic Publishers, p. 477-504.
- Grauch, V.J.S., and Cordell, L., 1987, Limitations of determining density or magnetic boundaries from the horizontal gradient of gravity or pseudogravity data: *Geophysics*, v. 52, p. 118-121.
- Hinze, W.J., 2003, Bouguer reduction density: why 2.67?: *Geophysics*, v. 68, p. 1559-1560.
- Ishihara, S., 1977, The magnetite-series and ilmenite-series granitic rocks: *Mining Geology*, v. 27, p. 293-305.
- , 1981, The granitoid series and mineralization: *Economic Geology 75th Anniversary Volume*, p. 458-484.
- Jadoon, I.A.K., and Khurshid, A., 1996, Gravity and tectonic model across the Sulaiman fold belt and the Chaman fault zone in western Pakistan and eastern Afghanistan: *Tectonophysics*, v. 254, p. 89-109.
- Maniar, P.D., and Piccoli, P.M., 1989, Tectonic discrimination of granitoids: *Geological Society of America Bulletin*, v. 101, p. 635-643.
- McGinnis, L.D., 1971, Gravity fields and tectonics of the Hindu Kush: *Journal of Geophysical Research*, v. 76, p. 1894-1904.
- Molnar, P., and Tapponnier, P., 1975, Cenozoic tectonics of Asia: effects of a continental collision: *Science*, v. 189, p. 419-426.
- Mushayandebvu, M.F., van Driel, P., Reid, A.B., and Fairhead, J.D., 2001, Magnetic source parameters of two-dimensional structures using extended Euler deconvolution: *Geophysics*, v. 66, p. 814-823.

- Nabighian, M.N., and Hansen, R.O., 2001, Unification of Euler and Werner deconvolution in three dimensions via the generalized Hilbert transform: *Geophysics*, v. 66, p. 1805-1810.
- Parker, R.L., 1972, The rapid calculation of potential anomalies: *Geophysical Journal of the Royal Astronomical Society*, v. 31, p. 447-455.
- Peters, S.G., Ludington, S.D., Orris, G.J., Sutphin, D.M., Bliss, J.D., and Rytuba, J.J., 2007, Preliminary Non-Fuel Mineral Assessment of Afghanistan: U.S. Geological Survey Open-File Report 2007-1214, p. 810.
- Phillips, J.D., 2002, Two-step processing for 3D magnetic source locations and structural indices using extended Euler or analytic signal methods: *Society of Exploration Geophysicists Technical Program Expanded Abstracts*, v. 19, p. 4.
- , 2005, Can we estimate total magnetization directions from aeromagnetic data using Helbig's integrals?: *Earth, Space, and Planets*, v. 57, p. 681-689.
- Reid, A.B., Allsop, J.M., Granser, H., Millett, A.J., and Somerton, I.W., 1990, Magnetic interpretation in three dimensions using Euler deconvolution: *Geophysics*, v. 55, p. 80-91.
- Ruleman, C.A., Crone, A.J., Machette, M.N., Haller, K.M., and Rukstales, K.S., 2007, Map and Database of Probable and Possible Quaternary Faults in Afghanistan: U.S. Geological Survey Open-File Report 2007-1103.
- Sengor, A.M.C., 1984, The Cimmeride Orogenic System and the Tectonics of Eurasia: *Geological Society of America Special Paper*, v. 195, p. 82.
- Sengor, A.M.C., Altmer, D., Cin, A., Ustaomer, T., and Hsu, K.J., 1988, Origin and assembly of the Tethyside orogenic collage at the expense of Gondwana Land, *in* Audley-Charles, M.G., and Hallam, A., eds., *Gondwana and Tethys: Geological Society Special Publication, Volume 37*, p. 119-181.
- Sengor, A.M.C., and Natal'in, B.A., 1996, Paleotectonics of Asia - fragments and synthesis, *in* Yin, A., and Harrison, M., eds., *The tectonic evolution of Asia*, Cambridge University Press, p. 486-640.

- Simpson, R.W., Jachens, R.W., Blakely, R.J., and Saltus, R.W., 1986, A new isostatic residual gravity map of the conterminous United States with a discussion on the significance of isostatic residual anomalies: *Journal of Geophysical Research*, v. 91, p. 8348-8372.
- Sweeney, R.E., Kucks, R.P., Hill, P.L., and Finn, C.A., 2006a, Aeromagnetic and gravity surveys in Afghanistan, U.S. Geological Survey Open-File Report 2006-1204.
- , 2006b, Aeromagnetic survey in western Afghanistan, U.S. Geological Survey Open-File Report 2006-1325.
- Tapponnier, P., Mattauer, M., Proust, F., and Cassaigneau, C., 1981, Mesozoic ophiolites, sutures, and large-scale tectonic movements in Afghanistan: *Earth and Planetary Science Letters*, v. 52, p. 355-371.
- Tapponnier, P., and Molnar, P., 1976, Slip-line field theory and large-scale continental tectonics: *Nature*, v. 264, p. 319-324.
- Telford, W.M., Geldart, L.P., Sheriff, R.E., and Keys, D.A., 1990, *Applied Geophysics*, 2nd Ed., Cambridge University Press, 770 p.
- Thompson, D.T., 1982, EULDPH: A new technique for making computer-assisted depth estimates from magnetic data: *Geophysics*, v. 47, p. 31-37.
- Treloar, P.J., and Izatt, C.N., 1993, Tectonics of the Himalayan collision between the Indian plate and the Afghan block- a synthesis, *in* Treloar, P.J., and Searle, M.P., eds., *Himalayan Tectonics: Geological Society Special Publication, Volume 74*, p. 69-87.
- Vikhter, B.Y., Yeremenko, G.K., and Chmyrev, V.M., 1976, A young volcanogenic carbonatite complex in Afghanistan: *International Geology Review*, v. 18, p. 1305-1312.

Vikhter, B.Y., Yeremenko, G.K., Chmyrev, V.M., and Abdullah, D., 1978, Pliocene-Quaternary volcanism of Afghanistan: *International Geology Review*, v. 20, p. 525-536.

Wheeler, R.L., Bufe, C.G., Johnson, M.L., and Dart, R.L., 2005, *Seismotectonic Map of Afghanistan, with Annotated Bibliography*: U.S. Geological Survey Open-File Report 2005-1264.

Wheeler, R.L., and Rukstales, K.S., 2007, *Seismotectonic Map of Afghanistan and adjacent areas, with Annotated Bibliography*: U.S. Geological Survey Open-File Report 2007-1104.

CONCLUSIONS

This dissertation demonstrates the utility of gravity and magnetic (potential field) methods for geologic interpretation in different tectonic environments and at different scales. In the central San Luis Basin of Colorado and New Mexico, inversion of gravity anomalies revealed patterns of sediment thickness and basin subsidence, and aeromagnetic anomalies reflect the distribution of interbedded volcanic rocks. The geometry of a batholith complex under the San Juan volcanic field in southwestern Colorado is revealed by integrated modeling of gravity and seismic refraction data, showing an average batholith thickness of 8-12 km with the greatest thicknesses under the western part of the volcanic field. In Afghanistan, major plutonic belts related to prior subduction events were mapped, and inferred tectonic blocks were shown to have distinctive geophysical signatures.